Structural Insights into the Assembly and Dynamics of the ATP-Dependent Chromatin-Remodeling Complex SWR1

A dissertation presented

by

Vu Quang Nguyen

to

The Department of Molecular and Cellular Biology

in partial fulfillment of the requirements
for the degree of
Doctor of Philosophy
in the subject of

Biochemistry

Harvard University
Cambridge, Massachusetts

April 2014

Professor Andres E. Leschziner
Research Advisor

Vu Quang Nguyen

Structural Insights into the Assembly and Dynamics of the ATP-Dependent Chromatin-Remodeling Complex SWR1

Abstract

Chromatin—the condensed genetic material in eukaryotes—undergoes dynamic compaction and decompaction as a means to regulate DNA accessibility. ATP-dependent chromatin-remodeling complexes (remodelers) are essential regulators of this process. These sophisticated assemblies, many of which contain over a dozen subunits and are megadalton-sized, target the nucleosome, which is the smallest repeating unit of chromatin and is comprised of ~150 DNA base-pairs wrapped around a core of histone proteins. ATP-driven DNA translocation by a catalytic ATPase, which is conserved among remodelers, leads to unraveling of the DNA from the histones. This fundamental activity then primes different remodelers to perform their specialized functions, among which are nucleosome repositioning, clearance, and histone exchange. Importantly, perhaps to prevent depletion of the nuclear ATP pool, these ATP-hydrolyzing machines have evolved autoinhibitory schemes that are only relieved upon their recognizing specific nucleosomal epitopes, such as linker DNA or histone modifications. These properties—functional specificity and autoinhibition—rely on accessory domains and subunits associated with the core ATPase. However, our knowledge of the assembly, substrate interaction and dynamics of remodelers, especially of the larger complexes, is extremely limited and remains an important goal in chromatin biology.

Large remodelers are recruited to specific sites in the genome to generate open chromatin, thus facilitating processes such as transcription initiation and DNA repair. Their

collective activity results in a nucleosome-depleted region (NDR) flanked by nucleosomes enriched in the histone variant H2A.Z. While the NDR forms as a result of remodelers repositioning or evicting nucleosomes, H2A.Z incorporation, which may function to stabilize the NDR, occurs *via* ATP-dependent exchange of histone dimers. This reaction is catalyzed by the remodeler SWR1, which, unlike other remodelers, does not reposition its nucleosome substrate. In *Saccharomyces cerevisiae*, where it is best characterized, SWR1 functions as a 1 MDa complex containing 14 different subunits that are suggested to form four modules: the catalytic ATPase, two multi-subunit substrate-handling modules, and the intriguing AAA+ proteins Rvb1/Rvb2 of unclear function. *How is a specialized dimer exchanger built from these functional modules? What role do AAA+ proteins, which are unique to dimer exchangers among remodelers, play in remodeling?* Furthermore, it has also been shown that regulation of SWR1's ATPase activity relies on the enzyme's unique requirement for two substrates—the nucleosome and the histone dimer. Interestingly, while dual substrate binding must occur to sufficiently activate SWR1 for exchange, nucleosome binding alone partially activates the complex. *What is the functional significance of this complex synergistic activation of the enzyme, which is not observed in other remodelers?* To address these important questions, my graduate research has aimed to characterize the molecular architecture of SWR1 during complex assembly and activation by its obligate substrates.

In this thesis work, we used electron microscopy to obtain the 3D structure of SWR1 and map the locations of its functional modules, which we showed to associate as structurally discrete entities in the complex. Remarkably, Rvb1 and Rvb2 form a hetero-hexameric ring and serve as a docking platform for the substrate-handling modules. As a result, these modules adopt a side-by-side arrangement, which may be important for spatial coordination of the two

substrates during exchange. This annotated SWR1 structure provides a framework to analyze conformational dynamics within the activated complex. Towards this goal, we have obtained the 3D structure of a SWR1-nucleosome co-complex, which showed that SWR1 significantly extends as the catalytic ATPase forms the main contact with the nucleosome core particle. Our current work aims to structurally characterize the ternary SWR1-nucleosome-H2A.Z/H2B complex. These 3D structures will allow visualization of conformational changes among the functional modules during partial and complete activation of SWR1. This information will be crucial to understand the mechanism and substrate-based regulation of the dimer-exchange activity in chromatin remodeling. In a broader context, insights gained from this functionally unique remodeler will be instrumental to our understanding of the functional divergence within this complex family of molecular machines.

Acknowledgments

The past six years have been the most intellectually invigorating time of my life. I had decided very early on that if I were to pursue a PhD, I would choose to work on chromatin remodelers. Looking back, I am still amazed that it had materialized, and that I was able to join the group of my thesis advisor, Andres Leschziner, whose work on the RSC complex inspired me to join the field of chromatin regulation. I owe it to the BOSS for giving me a challenging project, the freedom to explore it, and the very high standards by which I evaluate my and others' science. Most importantly, I thank him for sticking with me until the end. I am very proud of the work that we have done *together*.

The past six years have also been incredibly fun. There is no better lab in which to do research than the Leschziner Lab. I am indebted to Berith Isaacs and Preethi Chandramouli for familiarizing me with the biochemical and computational routines of the lab, and for being fantastic colleagues and friends. John Srouji, Bret Redwine, and Brandy Pappas, and I were the first students to join the lab, and I appreciate the friendships and intellectual support that we shared. Rogelio Hernandez-Lopez joined us the next year and he has become one of my closest friends. I thank Roger for patiently answering my computer-related questions and for all the fun. Three years ago, Kat Toropova entered the lab and has since become the glue that holds us together. Thanks to Katsch, I worked up the courage to get started on cryo-EM, by which I was very intimidated. Mike Cianfrocco recently became a member of our lab and has already given great advice on my research. To the undergrads—Koning Shen, Viviana Neviani, and Emily Boggs: thanks for teaching me how to teach. I had a lot of fun with you guys. And to the only member in the lab who will never read this: you know how much you mean to me, Locks!

Joining the Leschziner Lab is a buy-one-get-three-free deal because we share our space, science, and lots of fun with the Gaudet, D'Souza, and Jeruzalmi groups. Together we make up the Structural Biology Supergroup. Over the years, people have come and gone but the friendships that I have made here will last me a very long time. There are too many names to list here. Suffice it to say that thanks to all the members, past and present, of our beloved supergroup, it was always fun to come to work. I also owed it to the formidable Liza Sholl for keeping us stocked and reimbursed and for always saying yes when I needed help.

One of the most rewarding experiences of my graduate career is the three semesters I spent teaching undergrads. I especially enjoyed teaching MCB 52 and I have Mary Ellen Wiltrout, along with roughly two dozens fellow teachers, to thank for two wonderful semesters. I am also thankful for Briana Burton and Tom Torrello for allowing me more involvement with the course than I was paid to be. I have taught almost 50 undergrads here, and I thank most of them for helping be become a better teacher and communicator. I would like to also thank John Girash from the Bok Center for hiring me to be a teaching consultant. I have learned so much from working with you and my fellow consultants in this capacity.

I would like to express my gratitude to members of my exam and thesis committees: Susan Mango, Jim Hogle, Xiaowei Zhuang, Erin O'Shea, Nicole Francis, and Vlad Denic. I always enjoyed presenting my research to you. Your advice, support, and enthusiasm meant very much to me. Outside of my committee, Rachelle Gaudet, Samara Reck-Peterson and Briana Burton have provided me with valuable mentorship, for which am I very grateful. I also enjoyed my time rotating in David Jeruzalmi's and Alan Saghatelian's labs, and I thank the two advisors for their support during my first year in graduate school.

I would like to thank the Department of Molecular and Cellular Biology at Harvard for having taken a chance on me, especially considering that I was rejected by Stanford, Berkeley and UCSF. Here in MCB, I have made wonderful friends, not only among my terrific classmates, but also among the younger G's and within the rich and interactive MCB community. I must especially thank my good friends Jessica Liu and Steven Chao. You two have been more supportive of me than I could have ever asked for. Thanks for always listening and talking and texting and for providing a roof over my head during the summer months. Also, many thanks to Mike Lawrence and Debra Maddalena for a tremendous amount of advice and support during my years at MCB.

Lastly, I thank my phenomenal parents for giving me life and love. Making them proud has been and will always be my greatest motivation in life. I hope that what I have accomplished here does just that.

Table of Contents

List of Figures

List of Tables

Chapter One

Introduction

to chromatin structure and regulation by ATP-dependent remodeling complexes

PACKAGING OF THE EUKARYOTIC GENOME

During interphase, the eukaryote's DNA is confined to the nucleus—a double-membraned organelle of 1-2 μm diameter. Within this compartment, roughly 2 meters of genetic material exists as a highly condensed structure referred to as the chromatin. This condensation relies on histones—evolutionarily conserved proteins that associate with the majority of the DNA. Canonical histones H3, H4, H2A, and H2B are globally distributed and bind the DNA together to form nucleosomes—the smallest repeating structural unit of chromatin (Tan and Davey, 2011). Linker histones, such as H1 and H5, ubiquitously bind and stabilize nucleosomes, as well as facilitate higher-order packaging (Carter and van Holde, 1998; PRIETO et al., 2012). In contrast, histone variants, such as H2A.Z, H2A.X, and H3.3, function outside of DNA packaging and localize to specific regions in the chromatin (Volle and Dalal, 2014).

Why is the DNA packaged in eukaryotes? Is its compartmentalization during most of the cell's life cycle the main driving force for this complex feature? A recent study, which reported chromatinization involving histone homologs in the archaea *Haloferax volcanii*, which lacks a nucleus, proposed that packaging of the genetic material mainly serves to regulate gene expression (Ammar et al., 2012). In such case, the DNA must be packaged in a manner that allows for dynamic and context-specific patterns of expression. Understanding this process has been a decades-long pursuit and recent progress has begun to unveil the complex organization of the chromatin.

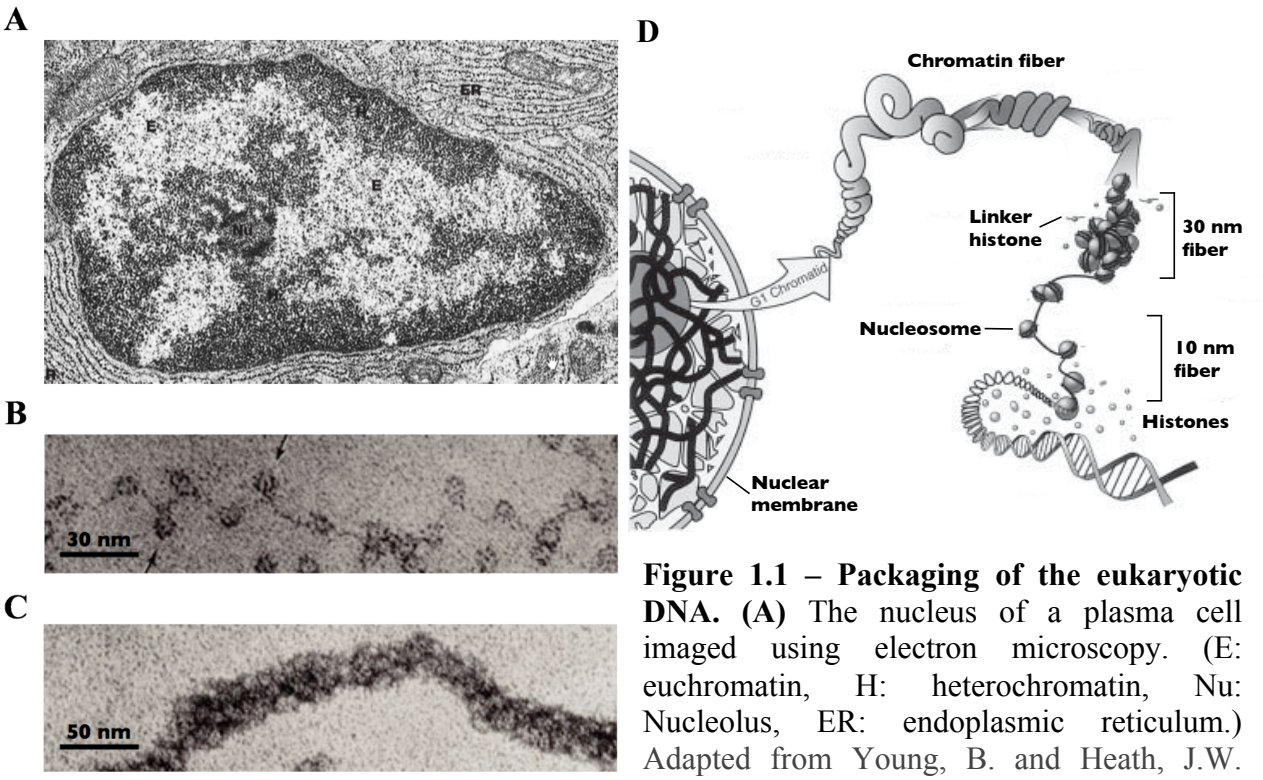

Figure 1.1 – Packaging of the eukaryotic DNA. (A) The nucleus of a plasma cell imaged using electron microscopy. (E: euchromatin, H: heterochromatin, Nu: Nucleolus, ER: endoplasmic reticulum.) Adapted from Young, B. and Heath, J.W. "Wheater's Functional Histology", 4th edition, 2000, Harcourt publishers Limited, Edinburgh. **(B)** Electron micrograph of the 10 nm chromatin fiber isolated at low ionic strength (Olins and Olins, 2003). Arrows indicate single nucleosomes. **(C)** Electron micrograph of the 30 nm chromatin fiber isolated at moderate ionic strength (Olins and Olins, 2003). **(D)** Schematic model of hierarchical DNA packaging in the interphase nucleus. Adapted from Hansen and Turgeon, 1999 (Hansen and Turgeon, 1999).

The chromatin is structurally heterogeneous. Early visualizations using electron microscopy of a fixed, sectioned, and negatively stained nucleus revealed varying densities of the genetic material (Figure 1.1A) (Olins and Olins, 2003). A relative enrichment of denser chromatin was observed associated with the inner nuclear membrane, while chromatin located more internally appeared less dense. The nucleolus, the site of synthesis of ribosomal RNAs, exists as a compact and dense chromatin region near the center of the nucleus. These observations underlie the dichotomous classification of genetic material as euchromatin and heterochromatin. While this classification was based on gross structure, or more precisely appearance, of chromatin, it carries important functional implications. Euchromatin is

commonly considered "active" chromatin due to its open structure, whereas heterochromatin is densely packaged and thus rendered "inactive." Chromatin activity generally refers to transcriptional competency, which correlates positively with accessibility of the DNA and thus negatively with the degree of compaction. However, transcriptional activity of single genes spans a complex spectrum from ubiquitously expressed, such as house-keeping genes, to repressed, such as those residing on the inactive X chromosome (Lee and Young, 2013). Gene expression can be temporally induced, inhibited, or poised, whereby the gene is transcriptionally competent but not yet transcribed. Does this simple classification of chromatin then sufficiently describe organizational and regulatory aspects of chromatin that enable its functional plasticity?

The structure of chromatin is a matter of debate (Ghirlando and Felsenfeld, 2013). Two configurations of isolated chromatin have been observed using electron microscopy (Figure 1.1B-C). The 10 nm fiber, observed in low ionic conditions, comprises linear repeats of single nucleosomes—this is often referred to as the "beads-on-a-string" structure of chromatin (Figure 1.1B). This fiber has been shown to compact into the 30 nm fiber (Figure 1.1C) at moderate ionic strength, of whose detailed structure several models exist (Ghirlando and Felsenfeld, 2013). Higher-order folding of the chromatin fiber, which must occur to achieve the observed level of DNA compaction, is unclear. It has been proposed that chromatin folding follows a hierarchical order starting from the 10 nm fiber (Figure 1.1D). This mode of compaction would allow for the drastic condensation of mitotic chromosomes. However, recent efforts in probing the structure of mitotic chromatin *in vivo* reported no structural features larger than 11 nm when measured by small-angle X-ray scattering (SAXS) (Joti et al., 2012). These authors reached the same conclusion for interphase chromatin in HeLa cells. Another study in mouse cells demonstrated that both open and closed chromatin regions exist inside the nucleus as the 10 nm fiber (Fussner

et al., 2012). Therefore, it is possible that the 30 nm fiber results from extraction of the chromatin, and that *in vivo*, chromatin folding is more irregular, and thus dynamic, than previously thought (Ghirlando and Felsenfeld, 2013).

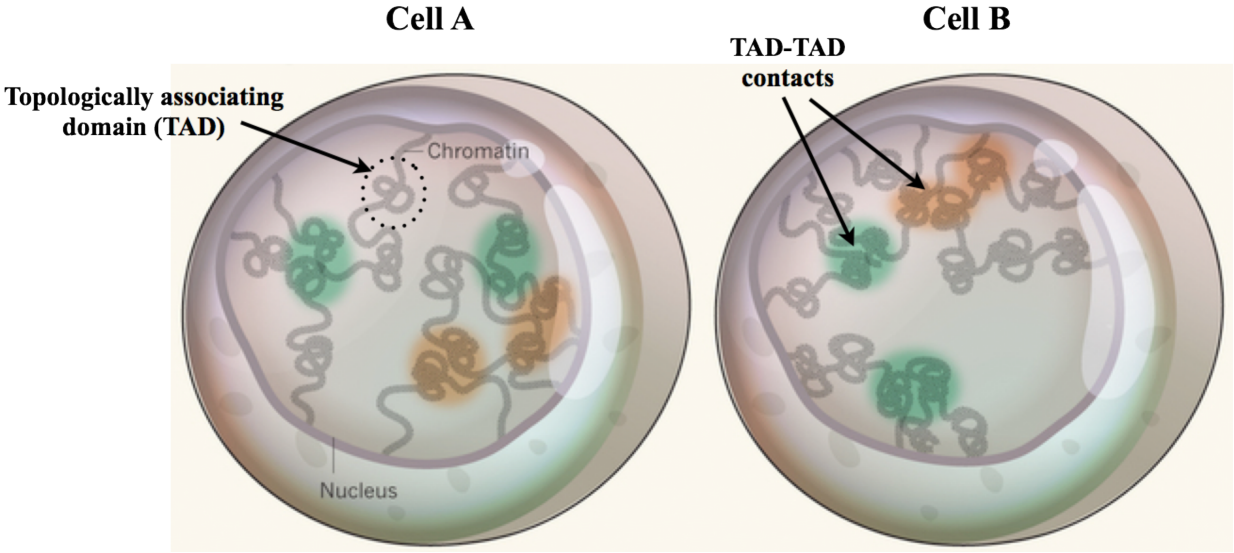

Figure 1.2 – Chromatin exists as separate structural domains inside the nucleus. Chromosome conformation capture was employed to probe the configuration of the chromatin in single cells (Nagano et al., 2013). This study showed that chromatin exists as individual topologically associating domains (TAD). Interactions between TADs, which may influence gene expression, vary in single cells within a population. Adapted from Dekker & Mirny (Dekker and Mirny, 2013).

Chromosome conformation capture (3C) is a technique frequently used to investigate interactions among specific genomic regions *in vivo* (Dekker et al., 2002). Recently, variations of this approach have accomplished genome-wide mapping of chromatin interactions (Dixon et al., 2012). These studies revealed that the chromatin is organized into distinct megabase-sized topologically associating domains (TADs) (Dixon et al., 2012) (Figure 1.2). Within these domains, genomic regions may interact with and regulate each other. Remarkably, these domains are conserved across mammalian species (Ammar et al., 2012; Dixon et al., 2012), suggesting a common structural organization of the chromatin, which may have been driven by

the conserved regulatory networks. This organization mode is erased in mitosis, suggesting that chromatin organization is highly dynamic during the cell cycle and that TADs are reversible structural features unique to interphase (Naumova et al., 2013). A recent 3C-type study examining chromatin organization in single cells found that TAD-TAD interactions vary from cell to cell within a population (Nagano et al., 2013) (Figure 1.2), further demonstrating the remarkably labile nature of chromatin.

It remains to be seen what governs these variable inter-TAD contacts and how they correlate with regulation of gene expression. While these aspects of DNA packaging in eukaryotes at the global level remain a challenging pursuit, they are much better understood at the smallest structural level of chromatin—the nucleosome.

THE NUCLEOSOME – STRUCTURE AND DYNAMICS

In 1975, the nucleosome was visualized for the first time by electron microscopy as the smallest repeating unit of chicken chromatin, measuring 125 Å in diameter, containing stoichiometric amounts of four histone proteins H2A, H2B, H3, and H4, and compacting ~ 200 bps to ~ 1/5 of its extended length (Oudet et al., 1975). It would take over 2 decades later for the structure of this nucleoprotein complex to be unveiled at atomic resolution (Luger et al., 1997). At the present, crystal structures are available for canonical nucleosomes from yeast (White et al., 2001), fly (Clapier et al., 2008), Xenopus (Davey et al., 2002; Luger et al., 1997), and human (Tsunaka et al., 2005). All of these structures revealed a remarkable structural conservation of the nucleosome core particle (Andrews and Luger, 2011). Two copies of H3/H4 heterodimers form a histone tetramer, which assembles with two H2A/H2B heterodimers into a globular core called the histone octamer, around which 147 DNA basepairs wrap in ~1.65 left-handed turns

(Figure 1.3 A-D). The resulting complex exhibits a pseudo two-fold symmetry in its 3 dimensional structure (Figure 1.3B-C). The symmetry axis intersects the dyad basepair, which is at the very center of the nucleosomal DNA. The H3/H4 tetramer binds the central portion of the DNA flanking the dyad region. A H2A/H2B dimer binds each terminal segment of the DNA.

The nucleosome structure reveals an extensive network of ~500 direct, indirect, and water-mediated electrostatic interactions between the DNA and the histone octamer (Davey et al., 2002), explaining the remarkable stability of the complex *in vitro*. Such extensive histone-DNA interactions also render nucleosomal DNA largely inaccessible to DNA-binding factors. None of these interactions occur in a base-specific manner, thus nucleosomes form independent of the DNA sequence, although certain sequence features are more favorable than others (Battistini et al., 2012; Kaplan et al., 2010). Among these interactions, 14 are crucial to the structural integrity of the nucleosomes. At each of these sites, the minor groove of the DNA faces the histone octamer and an arginine side chain inserts between the two DNA strands (Figure 1.3F) (Luger et al., 1997). These interactions occur independently of each other and help to maintain structural integrity of the nucleosome while accommodating the conformational dynamics intrinsic to the complex (Andrews and Luger, 2011).

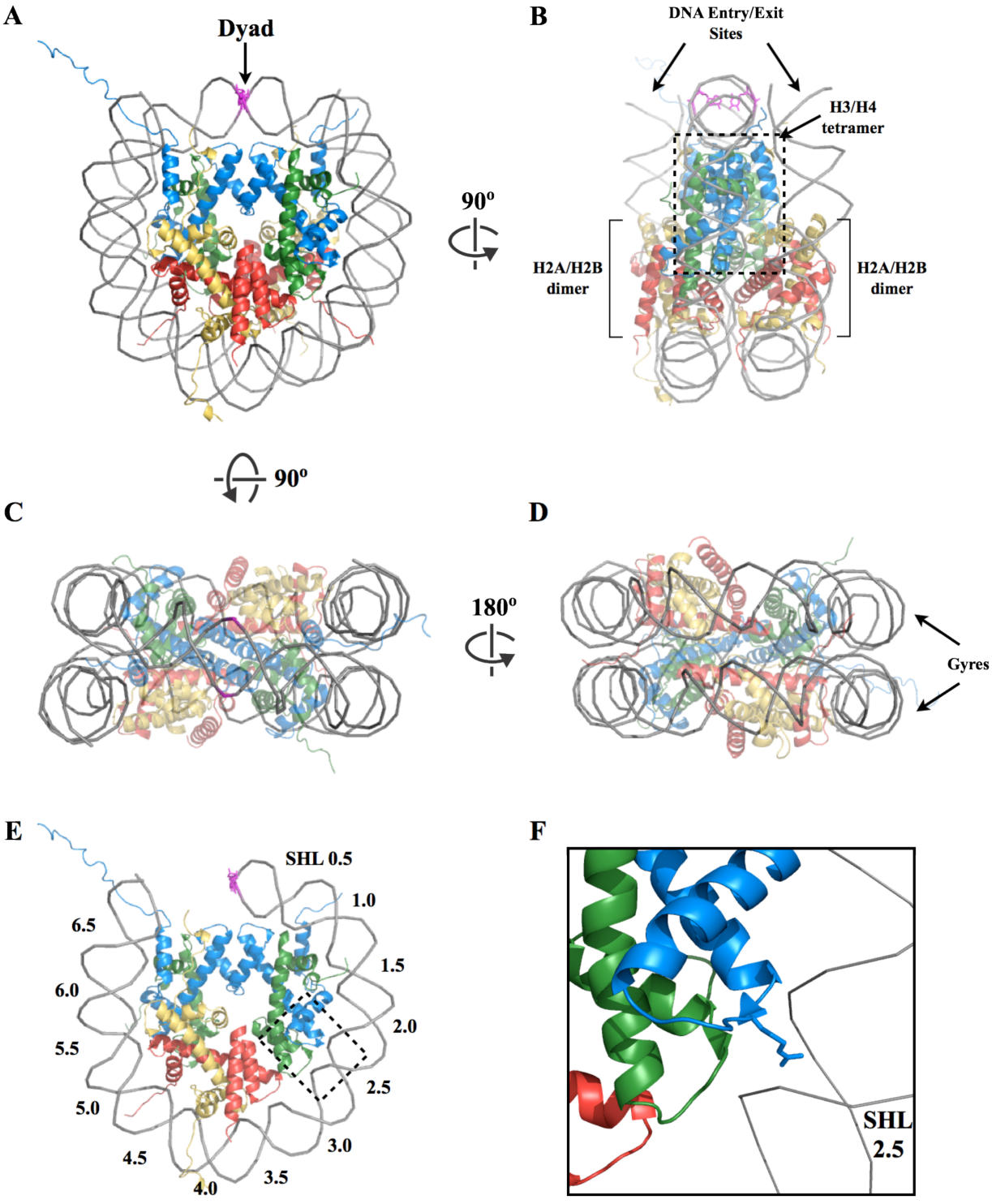

Figure 1.3 – The structure of the nucleosome. **(A)** The X-ray crystal structure of the nucleosome (Luger et al., 1997). The DNA is shown in grey, with the central dyad basepair shown as sticks in magenta. H3, H4, H2A and H2B are colored blue, green, yellow, and red, respectively. **(B)** Side view of the nucleosome structure. The main structural components of the

histone octamer, the H3/H4 tetramer and two flanking H2A/H2B dimers, as well as the two ends of the DNA, called the entry/exit sites, are labeled. **(C)** The structure viewed from the top of the dyad region. **(D)** View opposite from the dyad shows the two gyres of the negatively supercoilded DNA. **(E)** The same view as in (A) is shown, with the back half of the DNA segment (73 basepairs) and the back H2A/H2B dimer removed. Superhelical locations (SHL) are labeled for the nucleosomal DNA. The corresponding negative values are assigned to the SHLs on the other side of the dyad. **(F)** A close-up view of the region around SHL 2.5 boxed out in (E). An arginine side chain on H3 (shown in sticks) inserts between the two DNA strands. Similar interactions are observed at other SHLs where the minor groove of the DNA faces the histone octamer.

The histones interact in a similar manner with the DNA at each minor groove and all interactions appear to mirror each other across the dyad axis (Davey et al., 2002). However, the energetic landscape of histone-DNA interactions is surprisingly non-uniform and asymmetric (Figure 1.4). Hall and colleagues measured these interactions at single-basepair resolution by mechanically unzipping nucleosomal DNA using an optical trap setup (Hall et al., 2009). Strand separation is hindered by interaction of the DNA with the histones, causing pauses in the unzipping progress. The lengths of these pauses, called dwell times, reflect the strength of histone-DNA interactions at that location. This approach resulted in two major observations: (1) histones interact with the DNA in an energetically asymmetric manner around the dyad axis, and (2) there are three regions of strong interactions throughout the nucleosomes (Figure 1.4). The first observation demonstrates that the DNA sequence, although not recognized by the histones, affects the stability of the nucleosome. This is due to the sequence-dependent bendability of the DNA molecule that allows it to wrap around the histone octamer. This property has also been observed for nucleosomes that occur *in vivo* (Kaplan et al., 2009). Secondly, instead of 14 sites of strong histone-DNA interactions, only 3 such sites were observed, with the strongest interactions occurring between superhelical location (SHL) +/-1.0 and the dyad (Figure 1.4). Two other energetically significant interaction sites occur between SHL +/-5 and +/-4, where the H2A/H2B dimers bind to the DNA. The terminal ~20 basepairs of nucleosomal DNA on each

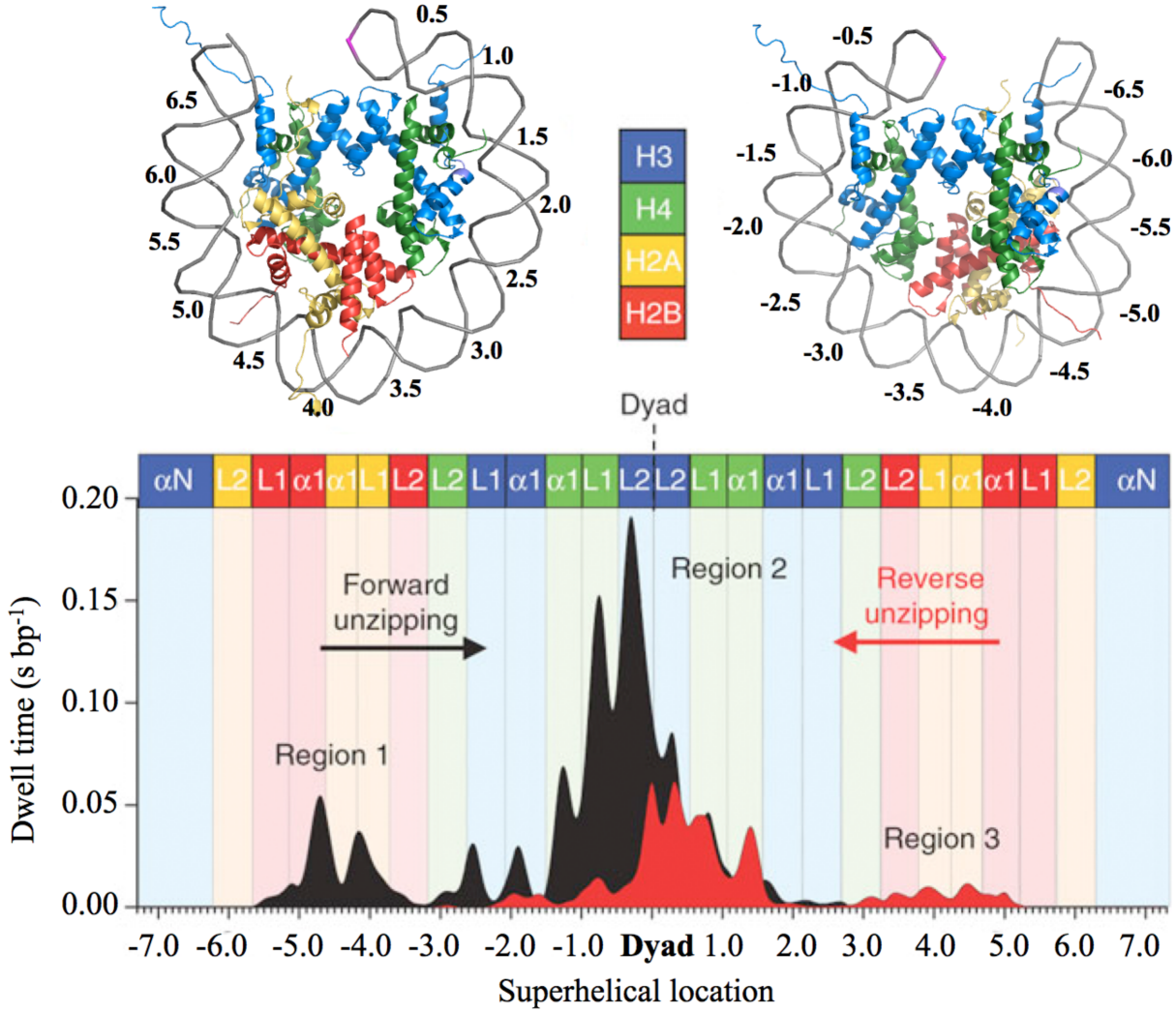

Figure 1.4 – The energetic landscape of histone-DNA interactions within the canonical nucleosome. **(Top)** Front and back halves of the nucleosome structure. Each view has one H2A/H2B dimer and ½ of the nucleosomal DNA removed. Coloring scheme for the histones is similar to that in Figure 1.3. Superhelical locations are indicated. **(Bottom)** Energetic assessment of histone-DNA interactions throughout the nucleosome. The nucleosomal DNA is mechanically unzipped from both ends (forward and reverse unzipping) at constant force (28 pN) in a single-molecule optical-trap setup (Hall et al., 2009). The dwell time (seconds/basepair) measures pauses in unzipping due to interaction of the DNA with the histones. It represents the strength of the interaction and is plotted for each basepair of the DNA. Adapted from Hall *et al.* (Hall et al., 2009).

side of the dyad interact weakly with the histones, which is consistent with the observation of spontaneous partial unwrapping, or "breathing," of the outer DNA segments (Li and Widom,

2004). Importantly, only 2 of 3 strong interaction sites were observed when the DNA was unzipped from either side of the dyad, suggesting that the nucleosome disintegrates when the DNA is unraveled past the dyad region. Thus, enzymes that function in the repositioning, disassembly or major structural reconfiguration of the nucleosome must overcome the energetic barrier present near the dyad region.

Nucleosomes are commonly reconstituted *in vitro* for various experimental purposes. This technique involves mixing recombinantly expressed histones, which may be pre-assembled into octamers, with pure DNA in high salt. Then, the salt concentration is lowered gradually, a process called salt-gradient dialysis, or in a stepwise manner (Dyer et al., 2004). As this proceeds, the histones sequentially bind to the DNA, starting with the H3/H4 dimer or tetramer, which interacts with the DNA at higher ionic strength, and followed by cooperative association of the two H2A/H2B dimers (Polo and Almouzni, 2006). *In vivo*, where histones are abundant, nonspecific histone-DNA aggregation is prevented by various histone chaperones, which bind to specific histone dimers and tetramers inside the nucleus (Burgess and Zhang, 2013). Together with chromatin assembly factors, they guide the sequential deposition of the histones onto the DNA and ensure proper nucleosome formation (Burgess and Zhang, 2013; Torigoe et al., 2011). While these activities peak during DNA replication as the newly synthesized DNA is chromatinized, chaperones are also involved during transcription and DNA repair to facilitate assembly and disassembly of the nucleosomes (Birch et al., 2009).

Despite the remarkable structural conservation across species, it has become increasing clear that the crystal structures reported for the nucleosome do not tell the whole story about its biophysical properties. Single-molecule studies have revealed the nucleosome to be highly structurally dynamic *in vitro* (Buning and van Noort, 2010). In addition to spontaneous DNA

breathing discussed above (Li and Widom, 2004), more internal sites in the nucleosome are also transiently exposed (Koopmans et al., 2009). Furthermore, a single-molecule fluorescence resonance energy transfer (FRET) analysis revealed more significantly open states that the nucleosome adopts in solution (Böhm et al., 2010). In one state, estimated to occur in 0.2-3% of the population under physiological salt conditions, the H2A/H2B dimers dissociate from the H3/H4 tetramer while all histones remain bound to the DNA. This open state is fundamentally different from that caused by DNA breathing. It is important to note that all experiments described so far were carried out on nucleosomes reconstituted using nucleosome-positioning sequences (NPS). These sequences intrinsically favor nucleosome formation due to their high bendability (Battistini et al., 2012). It is expected that *in vivo*, the nucleosomes, most of which form over less favorable sequences, exhibit even more structural plasticity. This property is crucial for chromatin function as it allows for dynamic reconfiguration of the nucleosomes while enzymes such as the RNA polymerase and helicases processively traverse the chromatinized template.

In additional to its intrinsic structural dynamics, posttranslational modifications (PTMs) of histones can alter the stability of the nucleosome. Histones are chemically modified inside the nucleus, and the majority of these covalent modifications are reversible and take place on the long, flexible, lysine-rich histone tails (Bannister and Kouzarides, 2011). Here, residue-specific acetylation, methylation, phosphorylation, and other PTMs are carried out by various histone acetyl/methyltransferases and kinases. Acetylations are generally considered to destabilize the nucleosome due to neutralization of the basic lysines that interact favorably with the phosphate backbone (ALLFREY et al., 1964). Therefore, this mode of modification has been shown to take place at sites of high gene activity, where as histone methylation is generally found in more

inactive regions of the chromatin (Bannister and Kouzarides, 2011). However, histone marks generally co-occur in the same nucleosome, and given the pseudo two-fold symmetry of the complex, both symmetric and asymmetric modifications have been detected *in vivo* (Voigt et al., 2012). It remains a major challenge to determine the combinatorial effect of various PTMs on the biophysical properties of the modified nucleosome. To further complicate matters, PTMs also correlate with recruitment of a diverse set of chromatin-binding factors, such as transcription factors and polycomb complexes (Bannister and Kouzarides, 2011). Thus, activities downstream of PTMs may further influence chromatin function. It is, however, not clear whether PTMs serve to promote future gene activity or as memory of recent activity (Henikoff and Shilatifard, 2011). Furthermore, PTMs are reversible marks that can be removed by deacetylases and demethylases (Bannister and Kouzarides, 2011). Therefore, histone modifications that alter nucleosomal stability and chromatin function are dynamic processes that facilitate highly specific patterns of gene expression.

Histone variants also confer upon the nucleosome distinct biophysical and functional properties (Volle and Dalal, 2014). Unlike the canonical histones, which are synthesized during DNA replication and present throughout the chromatin, histone variants are made throughout the cell cycle and localize to very specific regions. CENP-A, a variant of the canonical H3, is found at centromeres (Hasson et al., 2013; Mendiburo et al., 2011) and is required for attachment to the kinetochore (Guse et al., 2011). Another H3 variant, H3.3, although only differing from its canonical form by 4 amino acids, is enriched within the bodies of active genes, peaking near the 3' ends (Stroud et al., 2012). H2A.X, an H2A variant, is restricted to chromatin proximal to sites of DNA damage and plays a crucial role in mediating the repair process (Bassing et al., 2002). H2A.Z, the most evolutionarily conserved histone variant in eukaryotes, localizes to a few

nucleosomes flanking gene promoters (Zhang et al., 2005). These variants are incorporated into the chromatin by specialized histone chaperones (Banaszynski et al., 2013; Barnhart et al., 2011; Lewis et al., 2010), the exception being H2A.Z, whose deposition requires a unique ATP-dependent chromatin remodeler called SWR1 (Mizuguchi et al., 2004). The resulting variant-containing nucleosomes clearly mark specific functional regions in the genome; however, how histone variants affect stability of the nucleosome is unclear. Crystal structures have been obtained for H2A.Z- (Suto et al., 2000) and CENP-A- (Tachiwana et al., 2011) containing nucleosomes, which are remarkably similar to the canonical nucleosome. However, covalent modifications of the variants themselves, which often take place post-deposition (Ishibashi et al., 2009; Meyer et al., 2013; Thambirajah et al., 2009; Valdés-Mora et al., 2012), may confer more significant structural reconfiguration to the nucleosome, as well as mediate downstream activities. The dynamic association of histone variants during the cell cycle is an indispensible task to ensure proper remodeling of the chromatin to support a diverse set of functions (Nashun et al., 2011; Skene and Henikoff, 2013).

Many layers of regulatory features exist to diversify the biophysical and functional properties of nucleosomes that form throughout the genome. While the details of this phenomenon await further studies, two basic principles can be stated for the role of the nucleosome *in vivo*. First, it presents a steric barrier to DNA-templated transactions, such as transcription, replication, and repair. Secondly, its stability is strictly and specifically modulated by PTMs and histone variants. Therefore, the nucleosome provides a means for the cell to fine-tune DNA accessibility to support its activity. Valuable insights into this regulation have been gained from genome-wide mapping of nucleosome locations, modifications, and histone variants.

GENOME-WIDE NUCLEOSOME DISTRIBUTION

Mapping nucleosome positions is typically carried out using the chromatin immuno-precipitation (ChIP) approach (Solomon and Varshavsky, 1985), where the native chromatin, which could be chemically fixed, is treated with an endonuclease, most commonly micrococcal nuclease (MNase). This treatment removes DNA not associated with proteins, such as linker DNA between nucleosomes. The resulting chromatin thus contains primarily mononucleosomes, which are immuno-precipitated using an anti-histone resin. Then, the histone-bound DNA is isolated and sequenced. The density of each sequence read represents the level of histone enrichment and thus nucleosome presence at that genomic region. ChIP is also used to map the locations of functional histone modifications, histone variants and binding sites of chromatin-associated factors, given that antibodies against these features and factors are available for immune-precipitation (Jiang and Pugh, 2009; Zhang and Pugh, 2011). Recent advances in ChIP and next-generation sequencing technologies have allowed single-base-pair-resolution determination of these binding sites (Rhee and Pugh, 2011).

Using this approach, genome-wide nucleosome maps have been obtained for *Saccharomyces cerevisiae* (Albert et al., 2007), *Drosophila melanogaster* (Mavrich et al., 2008b), *Caenorhabditis elegans* (Valouev et al., 2008) and humans (Valouev et al., 2011). These maps converge on a striking stereotypical structure of promoter chromatin (Figure 1.5). Remarkably, promoter regions are generally depleted of histones, thus they are termed the nucleosome-free regions (NFR). The NFRs are also observed near transcription termination sites (Figure 1.5). When nucleosomes were assembled *in vitro* on genomic yeast DNA, histone depletion was observed at similar sites, indicating that the DNA sequences at these functional genomic regions intrinsically disfavor nucleosome formation (Kaplan et al., 2009). Detailed

analysis of the *in vivo* nucleosomal DNA sequences unveiled 10 basepair periodicity of alternating AT and CG dinucleotides, which promotes bending of the DNA at the superhelical locations (Figure 1.3 E) (Albert et al., 2007; Kaplan et al., 2010). This unique sequence feature is depleted at gene promoters, thus consistent with the absence of nucleosomes at these sites. In addition to promoters and termination regions, origins of replication (Eaton et al., 2010; Givens et al., 2012) and regulatory factor binding sites (Kaplan et al., 2009) are also depleted for histones. These studies demonstrated that even though the histones interact with the DNA in a sequence-independent manner (Luger et al., 1997), the genomic DNA sequence harbors.

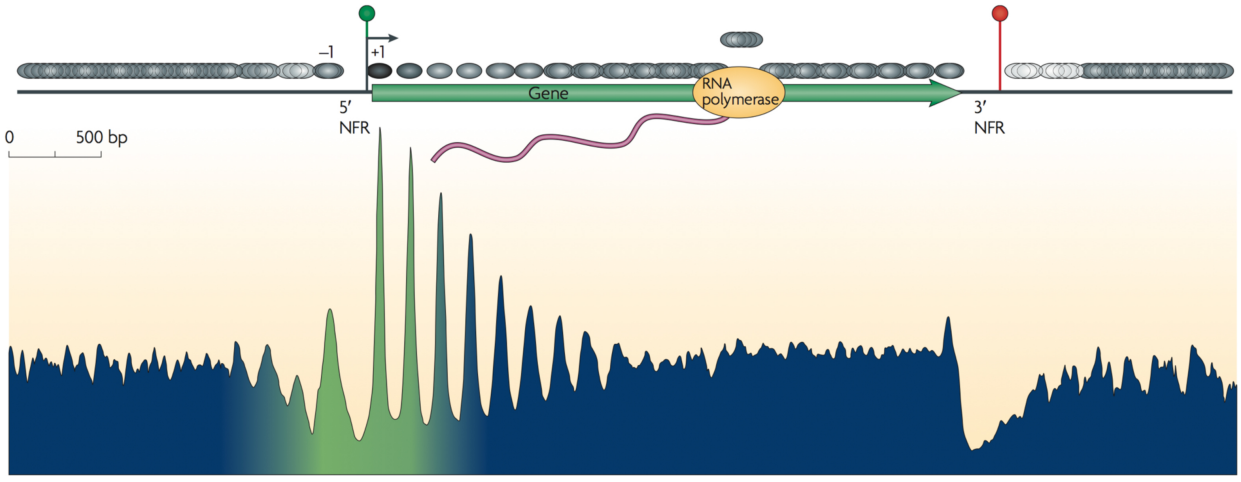

Figure 1. 5 – Stereotypical chromatin structure across a eukaryotic gene. (Top) Schematic depiction of consensus nucleosome distribution across a yeast gene. All genes are aligned by the transcription start sites (green circle) and termination sites (red circle). Nucleosomes are shown as grey ovals. The transcribed region is shown as a green arrow. The direction of transcription is shown. Nucleosomes flanking the nucleosome-free region (NFR) are called -1 and +1. **(Bottom)** Plot representing relative levels of H2A.Z, histone acetylation, H3K4 methylation and nucleosome phasing, or positional stability, at corresponding sites across the gene. Green shading indicates regions enriched for these features. Adapted from Mavrich *et al.* (Mavrich et al., 2008a) and Jiang and Pugh (Jiang and Pugh, 2009).

information that dictates nucleosome occlusion at specific regions. Interestingly, modifications to the ChIP protocol that allowed preservation of more labile nucleosomes led to the discovery

that particularly unstable nucleosomes are present at promoters (Jin et al., 2009). They contain both histone variants H2A.Z and H3.3. Thus, the NFRs should be more accurately referred to as nucleosome-depleted regions (NDRs).

Nucleosomes flanking the NDRs carry a unique set of features. First, they are the most phased, or positionally stable, nucleosomes across the gene (Figure 1.5) (Mavrich et al., 2008a). Gene-body nucleosomes are significantly less phased, or "fuzzy," as the histone octamers can adopt multiple rotational positions on an extended stretch of DNA (Figure 1.5) (Albert et al., 2007). The phasing property of promoter-proximal nucleosomes may result from the DNA sequence preventing promiscuous positioning of the octamer. Furthermore, factors that bind promoters may also block this from happening. As a result, these highly phased nucleosomes have been proposed to serve as initial barriers that promote statistical positioning, which occurs with a probability that decreases with increasing distance from the promoter, of downstream nucleosomes (Mavrich et al., 2008a). However, positional stability is separate from physical stability, as highly phased promoter-proximal nucleosomes are subjected to high turnover, especially at active genes (Dion et al., 2007).

Promoter nucleosomes are also compositionally unique. They are enriched in histone acetylation and the active-chromatin mark H3 lysine 4 trimethylation (H3K4-me3) (Figure 1.5) (Jiang et al., 2010; Narlikar et al., 2013). The presence of these PTMs suggest that these nucleosomes are physically unstable and may facilitate their high turnover (Dion et al., 2007), which is important for transcriptional activity. In addition, the histone variant H2A.Z is also highly enriched in promoter-proximal nucleosomes (Zhang et al., 2005). This is in marked contrast to another transcription-related variant, H3.3, which is more abundant in gene bodies and around termination sites (Stroud et al., 2012). Unlike the PTMs, it is not yet clear how the

presence of H2A.Z affects the stability of the host nucleosome (Bönisch and Hake, 2012). First of all, H2A.Z is found around promoters of both active and inactive genes in yeast (Raisner et al., 2005). Thus, it correlates poorly with transcriptional activity. It is then proposed that H2A.Z

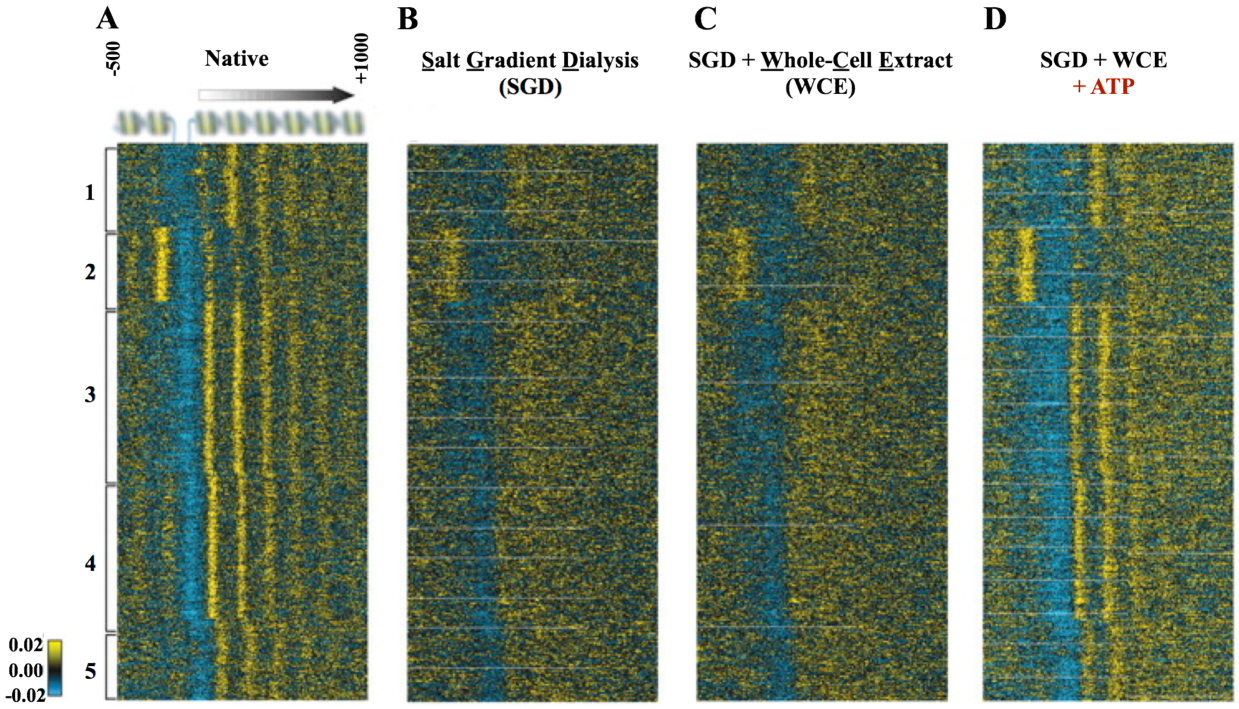

Figure 1.6 – Establishment of promoter chromatin structure is an ATP-dependent process. **(A)** Relative histone occupancy levels measured by ChIP for *Saccharomyces cerevisiae* are indicated for a 1,500 basepair region spanning the promoter (-500 and +1,000 basepairs from the transcription start sites—TSS). All yeast genes are aligned by their TSSs and are divided into 5 groups with unique promoter chromatin features. **(B)** A similar analysis was done for chromatin reconstituted *in vitro* using purified genomic DNA and histones *via* the salt-gradient dialysis (SGD) technique (Dyer et al., 2004). **(C)** Whole-cell extract was added to the *in vitro* chromatin reconstitution reaction. **(D)** ATP was included in the SGD + WCE reaction. Adapted from Zhang *et al.* (Zhang et al., 2011).

serves to poise genes for subsequent activation through facilitating histone loss (Zhang et al., 2005). However, *in vitro* stability assessment of H2A.Z-containing nucleosomes gave conflicting results (Fan et al., 2002; Guillemette and Gaudreau, 2006; Park et al., 2004; Suto et al., 2000). One study on the effect of H2A.Z on *in vitro* transcription through a nucleosome

reported that the variant renders its host nucleosome refractive to transcription (Thakar et al., 2010). The complete story on H2A.Z function must then involve the role of post-deposition modifications of the variant (Halley et al., 2010; Ishibashi et al., 2009; Mehta et al., 2010; Valdés-Mora et al., 2012) as well as H2A.Z-dependent recruitment of various factors (Draker et al., 2012; Santisteban et al., 2011).

What are the factors involved in the establishment and maintenance of promoter chromatin? A ChIP-based study by Zhang and colleagues highlighted several important features of chromatin assembly *in vivo* (Zhang et al., 2011). The authors analyzed chromatin organization around promoters of all genes in *Saccharomyes cerevisiae* and observed the expected phased nucleosomes flanking NDRs (Figure 1.6A). They then compared results from native chromatin to those from chromatin reconstituted *in vitro* using purified genomic DNA and histones (Figure 1.6B). The latter sample exhibited general histone depletion at promoters, further demonstrating that site-specific nucleosome occlusion is encoded by the DNA sequence. However, *in vitro* generated chromatin lacks phased promoter-proximal nucleosomes (Figure 1.6B). Addition of whole-cell extract (WCE) to the reconstitution reaction failed to generate this feature of native chromatin (Figure 1.6C)—a surprising result suggesting that factors involved in chromatin assembly at promoters are not active in the *in vitro* setup. However, upon addition of the nucleoside triphosphate (NTP) ATP, phased nucleosomes similar to those observed for native chromatin were generated (Figure 1.6D). Since other NTPs were removed from the WCE *via* dialysis, active transcription, which has been implicated in maintaining promoter chromatin (Struhl and Segal, 2013), was not involved. Therefore, establishment of promoter chromatin structure is tasked to dedicated ATP-dependent factors.

ATP-DEPENDENT CHROMATIN REMODELERS

In 1994, three research groups discovered and purified from *Saccharomyces cerevisiae* a multi-subunit complex containing products from genes defective in mating-type switching (*swi*) and sucrose non-fermenting (*snf*) mutants (Cairns et al., 1994; Côté et al., 1994; Peterson et al., 1994). The complex was subsequently named SWI/SNF. A robust DNA-dependent ATPase, called Snf2, was identified as the catalytic component of the complex (Cairns et al., 1994). SWI/SNF was shown to interact with the nucleosome and promote, in an ATP-dependent manner, binding of the transcription activator GAL4 to chromatin (Côté et al., 1994). Two years later, a related and more abundant complex was purified from yeast and named RSC (Remodel the Structure of Chromatin) (Cairns et al., 1996). This 15 subunit complex harbors the catalytic subunit Sth1 that is highly similar to SWI/SNF's Snf2. It was shown to directly perturb nucleosome structure. SWI/SNF and RSC are the first members of a large family of ATP-dependent chromatin remodeling complexes (remodelers) identified.

Table 1.1 – Compositions and homologues of known remodeling complexes. Adapted from Clapier and Cairns (Clapier and Cairns, 2009).

Family and composition		Organisms								
		Yeast			Fly			Human		
SWI/SNF	Complex	SWI/SNF		RSC	BAP		PBAP	BAF		PBAF
	ATPase	Swi2/Snf2		Sth1	BRM/Brahma			hBRM or BRG1		BRG1
	Noncatalytic homologous subunits	Swi1/Adr6			OSA/eyelid			BAF250/hOSA1		
							Polybromo BAP170			BAF180 BAF200
		Swi3		Rsc8/Swh3	MOR/BAP155			BAF155, BAF170		
		Swp73		Rsc6	BAP60			BAF60a or b or c		
		Snf5		Sfh1	SNR1/BAP45			hSNF5/BAF47/INI1		
					BAP111/dalao			BAF57		
		Arp7, Arp9			BAP55 or BAP47			BAF53a or b		
					Actin			β-actin		
	Unique									
ISWI	Complex	ISW1a	ISW1b	ISW2	NURF	CHRAC	ACF	NURF	CHRAC	ACF
	ATPase	Isw1		Isw2	ISWI			SNF2L	SNF2H	
	Noncatalytic homologous subunits			Itc1	NURF301	ACF1		BPTF	hACF1/WCRF180	
						CHRAC14			hCHRAC17	
						CHRAC16			hCHRAC15	
					NURF55/p55			RbAp46 or 48		
	Unique	Ioc3	Ioc2, Ioc4		NURF38					
CHD	Complex	CHD1			CHD1	Mi-2/NuRD		CHD1	NuRD	
	ATPase	Chd1			dCHD1	dMi-2		CHD1	Mi-2α/CHD3, Mi-2β/CHD4	
	Noncatalytic homologous subunits					dMBD2/3			MBD3	
						dMTA			MTA1,2,3	
						dRPD3			HDAC1,2	
						p55			RbAp46 or 48	
						p66/68			p66α,β	
	Unique								DOC-1	
INO80	Complex	INO80		SWR1	Pho-dINO80	Tip60		INO80	SRCAP	TRRAP/Tip60
	ATPase	Ino80		Swr1	dIno80	Domino		hIno80	SRCAP	p400
	Noncatalytic homologous subunits	Rvb1,2			Reptin, Pontin			RUVBL1,2/Tip49a,b		
		Arp5,8		Arp6	dArp5,8	BAP55		BAF53a		
		Arp4, Actin1			dActin1	Actin87E		Arp5,8	Arp6	Actin
		Taf14		Yaf9		dGAS41			GAS41	
		Ies2,6						hIes2,6		
				Swc4/Eaf2		dDMAP1			DMAP1	
				Swc2/Vps72		dYL-1			YL-1	
				Bdf1		dBrd8				Brd8/TRC/p120
				H2AZ,H2B		H2Av,H2B			H2AZ,H2B	
				Swc6/Vps71					ZnF-HIT1	
						dTra1				TRRAP
						dTip60				Tip60
						dMRG15				MRG15 MRGX
						dEaf6				FLJ11730
						dMRGBP				MRGBP
						E(Pc)				EPC1, EPC-like
						dING3				ING3
	Unique	Ies1,Ies3-5,Nhp10		Swc3,5,7	Pho					

Remodelers are evolutionarily conserved multi-subunit complexes that can directly alter nucleosomal position and composition (Clapier and Cairns, 2009). To date, several dozens of remodelers have been identified in all organisms (Table 1.1), most of which exist as complexes containing between 2-15 subunits and all contain a Snf2-related ATPase domain—a member of the Super-Family 2 (SF2) of helicases/translocases (Byrd and Raney, 2012) (Figure 1.7 B-C)—within their core, catalytic subunits (Clapier and Cairns, 2009). In addition, remodelers also harbor domains located in *cis* to the ATPase that can regulate its activity and the coupling of ATP hydrolysis to DNA translocation (Clapier and Cairns, 2012; Hota and Bartholomew, 2011) and bind accessory subunits (Szerlong et al., 2008) and/or histone modifications (Clapier and Cairns, 2009). These auxiliary domains are the basis for the common classification of remodelers into four subfamilies: SWI/SNF, ISWI, CHD, and INO80 (Clapier and Cairns, 2009) (Figure 1.8A and Table 1.1).

The diversity of remodelers suggests that they are functionally specialized, and the presence of PTM-recognition domains may allow them to target specific nucleosomes. The most comprehensive study addressing this question was carried out by Yen and colleagues, who used ChIP to map the nucleosomal targets for various remodelers *in vivo* in yeast (Yen et al., 2012). To do this, the authors crosslinked the nuclear material, obtained mononucleosomes by MNase digestion and immuno-precipitated the sample using antibodies against specific subunits of a select set of remodelers. Members of the SWI/SNF, ISWI, and INO80 subfamilies were included in this analysis. The results indicate that remodelers are enriched near the 5' and 3' regions of the gene, close to the NDRs (Figure 1.7) (Yen et al., 2012). Many remodelers exhibit overlapping chromatin footprints. For example, the +1 nucleosome, where the transcription start site resides, is bound by all remodelers studied, except for ISW1b (Figure 1.7A). Nucleosomes

on the opposite side of the promoter are also bound by many remodelers. RSC and INO80 bind to many nucleosomes downstream of the +1. Near the 3' end, the terminal nucleosome interacts with INO80, ISW1a and ISW2 and appear to be very well phased (Figure 1.7B). The ISW1b complex appears to interact exclusively with chromatin within the gene body.

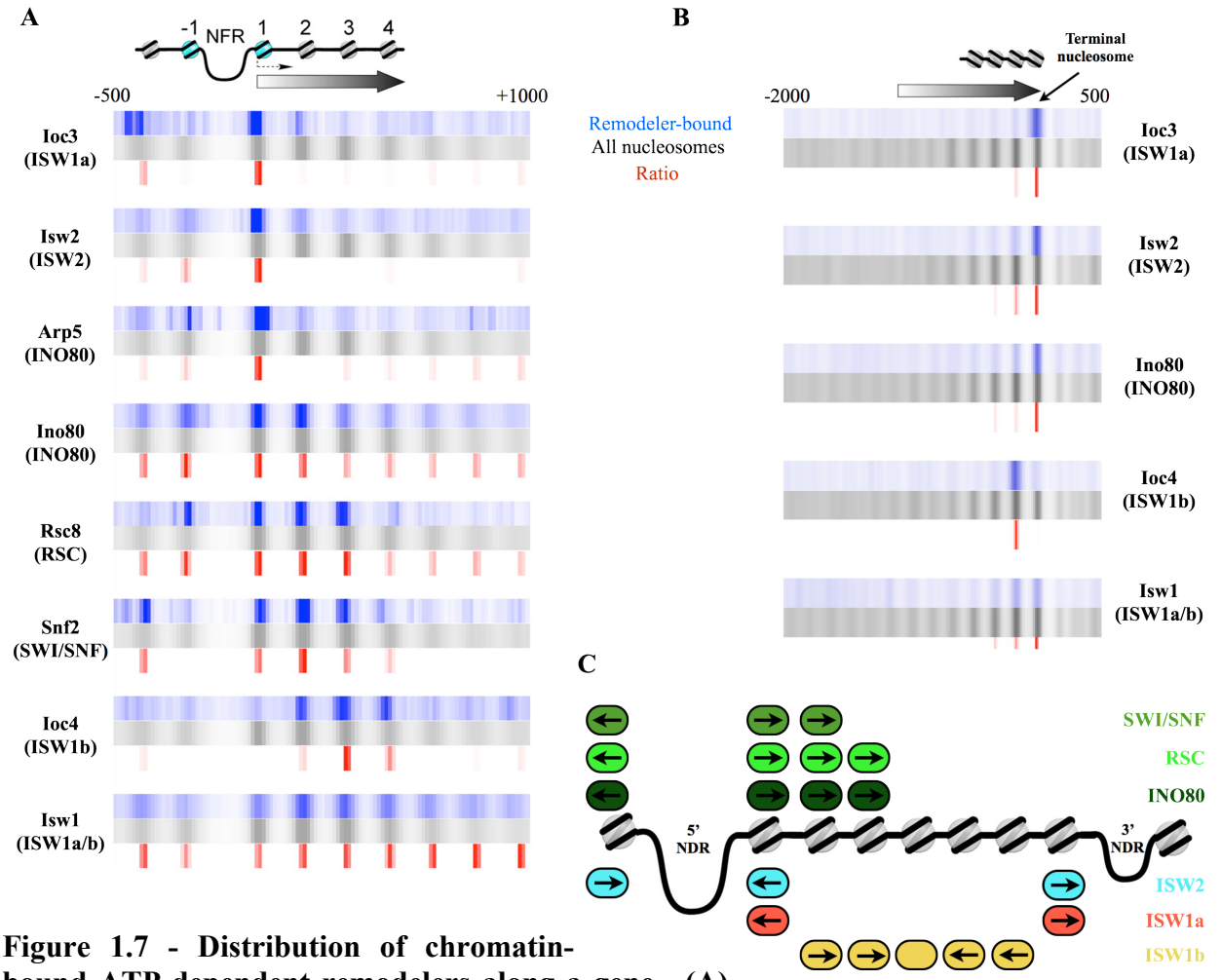

Figure 1.7 - Distribution of chromatin-bound ATP-dependent remodelers along a gene. (A) ChIP was performed to determine the target nucleosomes for select remodelers. Immuno-precipitation was carried out against specific subunits of each complex (parentheses). Regions enriched for remodeler-bound nucleosomes (blue), histones (grey), and the ratio of the two levels (red) are shown under a schematic representation of promoter chromatin spanning 1,500 basepairs. **(B)** A similar analysis as in (A) for a 2,500 basepair region spanning transcription termination sites. **(C)** Schematic representation of remodeler (colored ovals) distribution and directionality of nucleosome movement (arrows inside ovals). The names of the complexes studied are indicated on the right. Adapted from Yen *et al.* (Yen et al., 2012).

In addition, the authors also investigated the directionality of nucleosome movement by different remodelers by analyzing changes in nucleosome positions in strains lacking the activities of specific remodelers (Yen et al., 2012). The results revealed how their binding patterns allow remodelers to organize chromatin structure throughout the gene (Figure 1.7C). RSC, SWI/SNF, and INO80, which interact with nucleosomes flanking the 5' NDR, move their substrates away from the promoter and may be responsible for the maintenance of nucleosome depletion, consistent with their roles in stimulating transcription (Clapier and Cairns, 2009). ISW1a and ISW2, which are found at both ends of the gene, mobilize nucleosomes in the opposite direction—towards the NDRs. The ISW1b complex moves nucleosomes towards the middle to the gene, which results in formation of arrays of evenly spaced nucleosomes. Thus, the *in vivo* activities of ISWI remodelers are consistent with their roles in chromatin assembly and repression of transcription (Corona and Tamkun, 2004). CHD1, the only monomeric remodeler, has been shown in other studies to also function in chromatin assembly within gene bodies (Pointner et al., 2012; Zentner et al., 2013).

The Yen *et al.* study substantiated the observation that regulating promoter chromatin structure is an ATP-dependent process (Zhang et al., 2011). It demonstrated the role of ATP-dependent chromatin remodelers in mobilizing nucleosomes *in vivo*. They may influence transcription dynamics by directly regulating promoter accessibility. Their overlapping footprints do not necessarily mean that they compete for the substrates, as remodelers are targeted to unique sets of genes (Clapier and Cairns, 2009). This target specificity may rely on the accessory subunits and PTM-recognizing domains within the remodelers, and transcription factors may also recruit remodelers to specific promoters (Clapier and Cairns, 2009). Once

recruited, how remodelers perform their highly specific tasks (Figure 1.7C) is a topic of intense research.

MECHANISM(S) OF CHROMATIN REMODELING

All remodelers identified to date, with one exception, can mobilize the substrate nucleosome by repositioning, or "sliding," the histone octamer along the DNA (Mueller-Planitz et al., 2013; Narlikar et al., 2013). This is a very complex task. Firstly, the remodeler must overcome the extensive network of histone-DNA interactions (Figure 1.3 and corresponding discussion). In addition, as most remodeling reactions occur with only modest disruption to the histone octamer (Mueller-Planitz et al., 2013), the remodeler must also prevent disassembly of the octamer while the DNA is unraveled. The subsequent sliding direction is also intrinsic to each remodeler (Figure 1.7C). Remarkably, all remodeling reactions are catalyzed by a similar conserved ATPase/helicase domain, suggesting a common fundamental mechanism underlying nucleosome mobilization.

In contrast to bona-fide helicases, such as the SF1 ATPases, the remodeling ATPases, which are classified into the Swi2/Snf2 subfamily, lack the wedge domain that enables helicase, or strand-separating activity (Fairman-Williams et al., 2010). Therefore, remodelers generally do not possess helicase activity but function as DNA translocases (Saha et al., 2002). Crystal structures of the core ATPase domain have been reported for the Vasa ATPase in *D. melanogaster* (Sengoku et al., 2006), the Rad54 protein in zebrafish (Thomä et al., 2005) and *S. solfataricus* (Dürr et al., 2005), and the remodeler Chd1 from *S. cerevisiae* (Hauk et al., 2010). These structures suggest a common fold involving two RecA-like domains separated by a linker of variable lengths (Figure 1.8A-B). These domains contribute the Walker A lysine and the

arginine fingers crucial for the coordination and hydrolysis of ATP, which binds at this interface (Hauk and Bowman, 2011).

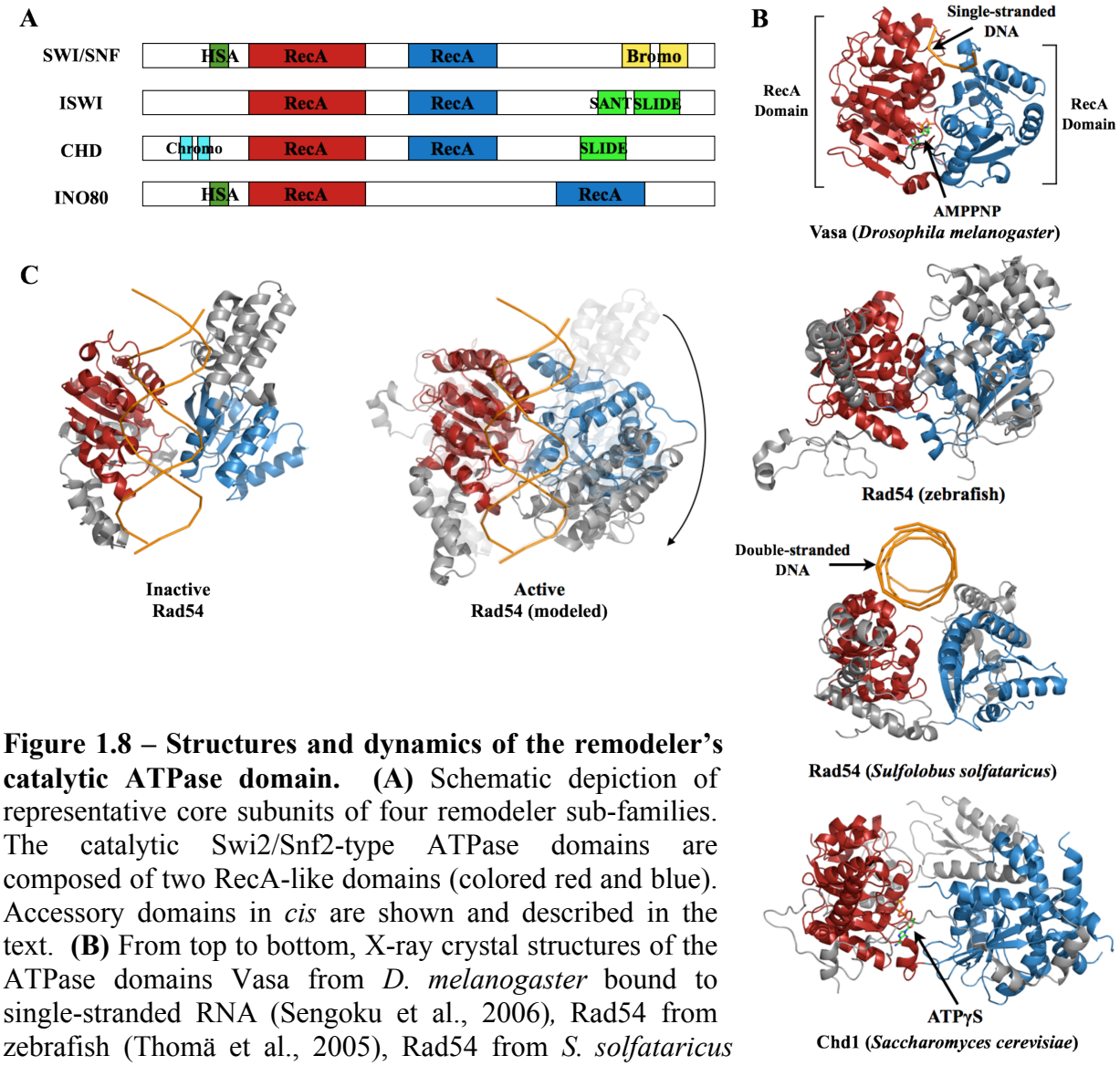

Figure 1.8 – Structures and dynamics of the remodeler's catalytic ATPase domain. **(A)** Schematic depiction of representative core subunits of four remodeler sub-families. The catalytic Swi2/Snf2-type ATPase domains are composed of two RecA-like domains (colored red and blue). Accessory domains in *cis* are shown and described in the text. **(B)** From top to bottom, X-ray crystal structures of the ATPase domains Vasa from *D. melanogaster* bound to single-stranded RNA (Sengoku et al., 2006), Rad54 from zebrafish (Thomä et al., 2005), Rad54 from *S. solfataricus* bound to double-stranded DNA (Dürr et al., 2005) and Chd1 from *S. cerevisiae* (Hauk et al., 2010). RecA-like domains are colored red and blue similar to (A). Swi2/Snf2-specific additional domains (not related to the colored domains in A) are colored grey. **(C)** The Rad54-dsDNA structure was crystallized in its inactive state (Dürr et al., 2005) (left). A rotation of the C-terminal RecA-like domain (blue) was modeled based on the active Rad54 structure (Thomä et al., 2005).

Both RecA-like domains also form the nucleic acid binding surface (Figure 1.8B) (Dürr et al., 2005; Sengoku et al., 2006). In the DNA-bound *S. solfataricus* Rad54 structure, the protein forms electrostatic interactions with the minor groove *via* the N-terminal RecA-like domain and one of the unique inserts (Dürr et al., 2005). The observation has an important implication: even though the core ATPase domain exhibits good homology among remodelers, divergent inserts within this domain may contribute to the observed functional diversity. Interestingly, in this structure, the RecA-like domains are oriented in a manner that prohibits ATP binding and hydrolysis—the two halves of the ATP binding pocket are not properly interfaced (Dürr et al., 2005). Structural modeling suggests that a significant rotation of one of the RecA-like domains is required to form this binding pocket (Figure 1.8C) and activate the enzyme. This significant conformational change has been detected *in vitro* (Lewis et al., 2008).

The core ATPase domain is anchored on the nucleosome at an internal site approximately two turns from the dyad (~SHL-2) (Dechassa et al., 2012; 2008; Gangaraju et al., 2009; Saha et al., 2005; Schwanbeck et al., 2004) (Figure 1.3 and 1.9). At this location, histone-DNA interactions energetically dip (Figure 1.4) (Hall et al., 2009), and their disruption is presumably favorable and more readily accommodated (Tan and Davey, 2011). Importantly, this interaction site brings the catalytic domain close to the main energetic barrier in the nucleosome—the dyad region (Figure 1.4) (Hall et al., 2009). Thus, it appears that remodelers have evolved to strategically recognize the most favorable nucleosomal site to initiate and propagate disruption. This is accomplished *via* ATP-dependent DNA translocation, which occurs on one strand of the DNA in a 3' to 5' direction (Saha et al., 2005; Whitehouse et al., 2003; Zofall et al., 2006). This fundamental activity has been reported for both the ISWI and RSC complexes, suggesting that it may be shared by all remodeler subfamilies.

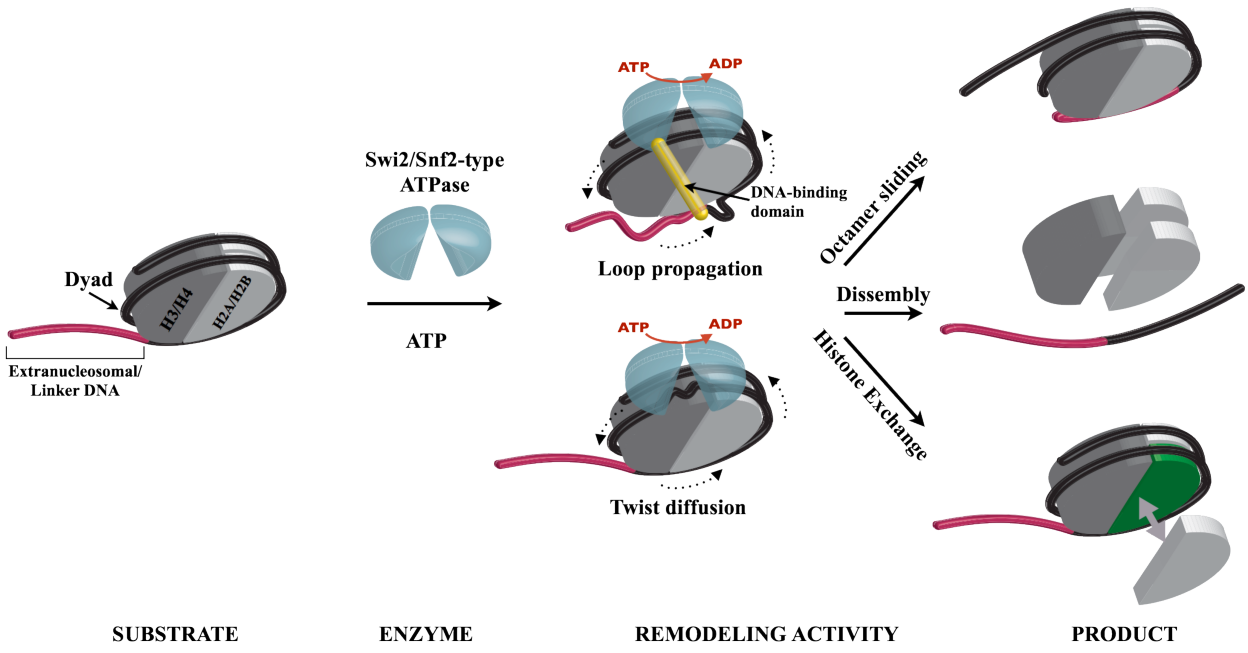

Figure 1.9 – Mechanistic models and possible outcomes of chromatin remodeling.

This strand-specific translocation by the immobilized translocase introduces torsional strain in the nucleosomal DNA (Mueller-Planitz et al., 2013). This strain arises from a twist defect in the DNA caused by "bunching" up of extra basepairs into a constrained DNA segment. It is relieved by dissociation of the DNA from the octamer. How the extra DNA is propagated past the dyad is likely to be context-specific. The octamer may be slid in single-basepair steps, as shown for the ISWI remodelers (Deindl et al., 2013). This mechanism is referred to as "twist diffusion" (Figure 1.9) (Bowman, 2010), highlighting the gradual transfer of DNA from one nucleosomal side the other. However, this mechanism may be more specific to subfamilies of smaller complexes, such as ISWI and CHD, which have been shown to remodel with minimal structural disruption to the substrate (Zofall et al., 2006). Alternatively, remodelers can pull and propagate larger segments of extranucleosomal DNA through the nucleosome in large loops, likely involving a linked DNA-binding domain/subunit and a conformational change in the

ATPase (Figure 1.8C) (Lewis et al., 2008). This is called the "loop propagation" model (Figure 1.9) (Bowman, 2010) and has been shown for SWI/SNF (Zofall et al., 2006) and RSC (Zhang et al., 2006), where loop sizes between 50 and 100 basepairs were reported. This mode of DNA transfer is more energetically costly, as many more histone-DNA interactions must be disrupted for the loop to be accommodated. Such significant disruption also requires the remodeler to ensure that the octamer remains intact if its goal is to slide the octamer.

Several studies have shown that the ATPase domains alone are capable of nucleosome mobilization (Clapier and Cairns, 2012; Mcknight et al., 2011; Mueller-Planitz et al., 2012; Saha et al., 2002). However, except for CHD1, remodelers function as assemblies of 2-15 subunits (Table 1.1) and are capable of nucleosome repositioning (sliding), assembly, disassembly, and histone exchange (Figure 1.9) (Clapier and Cairns, 2009). While all these activities must rely on disruption of histone-DNA interactions catalyzed by the core ATPase, accessory subunits may serve to fine-tune its activity and define functional specificity. Therefore, a more complete mechanistic understanding of chromatin remodeling requires studies that address how components of a remodeling machine assemble together and how the nucleosome is handled within this complex.

STRUCTURAL BIOLOGY OF REMODELING COMPLEXES

Genetics and biochemistry have uncovered the compositions of most known remodelers. Their interactions with the nucleosome have also been examined, in several cases in significant detail (Dang and Bartholomew, 2007; Dechassa et al., 2008; Gangaraju and Bartholomew, 2007; Saha et al., 2005), using nucleosome footprinting and site-specific DNA crosslinking. However, structural knowledge of how individual components assemble into a remodeling complex and spatially coordinate the substrate nucleosome is very limited. The multi-subunit compositions and relatively large sizes (200 – 1,400 kDa) of remodelers make them challenging subjects for structural studies.

Table 1.2 – Available structures of chromatin remodelers

Remodeler	Subunits MW (kDa)	Substrate	Technique	Resolution (Å)	Reference
SWI/SNF					
RSC (*S. cerevisiae*)	15; 1,300	None	NS-EM*	25	(Asturias et al., 2002)
		None	NS-EM	37	(Leschziner et al., 2007)
		None	NS-EM	40	(Skiniotis et al., 2007)
		None	Cryo-EM	25	(Chaban et al., 2008)
		Nucleosome	Cryo-EM		(Chaban et al., 2008)
SWI/SNF(*S. cerevisiae*)	11; 1,100	None	NS-EM	35-50	(Smith et al., 2003)
		None	Cryo-EM	25	(Dechassa et al., 2008)
PBAF (Human)		None	NS-EM	43-50	(Leschziner et al., 2005)
ISWI					
SFH2h (ACF) (Human)	1	Nucleosome	NS-EM	27	(Racki et al., 2009)
ISWIa (ΔATPase)	2; 100	None	X-ray	3.25	(Yamada et al., 2011)
(*S. cerevisiae*)		DNA	X-ray	3.60	
		Nucleosome	Cryo-EM	22-24	
CHD					
CHD1 (*S. cerevisiae*)	1; 80		X-ray	3.7	(Hauk et al., 2010)
INO80					
INO80 (*S. cerevisiae*)	15; 1,000	None	NS-EM	22	(Tosi et al., 2013)
			Cryo-EM	17.5	
SWR1 (*S. cerevisiae*)	14; 1,000	None	Cryo-NS-EM	28	(Nguyen et al., 2013)
		Nucleosome	Cryo-NS-EM	37	

*NS-EM: negative stain electron microscopy

Three-dimensional electron microscopy (3D EM) is the widely used technique to address the structures of remodeling complexes (Leschziner, 2011). Typically, this approach involves

obtaining electron micrographs of the purified samples in negative stain (NS). The electron-dense stain material (typically uranium) offers high signal-to-noise ratio, or contrast, in the data. However, incomplete stain absorption and structural artifacts due to dehydration limit the resolution and quality of the results. The 2D images of single protein complexes, or particles, are then computed to generate a low-resolution initial 3D model. The model is subsequently refined using either NS or cryo data, the latter are obtained for samples preserved in vitreous ice and thus are of optimal structural integrity. This technique has been utilized to obtain 3D structures of several complexes (Table 1.2 and Figure 1.10), mostly from *S. cerevisiae* due to relative ease of purifying the native samples.

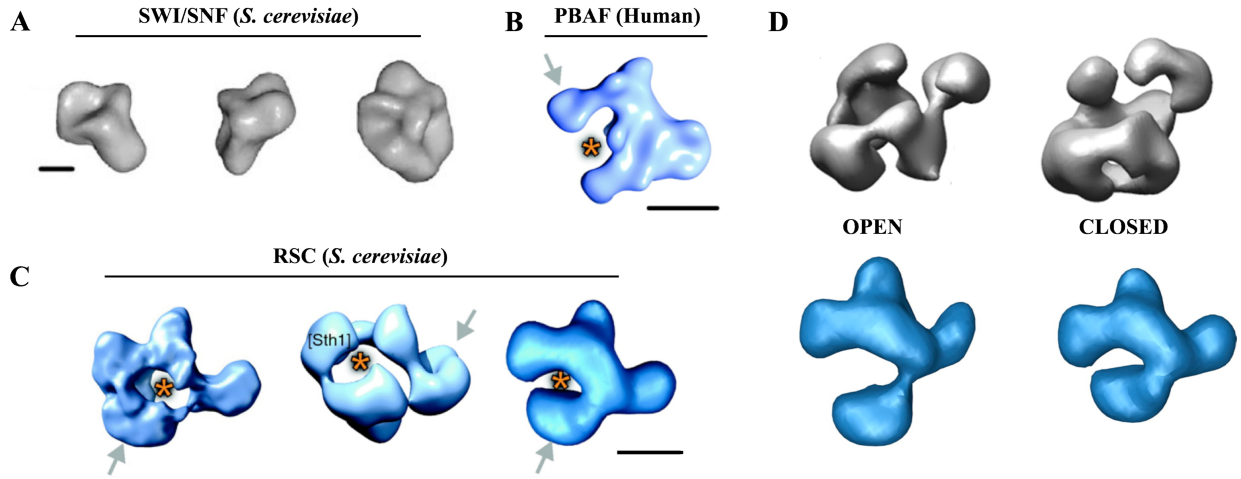

Figure 1.10 – 3D electron microscopy structures of SWI/SNF remodelers. (A) Three views of the SWI/SNF complex from *S. cerevisiae*. Adapted from Smith *et al.* (Smith et al., 2003). **(B)** 3D structure of PBAF, a SWI/SNF homologue in human (Leschziner et al., 2005). **(C)** Comparison among 3 reported structures for the RSC complex from *S. cerevisiae*. From left to right, Asturias *et al*. (Asturias et al., 2002), Leschziner *et al.* (Leschziner et al., 2007), Skiniotis *et al.* (Skiniotis et al., 2007). 3D structures were visually aligned. Arrows point to domains shown to be flexible. Asterisks mark proposed nucleosome binding cavity. All scale bars correspond to 10 nm. (B) and (C) were adapted from Leschziner (Leschziner, 2011). **(D)** Conformational flexibility reported for RSC by (top) Leschziner *et al.* (Leschziner et al., 2007) and (bottom) Skiniotis *et al.* (Skiniotis et al., 2007). Open and closed structural states are proposed.

The RSC complex, which is the most abundant and the only essential chromatin remodeler in yeast, has been structurally studied most extensively. The 3D EM structures, ranging from 25 Å to 40 Å resolution (Table 1.2), exhibit overall similarity (Figure 1.10C). These structures are significantly different from that of the SWI/SNF complex from yeast (Figure 1.10A) (Smith et al., 2003). However, the SWI/SNF homologous complex in human, PBAF, is more similar to RSC than SWI/SNF (Figure 1.10B) (Leschziner et al., 2005). According to these results, RSC, and perhaps SWI/SNF share an overall four-lobed shape with a central cavity that is proposed to serve as the nucleosome-binding site (Figure 1.10B-C). The nucleosome density can be very well accommodated in this density based on modeling (Asturias et al., 2002; Leschziner et al., 2007; Skiniotis et al., 2007). Interestingly, two conformations of the RSC complex have been reported that involve a flexible domain (Figure 1.10C-D) (Asturias et al., 2002; Leschziner et al., 2007; Skiniotis et al., 2007). These studies, however, differ in the location of this domain. It is worth noting that the three RSC structures were obtained using different computational approaches, which may have influenced differences in the results (Leschziner, 2011). However, there is an overall agreement among these studies about the shared architecture of and a potential substrate-binding mode by RSC.

Substrate-bound remodelers are much more complex samples to analyze structurally. Large remodelers, such as RSC, are inherently heterogenous (Figure 1.10D) and challenging samples to analyze. Addition of the substrate nucleosome or DNA may worsen this heterogeneity, which must now include sub-stoichiometric binding. In order for the bound nucleosome, which is ~1/5 the molecular weight of the enzyme, to be fully resolved, the complex must be very structurally stable. Efforts to obtain the RSC-nucleosome complex have been faced with this problem (Chaban et al., 2008). The reported structure included extra density in the

central cavity (Figure 1.11A); however, only a partial nucleosome, missing one H2A/H2B dimer and a portion of nucleosomal DNA, could be modeled into this density. This was surprising as the sample was imaged in the absence of ATP, and substrate disruption is unlikely to have taken place.

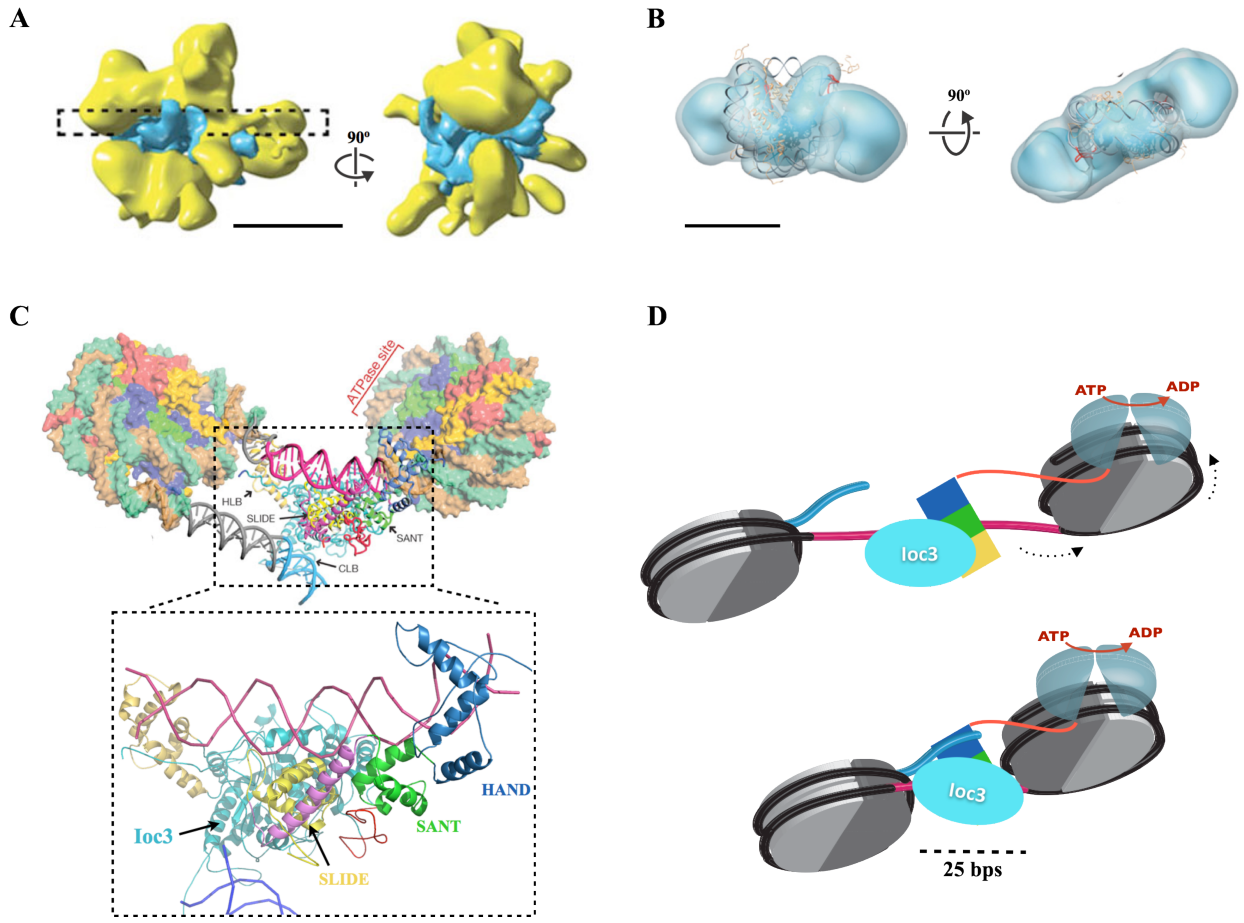

Figure 1.11 – Structural information on remodeler-nucleosome interaction. **(A)** Cryo-EM structure of the RSC-nucleosome complex. The cyan density was obtained from difference mapping between this complex and the apo-RSC complex. It is proposed to correspond to the bound nucleosome. Adapted from Chaban *et al*. (Chaban et al., 2008). **(B)** Negative-stain EM structure of the SFH2h translocase domain from the human ACF complex showing 2 units binding to one nucleosome (docked-in crystal structure). Adapted from Racki *et al*. (Racki et al., 2009). All scale bars correspond to 10 nm. **(C)** X-ray crystal structure of the yeast ISW1a complex, which includes the Ioc3 subunit and the non-translocase domains of the catalytic subunit, bound to 2 segments of double-stranded DNA (pink and blue). Top: the crystal structure is modeled into the structure of a dinucleosome array. Bottom: a close-up view of the crystallized portion. Adapted from Yamada *et al*. (Yamada et al., 2011). **(D)** Proposed mechanism for ISW1a-catalyzed nucleosome spacing according to the Yamada study.

Smaller complexes, such as those in the ISWI subfamily, are more amenable to this approach. The structure of nucleosome-bound ACF, a smaller remodeling complex in the ISWI subfamily, revealed that two remodelers bind to one nucleosome (Figure 1.11B) (Racki et al., 2009), a mechanism that may be shared by other remodelers which, like ACF, can generate arrays of evenly spaced nucleosomes. The remodeler ISW1a, which is also involved in array generation during replication, may have a different mode of measuring linker length. Yamada and colleagues crystallized the partial ISW1a complex containing the accessory subunit Ioc3 and the catalytic subunit missing the translocase domain (Figure 1.11C) (Yamada et al., 2011). Results from this study suggested a mechanism by which the HAND-SANT-SLIDE domains in *cis* to the translocase, together with the Ioc3 subunit, interact with linker DNA and serve as a "ruler" for linker length (Figure 1.11D). The nucleosome bound by the translocase is repositioned until it is 25 basepairs away from a neighboring nucleosome. In this case, accessory non-catalytic domains and subunits play an essential role in modulating the activity of the translocase. Again, this highlights the importance of investigating remodeling activities in the context of fully assembled complexes.

This thesis work focuses on the structural characterization of the ATP-dependent chromatin remodeling complex SWR1 from *S. cerevisiae*. This compositionally and functionally unique remodeler catalyzes the exchange of an H2A.Z/H2B dimer for the canonical H2A/H2B at nucleosomes flanking the NDRs (Kobor et al., 2004; Krogan et al., 2003; Mizuguchi et al., 2004). Therefore, it is responsible for the conserved localization of the important histone variant H2A.Z across the chromatin. SWR1 thus offers an excellent opportunity to address the structural and functional divergence among remodelers. We have obtained a 3D-EM structure of the complex, mapped the locations of its major functional modules, and showed a remarkably

modular assembly. These results will be the topic of Chapter 2. In addition, we also reconstructed the 3D structure of a SWR1-nucleosome complex and observed a significant conformational change. This structure will be discussed in Chapter 3, along with current progress on determining substrate-induced dynamics of SWR1.

REFERENCES

Albert, I., Mavrich, T.N., Tomsho, L.P., Qi, J., Zanton, S.J., Schuster, S.C., and Pugh, B.F. (2007). Translational and rotational settings of H2A.Z nucleosomes across the Saccharomyces cerevisiae genome. Nature *446*, 572–576.

ALLFREY, V.G., FAULKNER, R., and MIRSKY, A.E. (1964). ACETYLATION AND METHYLATION OF HISTONES AND THEIR POSSIBLE ROLE IN THE REGULATION OF RNA SYNTHESIS. Proc Natl Acad Sci USA *51*, 786–794.

Ammar, R., Torti, D., Tsui, K., Gebbia, M., Durbic, T., Bader, G.D., Giaever, G., and Nislow, C. (2012). Chromatin is an ancient innovation conserved between Archaea and Eukarya. Elife *1*, e00078.

Andrews, A.J., and Luger, K. (2011). Nucleosome structure(s) and stability: variations on a theme. Annual Review of Biophysics *40*, 99–117.

Asturias, F.J., Chung, W.-H., Kornberg, R.D., and Lorch, Y. (2002). Structural analysis of the RSC chromatin-remodeling complex. Proc Natl Acad Sci USA *99*, 13477–13480.

Banaszynski, L.A., Wen, D., Dewell, S., Whitcomb, S.J., Lin, M., Diaz, N., Elsässer, S.J., Chapgier, A., Goldberg, A.D., Canaani, E., et al. (2013). Hira-Dependent Histone H3.3 Deposition Facilitates PRC2 Recruitment at Developmental Loci in ES Cells. Cell *155*, 107–120.

Bannister, A.J., and Kouzarides, T. (2011). Regulation of chromatin by histone modifications. Cell Research *21*, 381–395.

Barnhart, M.C., Kuich, P.H.J.L., Stellfox, M.E., Ward, J.A., Bassett, E.A., Black, B.E., and Foltz, D.R. (2011). HJURP is a CENP-A chromatin assembly factor sufficient to form a functional de novo kinetochore. The Journal of Cell Biology *194*, 229–243.

Bassing, C.H., Chua, K.F., Sekiguchi, J., Suh, H., Whitlow, S.R., Fleming, J.C., Monroe, B.C., Ciccone, D.N., Yan, C., Vlasakova, K., et al. (2002). Increased ionizing radiation sensitivity and genomic instability in the absence of histone H2AX. Proc Natl Acad Sci USA *99*, 8173–8178.

Battistini, F., Hunter, C.A., Moore, I.K., and Widom, J. (2012). Structure-based identification of new high-affinity nucleosome binding sequences. Journal of Molecular Biology *420*, 8–16.

Birch, J.L., Tan, B.C.-M., Panov, K.I., Panova, T.B., Andersen, J.S., Owen-Hughes, T.A., Russell, J., Lee, S.-C., and Zomerdijk, J.C.B.M. (2009). FACT facilitates chromatin transcription by RNA polymerases I and III. Embo J *28*, 854–865.

Bowman, G.D. (2010). Mechanisms of ATP-dependent nucleosome sliding. Current Opinion in Structural Biology *20*, 73–81.

Böhm, V., Hieb, A.R., Andrews, A.J., Gansen, A., Rocker, A., Tóth, K., Luger, K., and Langowski, J. (2010). Nucleosome accessibility governed by the dimer/tetramer interface. Nucleic Acids Research.

Bönisch, C., and Hake, S.B. (2012). Histone H2A variants in nucleosomes and chromatin: more or less stable? Journal of Biological Chemistry.

Buning, R., and van Noort, J. (2010). Single- pair FRET experiments on nucleosome conformational dynamics. Biochimie.

Burgess, R.J., and Zhang, Z. (2013). Histone chaperones in nucleosome assembly and human disease. Nature Structural & Molecular Biology *20*, 14–22.

Byrd, A.K., and Raney, K.D. (2012). Superfamily 2 helicases. Front Biosci *17*, 2070–2088.

Cairns, B.R., Kim, Y.J., Sayre, M.H., Laurent, B.C., and Kornberg, R.D. (1994). A multisubunit complex containing the SWI1/ADR6, SWI2/SNF2, SWI3, SNF5, and SNF6 gene products isolated from yeast. Proc Natl Acad Sci USA *91*, 1950–1954.

Cairns, B.R., Lorch, Y., Li, Y., Zhang, M., Lacomis, L., Erdjument-Bromage, H., Tempst, P., Du, J., Laurent, B., and Kornberg, R.D. (1996). RSC, an essential, abundant chromatin-remodeling complex. Cell *87*, 1249–1260.

Carter, G.J., and van Holde, K. (1998). Self-association of linker histone H5 and of its globular domain: evidence for specific self-contacts. Biochemistry *37*, 12477–12488.

Chaban, Y., Ezeokonkwo, C., Chung, W.-H., Zhang, F., Kornberg, R.D., Maier-Davis, B., Lorch, Y., and Asturias, F.J. (2008). Structure of a RSC-nucleosome complex and insights into chromatin remodeling. Nature Structural & Molecular Biology *15*, 1272–1277.

Clapier, C.R., and Cairns, B.R. (2009). The biology of chromatin remodeling complexes. Annu Rev Biochem *78*, 273–304.

Clapier, C.R., and Cairns, B.R. (2012). Regulation of ISWI involves inhibitory modules antagonized by nucleosomal epitopes. Nature.

Clapier, C.R., Chakravarthy, S., Petosa, C., Fernández-Tornero, C., Luger, K., and Müller, C.W. (2008). Structure of the Drosophila nucleosome core particle highlights evolutionary constraints on the H2A-H2B histone dimer. Proteins *71*, 1–7.

Corona, D.F.V., and Tamkun, J.W. (2004). Multiple roles for ISWI in transcription, chromosome organization and DNA replication. Biochimica Et Biophysica Acta *1677*, 113–119.

Côté, J., Quinn, J., Workman, J.L., and Peterson, C.L. (1994). Stimulation of GAL4 derivative binding to nucleosomal DNA by the yeast SWI/SNF complex. Science *265*, 53–60.

Dang, W., and Bartholomew, B. (2007). Domain architecture of the catalytic subunit in the ISW2-nucleosome complex. Molecular and Cellular Biology *27*, 8306–8317.

Davey, C.A., Sargent, D.F., Luger, K., Maeder, A.W., and Richmond, T.J. (2002). Solvent mediated interactions in the structure of the nucleosome core particle at 1.9 a resolution. Journal of Molecular Biology *319*, 1097–1113.

Dechassa, M.L., Hota, S.K., Sen, P., Chatterjee, N., Prasad, P., and Bartholomew, B. (2012). Disparity in the DNA translocase domains of SWI/SNF and ISW2. Nucleic Acids Research.

Dechassa, M.L., Zhang, B., Horowitz-Scherer, R., Persinger, J., Woodcock, C.L., Peterson, C.L., and Bartholomew, B. (2008). Architecture of the SWI/SNF-nucleosome complex. Molecular and Cellular Biology *28*, 6010–6021.

Deindl, S., Hwang, W.L., Hota, S.K., Blosser, T.R., Prasad, P., Bartholomew, B., and Zhuang, X. (2013). ISWI Remodelers Slide Nucleosomes with Coordinated Multi-Base-Pair Entry Steps and Single-Base-Pair Exit Steps. Cell *152*, 442–452.

Dekker, J., and Mirny, L. (2013). Biological techniques: Chromosomes captured one by one. Nature.

Dekker, J., Rippe, K., Dekker, M., and Kleckner, N. (2002). Capturing chromosome conformation. Science *295*, 1306–1311.

Dion, M.F., Kaplan, T., Kim, M., Buratowski, S., Friedman, N., and Rando, O.J. (2007). Dynamics of replication-independent histone turnover in budding yeast. Science *315*, 1405–1408.

Dixon, J.R., Selvaraj, S., Yue, F., Kim, A., Li, Y., Shen, Y., Hu, M., Liu, J.S., and Ren, B. (2012). Topological domains in mammalian genomes identified by analysis of chromatin interactions. Nature *485*, 376–380.

Draker, R., Ng, M.K., Sarcinella, E., Ignatchenko, V., Kislinger, T., and Cheung, P. (2012). A Combination of H2A.Z and H4 Acetylation Recruits Brd2 to Chromatin during Transcriptional Activation. PLoS Genet *8*, e1003047.

Dürr, H., Körner, C., Müller, M., Hickmann, V., and Hopfner, K.-P. (2005). X-ray structures of the Sulfolobus solfataricus SWI2/SNF2 ATPase core and its complex with DNA. Cell *121*, 363–373.

Dyer, P.N., Edayathumangalam, R.S., White, C.L., Bao, Y., Chakravarthy, S., Muthurajan, U.M., and Luger, K. (2004). Reconstitution of nucleosome core particles from recombinant histones and DNA. Meth Enzymol *375*, 23–44.

Eaton, M.L., Galani, K., Kang, S., Bell, S.P., and MacAlpine, D.M. (2010). Conserved nucleosome positioning defines replication origins. Genes & Development *24*, 748–753.

Fairman-Williams, M.E., Guenther, U.-P., and Jankowsky, E. (2010). SF1 and SF2 helicases: family matters. Current Opinion in Structural Biology *20*, 313–324.

Fan, J.Y., Gordon, F., Luger, K., Hansen, J.C., and Tremethick, D.J. (2002). The essential histone variant H2A.Z regulates the equilibrium between different chromatin conformational states. Nat Struct Biol *9*, 172–176.

Fussner, E., Strauss, M., Djuric, U., Li, R., Ahmed, K., Hart, M., Ellis, J., and Bazett-Jones, D.P.

(2012). Open and closed domains in the mouse genome are configured as 10-nm chromatin fibres. EMBO Rep *13*, 992–996.

Gangaraju, V.K., and Bartholomew, B. (2007). Dependency of ISW1a Chromatin Remodeling on Extranucleosomal DNA. Molecular and Cellular Biology *27*, 3217–3225.

Gangaraju, V.K., Prasad, P., Srour, A., Kagalwala, M.N., and Bartholomew, B. (2009). Conformational changes associated with template commitment in ATP-dependent chromatin remodeling by ISW2. Molecular Cell *35*, 58–69.

Ghirlando, R., and Felsenfeld, G. (2013). Chromatin structure outside and inside the nucleus. Biopolymers *99*, 225–232.

Givens, R.M., Lai, W.K.M., Rizzo, J.M., Bard, J.E., Mieczkowski, P.A., Leatherwood, J., Huberman, J.A., and Buck, M.J. (2012). Chromatin architectures at fission yeast transcriptional promoters and replication origins. Nucleic Acids Research.

Guillemette, B., and Gaudreau, L. (2006). Reuniting the contrasting functions of H2A.Z. Biochem Cell Biol *84*, 528–535.

Guse, A., Carroll, C.W., Ben Moree, Fuller, C.J., and Straight, A.F. (2011). In vitro centromere and kinetochore assembly on defined chromatin templates. Nature *477*, 354–358.

Hall, M.A., Shundrovsky, A., Bai, L., Fulbright, R.M., Lis, J.T., and Wang, M.D. (2009). High-resolution dynamic mapping of histone-DNA interactions in a nucleosome. Nature Structural & Molecular Biology *16*, 124–129.

Halley, J.E., Kaplan, T., Wang, A.Y., Kobor, M.S., and Rine, J. (2010). Roles for H2A.Z and Its Acetylation in GAL1 Transcription and Gene Induction, but Not GAL1-Transcriptional Memory. PLoS Biol *8*, e1000401.

Hansen, J.C., and Turgeon, C.L. (1999). Analytical ultracentrifugation of chromatin. Methods Mol Biol *119*, 127–141.

Hasson, D., Panchenko, T., Salimian, K.J., Salman, M.U., Sekulic, N., Alonso, A., Warburton, P.E., and Black, B.E. (2013). The octamer is the major form of CENP-A nucleosomes at human centromeres. Nature Structural & Molecular Biology.

Hauk, G., and Bowman, G.D. (2011). Structural insights into regulation and action of SWI2/SNF2 ATPases. Current Opinion in Structural Biology *21*, 719–727.

Hauk, G., Mcknight, J.N., Nodelman, I.M., and Bowman, G.D. (2010). The chromodomains of the Chd1 chromatin remodeler regulate DNA access to the ATPase motor. Molecular Cell *39*, 711–723.

Henikoff, S., and Shilatifard, A. (2011). Histone modification: cause or cog? Trends Genet.

Hota, S.K., and Bartholomew, B. (2011). Diversity of operation in ATP-dependent chromatin

remodelers. Biochimica Et Biophysica Acta *1809*, 476–487.

Ishibashi, T., Dryhurst, D., Rose, K.L., Shabanowitz, J., Hunt, D.F., and Ausió, J. (2009). Acetylation of vertebrate H2A.Z and its effect on the structure of the nucleosome. Biochemistry *48*, 5007–5017.

Jiang, C., and Pugh, B.F. (2009). Nucleosome positioning and gene regulation: advances through genomics. Nat Rev Genet *10*, 161–172.

Jiang, Y., Wang, X., Bao, S., Guo, R., Johnson, D.G., Shen, X., and Li, L. (2010). INO80 chromatin remodeling complex promotes the removal of UV lesions by the nucleotide excision repair pathway. Proc Natl Acad Sci USA.

Jin, C., Zang, C., Wei, G., Cui, K., Peng, W., Zhao, K., and Felsenfeld, G. (2009). H3.3/H2A.Z double variant–containing nucleosomes mark "nucleosome-free regions" of active promoters and other regulatory regions. Nature Publishing Group *41*, 941–945.

Joti, Y., Hikima, T., Nishino, Y., Kamada, F., Hihara, S., Takata, H., Ishikawa, T., and Maeshima, K. (2012). Chromosomes without a 30-nm chromatin fiber. Nucleus (Austin, Tex) *3*, 404–410.

Kaplan, N., Moore, I.K., Fondufe-Mittendorf, Y., Gossett, A.J., Tillo, D., Field, Y., Hughes, T.R., Lieb, J.D., Widom, J., and Segal, E. (2010). Nucleosome sequence preferences influence in vivo nucleosome organization. Nature Structural & Molecular Biology *17*, 918–920.

Kaplan, N., Moore, I.K., Fondufe-Mittendorf, Y., Gossett, A.J., Tillo, D., Field, Y., Leproust, E.M., Hughes, T.R., Lieb, J.D., Widom, J., et al. (2009). The DNA-encoded nucleosome organization of a eukaryotic genome. Nature *458*, 362–366.

Kobor, M.S., Venkatasubrahmanyam, S., Meneghini, M.D., Gin, J.W., Jennings, J.L., Link, A.J., Madhani, H.D., and Rine, J. (2004). A protein complex containing the conserved Swi2/Snf2-related ATPase Swr1p deposits histone variant H2A.Z into euchromatin. PLoS Biol *2*, E131.

Koopmans, W.J.A., Buning, R., Schmidt, T., and van Noort, J. (2009). spFRET using alternating excitation and FCS reveals progressive DNA unwrapping in nucleosomes. Biophysical Journal *97*, 195–204.

Krogan, N.J., Keogh, M.C., Datta, N., Sawa, C., Ryan, O.W., Ding, H., Haw, R.A., Pootoolal, J., Tong, A., Canadien, V., et al. (2003). A Snf2 family ATPase complex required for recruitment of the histone H2A variant Htz1. Molecular Cell *12*, 1565–1576.

Lee, T.I., and Young, R.A. (2013). Transcriptional regulation and its misregulation in disease. Cell *152*, 1237–1251.

Leschziner, A.E. (2011). Electron microscopy studies of nucleosome remodelers. Current Opinion in Structural Biology.

Leschziner, A.E., Lemon, B., Tjian, R., and Nogales, E. (2005). Structural studies of the human

PBAF chromatin-remodeling complex. Structure *13*, 267–275.

Leschziner, A.E., Saha, A., Wittmeyer, J., Zhang, Y., Bustamante, C., Cairns, B.R., and Nogales, E. (2007). Conformational flexibility in the chromatin remodeler RSC observed by electron microscopy and the orthogonal tilt reconstruction method. Proc Natl Acad Sci USA *104*, 4913–4918.

Lewis, P.W., Elsaesser, S.J., Noh, K.-M., Stadler, S.C., and Allis, C.D. (2010). Daxx is an H3.3-specific histone chaperone and cooperates with ATRX in replication-independent chromatin assembly at telomeres. Proc Natl Acad Sci USA.

Lewis, R., Dürr, H., Hopfner, K.-P., and Michaelis, J. (2008). Conformational changes of a Swi2/Snf2 ATPase during its mechano-chemical cycle. Nucleic Acids Research *36*, 1881–1890.

Li, G., and Widom, J. (2004). Nucleosomes facilitate their own invasion. Nature Structural & Molecular Biology *11*, 763–769.

Luger, K., Mäder, A.W., Richmond, R.K., Sargent, D.F., and Richmond, T.J. (1997). Crystal structure of the nucleosome core particle at 2.8 A resolution. Nature *389*, 251–260.

Mavrich, T.N., Ioshikhes, I.P., Venters, B.J., Jiang, C., Tomsho, L.P., Qi, J., Schuster, S.C., Albert, I., and Pugh, B.F. (2008a). A barrier nucleosome model for statistical positioning of nucleosomes throughout the yeast genome. Genome Research *18*, 1073–1083.

Mavrich, T.N., Jiang, C., Ioshikhes, I.P., Li, X., Venters, B.J., Zanton, S.J., Tomsho, L.P., Qi, J., Glaser, R.L., Schuster, S.C., et al. (2008b). Nucleosome organization in the Drosophila genome. Nature *453*, 358–362.

Mcknight, J.N., Jenkins, K.R., Nodelman, I.M., Escobar, T., and Bowman, G.D. (2011). Extranucleosomal DNA Binding Directs Nucleosome Sliding By Chd1. Molecular and Cellular Biology.

Mehta, M., Braberg, H., Wang, S., Lozsa, A., Shales, M., Solache, A., Krogan, N.J., and Keogh, M.C. (2010). Individual lysine acetylations on the N-terminus of S. Cerevisiae H2A.Z are highly but not differentially regulated. J Biol Chem.

Mendiburo, M.J., Padeken, J., Fülöp, S., Schepers, A., and Heun, P. (2011). Drosophila CENH3 is sufficient for centromere formation. Science *334*, 686–690.

Meyer, B., Voss, K.-O., Tobias, F., Jakob, B., Durante, M., and Taucher-Scholz, G. (2013). Clustered DNA damage induces pan-nuclear H2AX phosphorylation mediated by ATM and DNA-PK. Nucleic Acids Research *41*, 6109–6118.

Mizuguchi, G., Shen, X., Landry, J., Wu, W.-H., Sen, S., and Wu, C. (2004). ATP-driven exchange of histone H2AZ variant catalyzed by SWR1 chromatin remodeling complex. Science *303*, 343–348.

Mueller-Planitz, F., Klinker, H., and Becker, P.B. (2013). Nucleosome sliding mechanisms: new

twists in a looped history. Nature Structural & Molecular Biology *20*, 1026–1032.

Mueller-Planitz, F., Klinker, H., Ludwigsen, J., and Becker, P.B. (2012). The ATPase domain of ISWI is an autonomous nucleosome remodeling machine. Nature Structural & Molecular Biology.

Nagano, T., Lubling, Y., Stevens, T.J., Schoenfelder, S., Yaffe, E., Dean, W., Laue, E.D., Tanay, A., and Fraser, P. (2013). Single-cell Hi-C reveals cell-to-cell variability in chromosome structure. Nature.

Narlikar, G.J., Sundaramoorthy, R., and Owen-Hughes, T. (2013). Mechanisms and Functions of ATP-Dependent Chromatin-Remodeling Enzymes. Cell *154*, 490–503.

Nashun, B., Akiyama, T., Suzuki, M.G., and Aoki, F. (2011). Dramatic replacement of histone variants during genome remodeling in nuclear-transferred embryos. Epigenetics *6*, 1489–1497.

Naumova, N., Imakaev, M., Fudenberg, G., Zhan, Y., Lajoie, B.R., Mirny, L.A., and Dekker, J. (2013). Organization of the Mitotic Chromosome. Science.

Nguyen, V.Q., Ranjan, A., Stengel, F., Wei, D., Aebersold, R., Wu, C., and Leschziner, A.E. (2013). Molecular Architecture of the ATP-Dependent Chromatin-Remodeling Complex SWR1. Cell *154*, 1220–1231.

Olins, D.E., and Olins, A.L. (2003). Chromatin history: our view from the bridge. Nat Rev Mol Cell Biol *4*, 809–814.

Oudet, P., Gross-Bellard, M., and Chambon, P. (1975). Electron microscopic and biochemical evidence that chromatin structure is a repeating unit. Cell *4*, 281–300.

Park, Y.-J., Dyer, P.N., Tremethick, D.J., and Luger, K. (2004). A new fluorescence resonance energy transfer approach demonstrates that the histone variant H2AZ stabilizes the histone octamer within the nucleosome. J Biol Chem *279*, 24274–24282.

Peterson, C.L., Dingwall, A., and Scott, M.P. (1994). Five SWI/SNF gene products are components of a large multisubunit complex required for transcriptional enhancement. Proc Natl Acad Sci USA *91*, 2905–2908.

Pointner, J., Persson, J., Prasad, P., Norman-Axelsson, U., lfors, A.S.A., Khorosjutina, O., Krietenstein, N., Svensson, J.P., Ekwall, K., and Korber, P. (2012). CHD1 remodelers regulate nucleosome spacing in vitro and align nucleosomal arrays over gene coding regions in S. pombe. Journal of Biological Chemistry –.

Polo, S.E., and Almouzni, G. (2006). Chromatin assembly: a basic recipe with various flavours. Current Opinion in Genetics & Development *16*, 104–111.

PRIETO, E., HIZUME, K., KOBORI, T., YOSHIMURA, S.H., and TAKEYASU, K. (2012). Core Histone Charge and Linker Histone H1 Effects on the Chromatin Structure of Schizosaccharomyces pombe. Journal of Biological Chemistry.

Racki, L.R., Yang, J.G., Naber, N., Partensky, P.D., Acevedo, A., Purcell, T.J., Cooke, R., Cheng, Y., and Narlikar, G.J. (2009). The chromatin remodeller ACF acts as a dimeric motor to space nucleosomes. Nature *462*, 1016–1021.

Raisner, R.M., Hartley, P.D., Meneghini, M.D., Bao, M.Z., Liu, C.L., Schreiber, S.L., Rando, O.J., and Madhani, H.D. (2005). Histone variant H2A.Z marks the 5' ends of both active and inactive genes in euchromatin. Cell *123*, 233–248.

Rhee, H.S., and Pugh, B.F. (2011). Comprehensive genome-wide protein-DNA interactions detected at single-nucleotide resolution. Cell *147*, 1408–1419.

Saha, A., Wittmeyer, J., and Cairns, B.R. (2002). Chromatin remodeling by RSC involves ATP-dependent DNA translocation. Genes & Development *16*, 2120–2134.

Saha, A., Wittmeyer, J., and Cairns, B.R. (2005). Chromatin remodeling through directional DNA translocation from an internal nucleosomal site. Nature Structural & Molecular Biology *12*, 747–755.

Santisteban, M.S., Hang, M., and Smith, M.M. (2011). Histone variant H2A.Z and RNA polymerase II transcription elongation. Molecular and Cellular Biology *31*, 1848–1860.

Schwanbeck, R., Xiao, H., and Wu, C. (2004). Spatial contacts and nucleosome step movements induced by the NURF chromatin remodeling complex. J Biol Chem *279*, 39933–39941.

Sengoku, T., Nureki, O., Nakamura, A., Kobayashi, S., and Yokoyama, S. (2006). Structural basis for RNA unwinding by the DEAD-box protein Drosophila Vasa. Cell *125*, 287–300.

Skene, P.J., and Henikoff, S. (2013). Histone variants in pluripotency and disease. Development *140*, 2513–2524.

Skiniotis, G., Moazed, D., and Walz, T. (2007). Acetylated histone tail peptides induce structural rearrangements in the RSC chromatin remodeling complex. J Biol Chem *282*, 20804–20808.

Smith, C.L., Horowitz-Scherer, R., Flanagan, J.F., Woodcock, C.L., and Peterson, C.L. (2003). Structural analysis of the yeast SWI/SNF chromatin remodeling complex. Nat Struct Biol *10*, 141–145.

Solomon, M.J., and Varshavsky, A. (1985). Formaldehyde-mediated DNA-protein crosslinking: a probe for in vivo chromatin structures. Proc Natl Acad Sci USA *82*, 6470–6474.

Stroud, H., Otero, S., Desvoyes, B., Ramírez-Parra, E., Jacobsen, S.E., and Gutierrez, C. (2012). Genome-wide analysis of histone H3.1 and H3.3 variants in Arabidopsis thaliana. Proceedings of the National Academy of Sciences *109*, 5370–5375.

Struhl, K., and Segal, E. (2013). Determinants of nucleosome positioning. Nature Structural & Molecular Biology *20*, 267–273.

Suto, R.K., Clarkson, M.J., Tremethick, D.J., and Luger, K. (2000). Crystal structure of a

nucleosome core particle containing the variant histone H2A.Z. Nat Struct Biol *7*, 1121–1124.

Szerlong, H., Hinata, K., Viswanathan, R., Erdjument-Bromage, H., Tempst, P., and Cairns, B.R. (2008). The HSA domain binds nuclear actin-related proteins to regulate chromatin-remodeling ATPases. Nature Structural & Molecular Biology *15*, 469–476.

Tachiwana, H., Kagawa, W., Shiga, T., Osakabe, A., Miya, Y., Saito, K., Hayashi-Takanaka, Y., Oda, T., Sato, M., Park, S.-Y., et al. (2011). Crystal structure of the human centromeric nucleosome containing CENP-A. Nature.

Tan, S., and Davey, C.A. (2011). Nucleosome structural studies. Current Opinion in Structural Biology *21*, 128–136.

Thakar, A., Gupta, P., McAllister, W.T., and Zlatanova, J. (2010). Histone variant H2A.Z inhibits transcription in reconstituted nucleosomes. Biochemistry *49*, 4018–4026.

Thambirajah, A.A., Li, A., Ishibashi, T., and Ausió, J. (2009). New developments in post-translational modifications and functions of histone H2A variants. Biochem Cell Biol *87*, 7–17.

Thomä, N.H., Czyzewski, B.K., Alexeev, A.A., Mazin, A.V., Kowalczykowski, S.C., and Pavletich, N.P. (2005). Structure of the SWI2/SNF2 chromatin-remodeling domain of eukaryotic Rad54. Nature Structural & Molecular Biology *12*, 350–356.

Torigoe, S.E., Urwin, D.L., Ishii, H., Smith, D.E., and Kadonaga, J.T. (2011). Identification of a rapidly formed nonnucleosomal histone-DNA intermediate that is converted into chromatin by ACF. Molecular Cell *43*, 638–648.

Tosi, A., Haas, C., Herzog, F., Gilmozzi, A., Berninghausen, O., Ungewickell, C., Gerhold, C.B., Lakomek, K., Aebersold, R., Beckmann, R., et al. (2013). Structure and Subunit Topology of the INO80 Chromatin Remodeler and Its Nucleosome Complex. Cell *154*, 1207–1219.

Tsunaka, Y., Kajimura, N., Tate, S.-I., and Morikawa, K. (2005). Alteration of the nucleosomal DNA path in the crystal structure of a human nucleosome core particle. Nucleic Acids Research *33*, 3424–3434.

Valdés-Mora, F., Song, J.Z., Statham, A.L., Strbenac, D., Robinson, M.D., Nair, S.S., Patterson, K.I., Tremethick, D.J., Stirzaker, C., and Clark, S.J. (2012). Acetylation of H2A.Z is a key epigenetic modification associated with gene deregulation and epigenetic remodeling in cancer. Genome Research *22*, 307–321.

Valouev, A., Ichikawa, J., Tonthat, T., Stuart, J., Ranade, S., Peckham, H., Zeng, K., Malek, J.A., Costa, G., McKernan, K., et al. (2008). A high-resolution, nucleosome position map of C. elegans reveals a lack of universal sequence-dictated positioning. Genome Research *18*, 1051–1063.

Valouev, A., Johnson, S.M., Boyd, S.D., Smith, C.L., Fire, A.Z., and Sidow, A. (2011). Determinants of nucleosome organization in primary human cells. Nature *474*, 516–520.

Voigt, P., Leroy, G., Drury, W.J., Zee, B.M., Son, J., Beck, D.B., Young, N.L., Garcia, B.A., and Reinberg, D. (2012). Asymmetrically modified nucleosomes. Cell *151*, 181–193.

Volle, C., and Dalal, Y. (2014). Histone variants: the tricksters of the chromatin world. Current Opinion in Genetics & Development *25C*, 8–14.

White, C.L., Suto, R.K., and Luger, K. (2001). Structure of the yeast nucleosome core particle reveals fundamental changes in internucleosome interactions. Embo J *20*, 5207–5218.

Whitehouse, I., Stockdale, C., Flaus, A., Szczelkun, M.D., and Owen-Hughes, T. (2003). Evidence for DNA translocation by the ISWI chromatin-remodeling enzyme. Molecular and Cellular Biology *23*, 1935–1945.

Yamada, K., Frouws, T.D., Angst, B., Fitzgerald, D.J., DeLuca, C., Schimmele, K., Sargent, D.F., and Richmond, T.J. (2011). Structure and mechanism of the chromatin remodelling factor ISW1a. Nature *472*, 448–453.

Yen, K., Vinayachandran, V., Batta, K., Koerber, R.T., and Pugh, B.F. (2012). Genome-wide nucleosome specificity and directionality of chromatin remodelers. Cell *149*, 1461–1473.

Zentner, G.E., Tsukiyama, T., and Henikoff, S. (2013). ISWI and CHD Chromatin Remodelers Bind Promoters but Act in Gene Bodies. PLoS Genet *9*, e1003317.

Zhang, H., Roberts, D.N., and Cairns, B.R. (2005). Genome-wide dynamics of Htz1, a histone H2A variant that poises repressed/basal promoters for activation through histone loss. Cell *123*, 219–231.

Zhang, Y., Smith, C.L., Saha, A., Grill, S.W., Mihardja, S., Smith, S.B., Cairns, B.R., Peterson, C.L., and Bustamante, C. (2006). DNA translocation and loop formation mechanism of chromatin remodeling by SWI/SNF and RSC. Molecular Cell *24*, 559–568.

Zhang, Z., Wippo, C.J., Wal, M., Ward, E., Korber, P., and Pugh, B.F. (2011). A Packing Mechanism for Nucleosome Organization Reconstituted Across a Eukaryotic Genome. Science *332*, 977–980.

Zhang, Z., and Pugh, B.F. (2011). High-Resolution Genome-wide Mapping of the Primary Structure of Chromatin. Cell *144*, 175–186.

Zofall, M., Persinger, J., Kassabov, S.R., and Bartholomew, B. (2006). Chromatin remodeling by ISW2 and SWI/SNF requires DNA translocation inside the nucleosome. Nature Structural & Molecular Biology *13*, 339–346.

Chapter Two

Molecular architecture of the ATP-dependent chromatin-remodeling complex SWR1

Part of this work was completed in collaboration with Anand Ranjan and Debbie Wei in Carl Wu's group (NIH-NCI/HHMI) and Florian Stengel in Ruedi Aebersold's group (ETH Zurich). A.R and D.W performed purification of endogenous SWR1 from *Saccharomyces cerevisiae* and *in vitro* assembly of recombinant mononucleosomes. F.S carried out isotopic crosslinking of SWR1 followed by mass-spectrometric analysis of crosslinked peptides.

INTRODUCTION

Many ATP-dependent chromatin remodelers collaborate at gene promoters to regulate transcriptional competency (Figure 1.7) (Yen et al., 2013). Results from several studies suggest that complexes of the SWI/SNF and ISWI families establish a nucleosome-free region (NFR) around the promoter, thus exposing it to the transcriptional machinery (Clapier and Cairns, 2009). SWR1, a member of the INO80 subfamily, is targeted to this region to deposit H2A.Z at flanking nucleosomes (Hartley and Madhani, 2009; Kobor et al., 2004; Krogan et al., 2003; Venters and Pugh, 2009). While the function of H2A.Z remains controversial (Chen et al., 2012; Guillemette and Gaudreau, 2006), it has been shown to affect the stability of its host nucleosome (Park et al., 2004; Suto et al., 2000; Yen et al., 2013), higher-order chromatin folding (Clapier and Cairns, 2009; Fan et al., 2002; 2004), and recruitment of transcriptional factors (Draker et al., 2012; Hartley and Madhani, 2009; Kobor et al., 2004; Krogan et al., 2003; Venters and Pugh, 2009). However, the most conserved characteristic of this histone variant is the striking positional stability of H2A.Z-containg nucleosomes, a majority of which is found at 5' ends of genes.

SWR1, like many other remodelers, is recruited to promoter NDRs; however, its activity targets primarily the +1 nucleosome (Chen et al., 2012; Guillemette and Gaudreau, 2006; Yen et al., 2013). It has been shown that free DNA regions within the NDRs serve to recruit SWR1 (Ranjan et al., 2013; Yen et al., 2013). Here, instead of repositioning the substrate, it catalyzes the unique dimer exchange reaction (Luk et al., 2010; Mizuguchi et al., 2004; Papamichos-Chronakis et al., 2011). This complex reaction must involve the enzyme ejecting a resident H2A-H2B dimer from its substrate nucleosome and inserting a H2A.Z-H2B dimer in its place

(Figure 2.1B). Besides this divergent remodeling activity, SWR1 also possesses an intriguingly sophisticated composition.

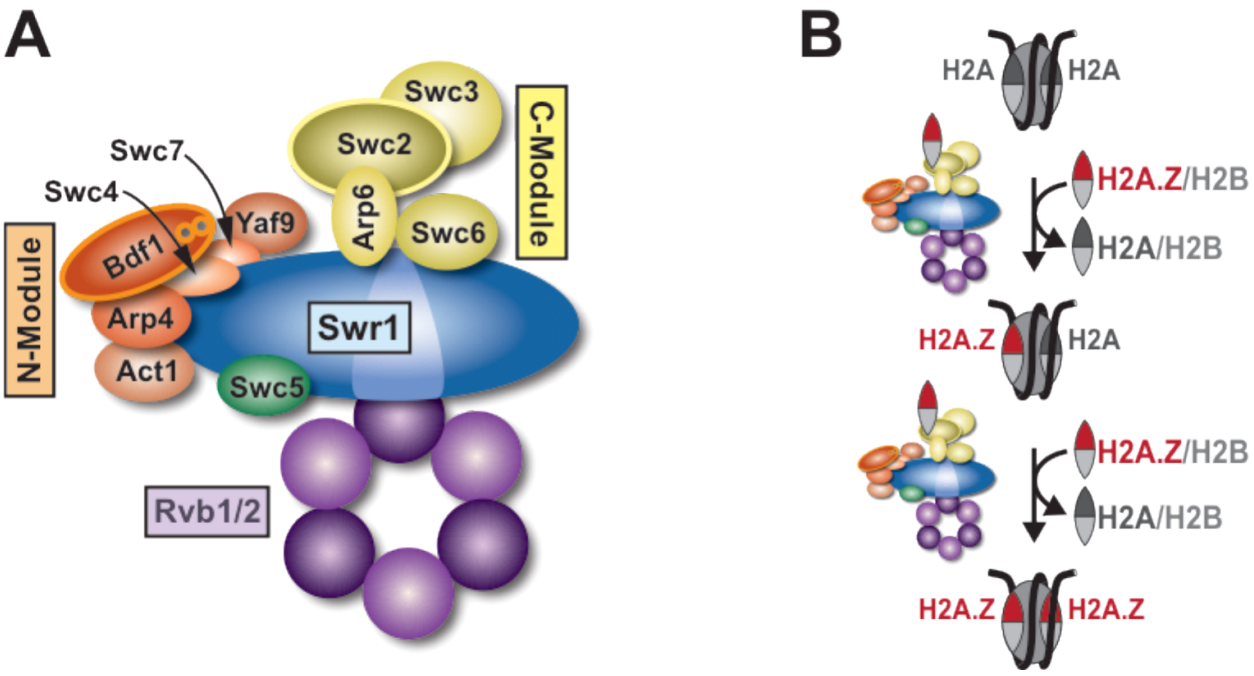

Figure 2.1 – Composition and remodeling activity of the SWR1 complex from *Saccharomyces cerevisiae*. **(A)** Schematic representation of the SWR1 complex. The arrangement of its 14 subunits is based on previous biochemical studies. **(B)** Schematic representation of the ATP-dependent histone-dimer exchange catalyzed by SWR1.

In *Saccharomyces cerevisiae*, SWR1 functions as a ~ 1 MDa complex containing 14 different polypeptides. By compositional analysis of affinity-purified sub-complexes from single-deletion mutants, Wu *et al.* identified three multi-subunit modules that assemble on the core, catalytic subunit Swr1 (Figure 2.1A) (Wu et al., 2009) (Wu et al., 2005). The N-terminal half of the Swr1 polypeptide contains the helicase-SANT-associated (HSA) domain, which is also present in the RSC and SWI/SNF complexes, and interacts with nuclear actin-related proteins (Arps) (Szerlong et al., 2008). Consistent with this report, the Bdf1-Arp4-Act1-Swc4-Yaf9-Swc7 module—referred to as the N-Module here—is recruited to this region. Arp4 has

been shown to interact directly with canonical nucleosomes and histones (Galarneau et al., 2000; Sunada et al., 2005), and Swc4 contains a SANT domain, which has been implicated in binding unmodified histone tails (Boyer et al., 2004). Moreover, Bdf1 contains tandem bromodomains with affinity for acetylated histone tails (Jacobson et al., 2000; Pamblanco et al., 2001). Therefore, the N-Module is likely involved in targeting and binding of SWR1 to hyper-acetylated nucleosomes (Durant and Pugh, 2007; Zhang et al., 2005). The conserved ATPase domain resides in the C-terminal half of Swr1, where its two RecA domains are separated by an extra-long, ~400 amino-acid insert that is characteristic of the INO80, or "split-ATPase," subfamily. Deletion of this insert eliminates association of the two remaining modules, Swc3-Swc2-Arp6-Swc6 (termed here the C-Module) and the putative hexameric helicases Rvb1/2 (Wu et al., 2005), the latter being another distinguishing characteristic of the INO80 subfamily. The C-Module binds the H2A.Z-H2B dimer, which is to be incorporated into the substrate nucleosome, *via* the Swc2 subunit (Wu et al., 2005). Lastly, as perhaps the most intriguing components in SWR1, Rvb1 and Rvb2 are AAA+ ATPases whose structure and function are still actively debated (Jónsson et al., 2004). In isolation, they have been shown to form single homo-hexameric (Matias et al., 2006) or hetero-hexameric ring structures (Gribun et al., 2008), but most studies show a stacked-ring, dodecameric arrangement (Cheung et al., 2010b; Puri et al., 2007; Torreira et al., 2008). Interestingly, although previous stoichiometric analysis suggested that there are two Rvb1/2 rings in the SWR1-related INO80 complex (Shen et al., 2000), robust ATPase and helicase activities have only been demonstrated for the single hetero-hexameric ring configuration (Gribun et al., 2008). Questions remain as to how these functional modules, all of which are essential to the dimer-exchange activity of SWR1, assemble as a remodeling complex.

To address these questions, we have undertaken a multi-pronged approach to characterize the SWR1 complex from *Saccharomyces cerevisiae* (Figure 2.1). Using electron microscopy (EM), we have determined the 3D structure of SWR1 and revealed that it contains a single hetero-hexameric Rvb1/2 ring. We have mapped the locations of all functional modules in SWR1 and show that the N- and C-Modules are bracketed by Swr1 and the Rvb1/2 ring. Furthermore, neighboring relationships within SWR1, as determined by chemical cross-linking and mass-spectrometric analysis of cross-linked peptides (CX-MS), show that its components are highly interconnected. Our results provide a structural framework for understanding SWR1's unique dimer-exchange activity.

RESULTS

Biochemical purification of a SWR1 sample suitable for structural determination

We obtained SWR1 from *S. cerevisiae* by affinity purification from a strain harboring a 3X FLAG tag at the C-terminus of the Swr1 core subunit (SWR1-3Flag, *htz1Δ*, Table 2.1). Although the sample was biochemically pure—all 14 components of SWR1 can be identified on a SDS-PAGE (Figure 2.2A)—it was structurally heterogeneous when observed under the electron microscope (Figure 2.2C, left and middle).

Table 2.1 – Yeast strains used in this study

SWR1-3Flag *htz1*Δ	*W1588C-4C swr1::SWR1-3Flag-P-KanMX-P htz1*Δ*::natMX4*	Kind gift of Wei-hua Wu
SWR1-2Flag (ΔN2)	*W1588-4C swr1::natMX [pRS416-swr1*Δ*N2-2Flag]*	Wei-hua et al 2006
SWR1-Flag arp6Δ	*W1588-4C SWR1-3Flag kanMX4 arp6::hphMX6 htz1::natMX*	Wei-hua et al 2006

We overcame this heterogeneity by using a modified version of the GraFix (Gradient with Fixation) technique (Figure 2.2A). This approach uses a combined glycerol and cross-linking gradient to both stabilize and purify macromolecular assemblies (Kastner et al., 2008; Stark, 2010). A key modification we made to the standard protocol was to replace glutaraldehyde with formaldehyde as the cross-linker to increase the stringency of the cross-linking and make the cross-links reversible. This reversibility allowed us to verify, in a small aliquot from each gradient fraction, that all SWR1 components were present (Figure 2.2A-B). We screened aliquots containing all the SWR1 components by electron microscopy before choosing a final sample for data collection. This two-step purification protocol significantly improved the homogeneity of the sample (Figure 2.2C). Stabilization by crosslinking allowed for preservation of this sample quality after glycerol removal via dialysis.

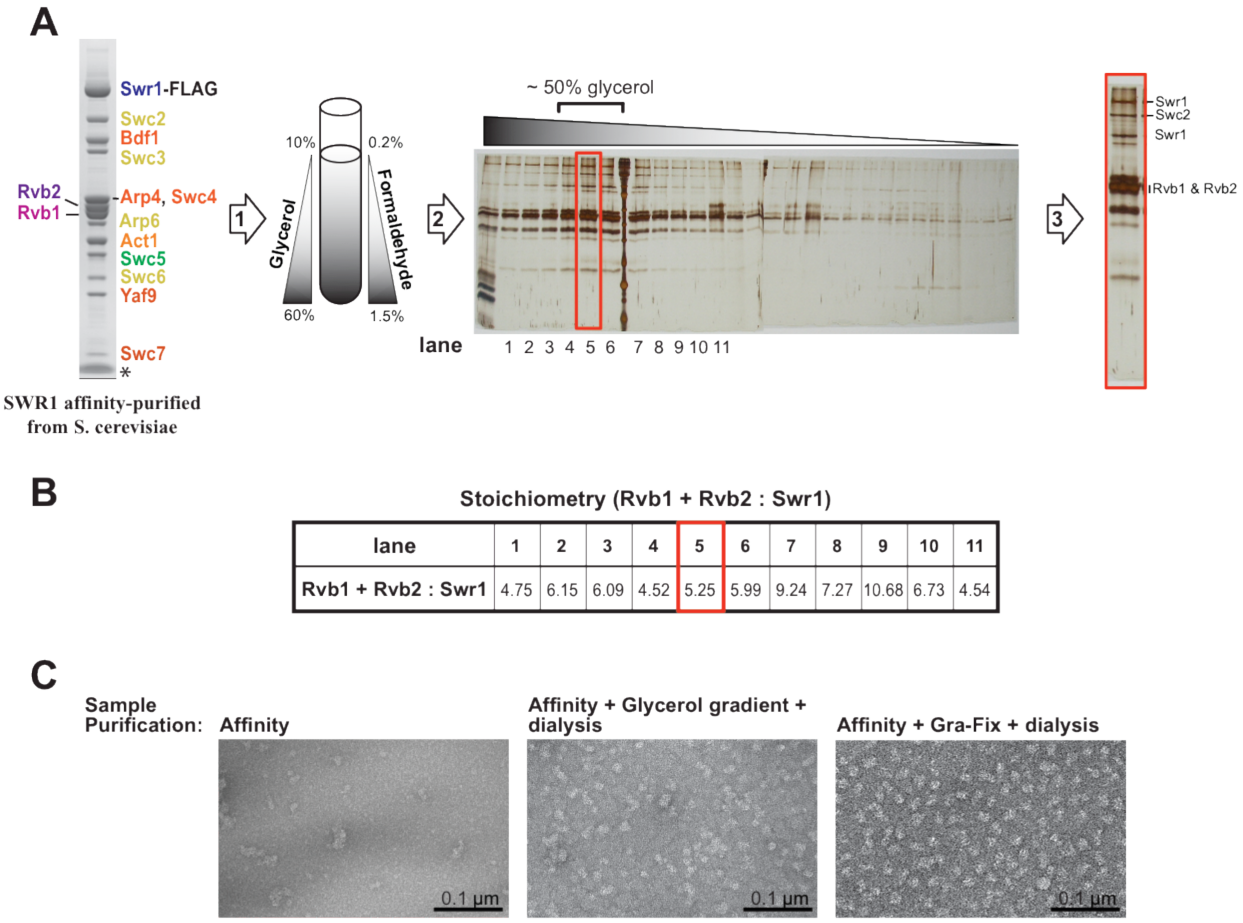

lane	1	2	3	4	5	6	7	8	9	10	11
Rvb1 + Rvb2 : Swr1	4.75	6.15	6.09	4.52	5.25	5.99	9.24	7.27	10.68	6.73	4.54

Figure 2.2 – Biochemical purification of a SWR1 sample suitable for imaging using the electron microscope. **(A)** Native SWR1 was affinity-purified from *S. cerevisiae* as described (Luk et al., 2010). Its 14 subunits are labeled and colored according to Figure 2.1A. The band at the bottom of the gel (*) corresponds to the 3x FLAG peptides used to elute the complex from the affinity resin. (1) The affinity-purified sample was run through a GraFix gradient (Kastner et al., 2008). (2) Upon fractionation of the gradient, small aliquots from all the fractions were treated to reverse the formaldehyde cross-links (Experimental Procedures) and were analyzed by SDS-PAGE. (3) After the main SWR1 peak was identified, the peak fractions were negatively stained and inspected for homogeneity in the electron microscope. The SDS-PAGE lane to the right represents the fraction from which data were collected; cross-links are only reversed for analytical purposes and not in the imaged samples. **(B)** The relative amounts of the Swr1 subunit and the Rvb's (Rvb1 + Rvb2) were measured for the different numbered fractions in (A). **(C)** Electron micrographs showing the appearance of the SWR1 after different purification strategies: affinity purification (left panel); affinity purification → glycerol gradient → dialysis (center panel); and affinity purification → GraFix → dialysis (right panel). The dialysis reduces the high glycerol concentration in the sample, which would otherwise affect the staining.

3D Reconstruction of SWR1

We obtained initial, low-resolution models of SWR1 using the Orthogonal Tilt Reconstruction (OTR) approach (Leschziner, 2010) and negatively-stained samples (Figure 2.3A-B). To refine the OTR models, we used cryo-negative stain (cryo-NS) data. This technique combines the high contrast provided by the heavy-atom negative stain with the structural preservation arising from the frozen-hydrated state of the sample (De Carlo and Stark, 2010). We performed projection-matching refinement, first against reference-free class averages and then against single particles (Figure 2.3C).

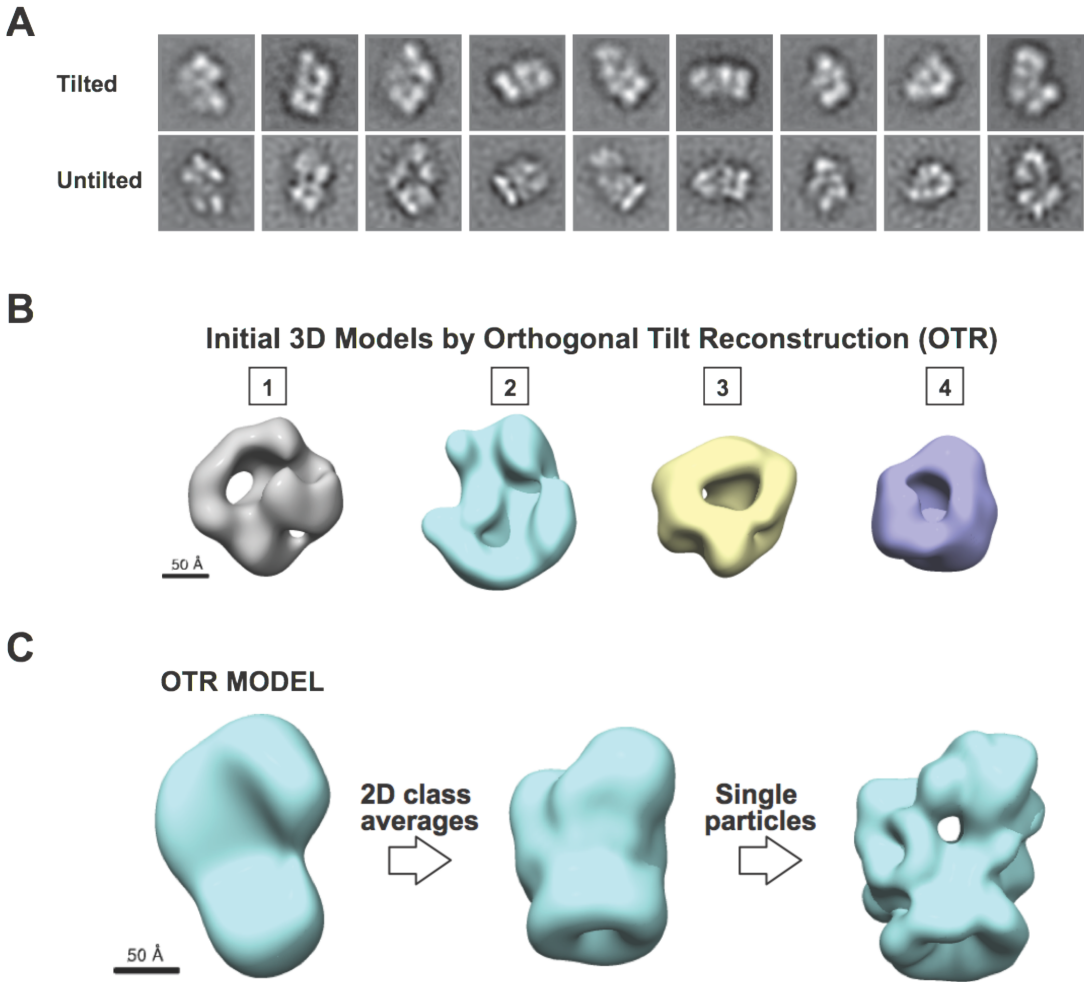

Figure 2.3 – 3D reconstruction and refinement of initial models. **(A)** 2D class averages obtained from data collected at (+/-) 45° tilt exhibit similarity to those obtained from untilted data, which indicates sampling of sufficiently random particle orientations for Orthogonal Tilt Reconstruction (OTR) (Chandramouli et al., 2011). **(B)** Initial 3D models obtained using the OTR approach (Leschziner, 2010). **(C)** The OTR initial model (left) was first refined by projection matching against reference-free class averages generated from untilted, cryo-negative stain (cryo-NS) images of SWR1. The resulting structure (middle) was further refined by projection matching against individual cryo-NS images of SWR1. The final refined structure is shown to the right. Scale bars measure 50 Å.

The resulting 3D structure has an estimated resolution of 28 Å (0.5 Fourier Shell Correlation) (Figure 2.4A-B) and has approximate dimensions of 250Å by 120Å by 120Å (Figure 1E and Movie S1). Two-dimensional projections calculated from this structure show a good match to reference-free class averages obtained from the cryo-NS data (Figure 2.4D).

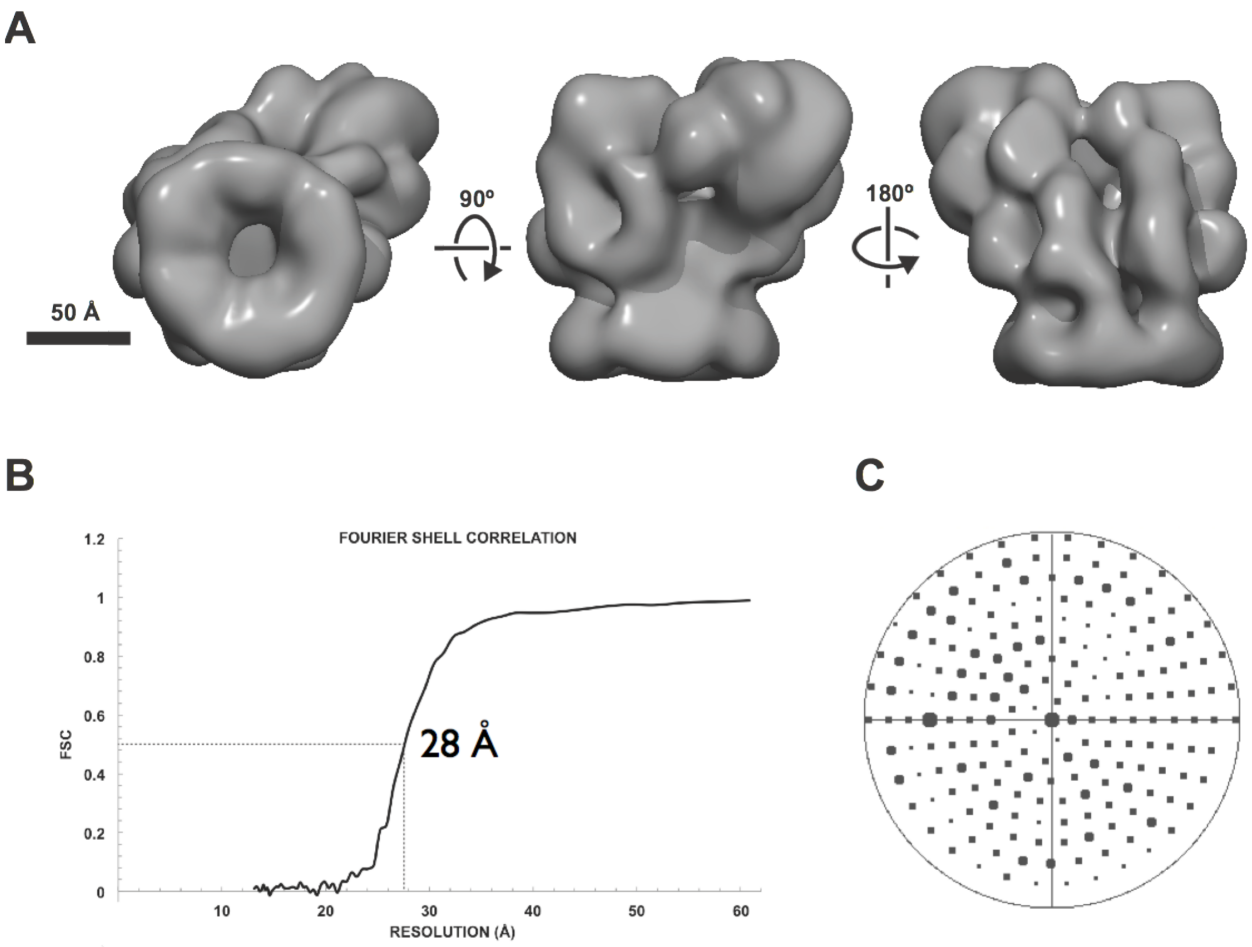

Figure 2.4 – 3D EM structure of the SWR1 complex. **(A)** Cryo-NS structure of SWR1 at 28 Å resolution. A hexameric feature can be seen in the left-most view of the complex. **(B)** Fourier Shell Correlation calculated for the final refined structure. The frequencies are shown as resolution, its inverse, in this graph. **(C)** Angular distribution of the images used for refinement. The position of each circle in the plot represents the set of Euler angles corresponding to one reference image using during projection matching. The radius of the circle is proportional to the number of particles assigned to that particular reference. **(D)** Comparison between re-projections of the SWR1 3D map and reference-free experimental class averages.

The SWR1 complex contains a single hetero-hexameric Rvb1/2 ring

Our cryo-NS map of SWR1 shows a clear ring-like density with hexameric features (Figure 2.4A, left, and Figure 2.5). Since a 13 Å cryo-electron microscopy (cryo-EM) structure of an Rvb1/2 dodecamer from *S.cerevisiae* is available (Torreira et al., 2008), we attempted to dock it into our map; we could only obtain a good match between one of its two rings and that in SWR1 (Figure 2.5A-C). This density fits well the crystal structure of a hexamer of RuvBL1 (Matias et al., 2006), the human ortholog of Rvb1 (Figure 2.5D-H). The only mismatch we observed between the RuvBL1 hexamer and SWR1 was at the distal ends of the insert domains; these domains, which are known to be flexible (López-Perrote et al., 2012; Petukhov et al., 2012), protrude from the EM map (Figure 2.5D-H). We further validated our structural data by performing a quantitative analysis of the Swr1:Rvb1:Rvb2 stoichiometry (Figure 2.5I), which we determined to be ~1:3:3. This result is consistent with the presence of a single Rvb1/2 ring in SWR1. This stoichiometry does not appear to be a feature unique to SWR1 as we obtained similar results for the highly related complex INO80 (Figure 2.5J).

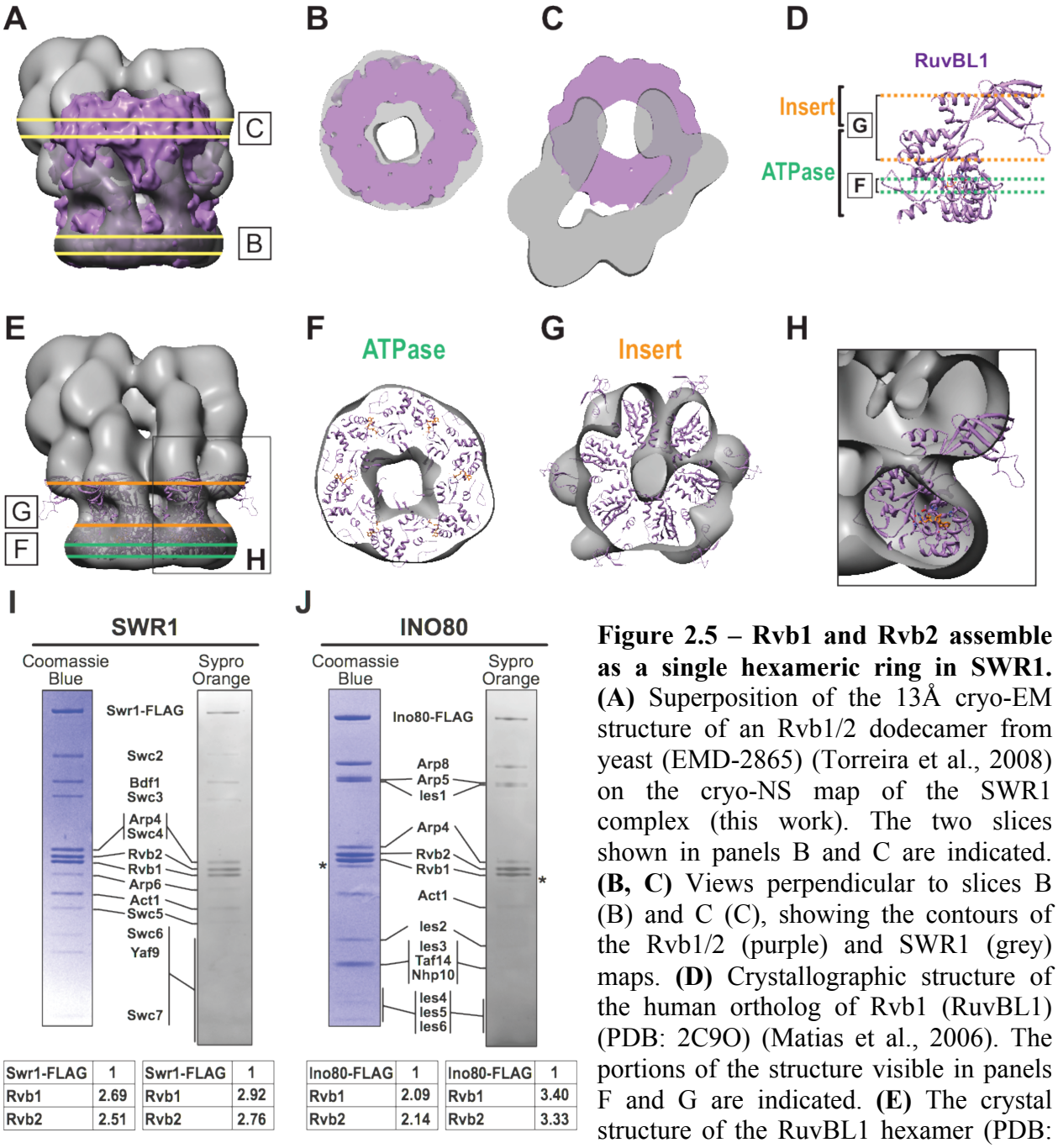

Swr1-FLAG	1
Rvb1	2.69
Rvb2	2.51

Swr1-FLAG	1
Rvb1	2.92
Rvb2	2.76

Ino80-FLAG	1
Rvb1	2.09
Rvb2	2.14

Ino80-FLAG	1
Rvb1	3.40
Rvb2	3.33

Figure 2.5 – Rvb1 and Rvb2 assemble as a single hexameric ring in SWR1. **(A)** Superposition of the 13Å cryo-EM structure of an Rvb1/2 dodecamer from yeast (EMD-2865) (Torreira et al., 2008) on the cryo-NS map of the SWR1 complex (this work). The two slices shown in panels B and C are indicated. **(B, C)** Views perpendicular to slices B (B) and C (C), showing the contours of the Rvb1/2 (purple) and SWR1 (grey) maps. **(D)** Crystallographic structure of the human ortholog of Rvb1 (RuvBL1) (PDB: 2C9O) (Matias et al., 2006). The portions of the structure visible in panels F and G are indicated. **(E)** The crystal structure of the RuvBL1 hexamer (PDB: 2C9O) docked into the hexameric density at the bottom of the SWR1 cryo-NS map. The two slices shown in panels F and G are indicated. **(F)** View perpendicular to slice F, corresponding to the ATPase domains. **(G)** View perpendicular to slice G, corresponding to the insert and a portion of the ATPase immediately adjacent to it. **(H)** The front half of the EM density was removed to show a single RuvBL1 monomer docked into the SWR1 EM density map. The orientation of the RuvBL1 structure is identical to that shown in panel D. **(I and J)** Biochemical quantifications of Swr1:Rvb1:Rvb2 revealed that both SWR1 (I) and the related complex INO80 (J) contain three copies each of Rvb1 and Rvb2.

While our structure contains a single Rvb ring, it does not establish whether both Rvb1 and Rvb2 are present in it. Although both variants copurify with Swr1 (Mizuguchi et al., 2004), and Rvb1 and Rvb2 can form a hetero-hexameric ring in isolation (Gribun, 2008), it was formally possible that two populations of SWR1 complex coexist in the nucleus, each containing a homo-hexameric ring of either Rvb1 or Rvb2. Using CX-MS (Leitner et al., 2010), we identified a cross-link between Rvb1 and Rvb2, but no homotypic (Rvb1-Rvb1 or Rvb2-Rvb2) cross-links (Figure 5 and Table S2). All Rvb1-Rvb1 and Rvb2-Rvb2 cross-links we identified corresponded to distances most compatible with their being intramolecular (Table S2). The Rv1-Rvb2 cross-link we observed is in agreement with the expected intersubunit interface based on a homology model built from the *S.cerevisiae* Rvb1 and Rvb2 sequences and the crystal structure of the human RuvBL1 homohexameric ring (Gorynia et al., 2011) (Figure 5B,C).

Two functional modules of SWR1 form discrete structural entities bracketed by Rvb1/2 and the Swr1 ATPase

To determine the location of the N- and C-Modules in the SWR1 structure, we obtained stable sub-complexes containing Swr1 and Rvb1/2, and either the N- or C-Module (Wu et al., 2009). We named these ~700 kDa sub-complexes SWR1-ΔC-Mod and SWR1-ΔN-Mod to indicate the missing module (Figure 2.6A). SWR1-ΔC-Mod was affinity-purified via Swr1-3X FLAG from an *arp6-/-* strain (Table 2.1), as elimination of Arp6 prevents association of the Swc2, Swc3, and Swc6 (the entire C-Module) with the complex (Wu et al., 2005) (Figure 2.6B). We obtained SWR1-ΔN-Mod from a strain harboring a truncation in Swr1 spanning residues 278 to 681 (Swr1-ΔN) (Table 2.1), which includes the HSA domain (Figure 2.6A). This truncation

results in the exclusion of the N-Module (Figure 2.6B). Each sub-complex was further purified by GraFix as described above (Figure 2.6C-D, top) and imaged under cryo-negative conditions.

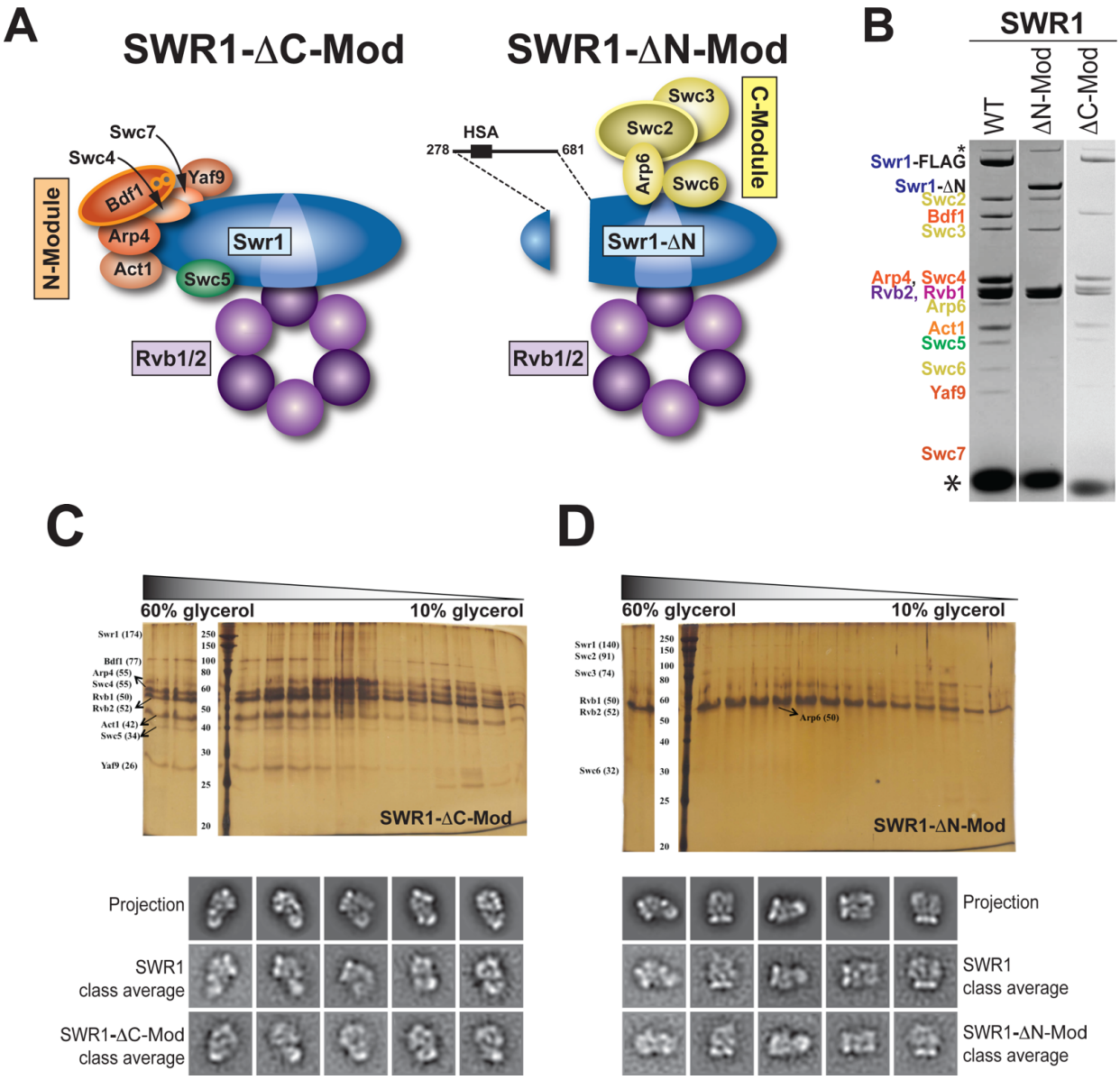

Figure 2.6 – Stable SWR1 subcomplexes structurally analyzed to map functional modules. **(A)** Schematic representation of the two sub-complexes used for our analysis, SWR1-ΔN-Mod and SWR1-ΔC-Mod. Both sub-complexes contain the Swr1 ATPase and Rvb1/2. They differ in the presence or absence of subsets of subunits, termed the N- and C-Module, based on the portion of Swr1 with which they are known to interact (Wu et al., 2009). **(B)** SDS-PAGE analysis of SWR1-ΔN-Mod and SWR1-ΔC-Mod showing their composition. The sub-complexes were affinity-purified from *S. cerevisiae* carrying an *arp6-/-* deletion or a *swr1-Δ278-681* truncation, respectively. The dark band at the bottom of the gels (*) is the 3X FLAG peptide

used to elute the complex from the affinity resin. **(C)** Stabilization and purification of SWR1-ΔC-Mod by GraFix, followed by SDS-PAGE analysis (top) and comparison between reference-free experimental class averages generated for SWR1-ΔC-Mod and the corresponding projections and class averages of full SWR1 (bottom). **(D)** Stabilization and purification of SWR1-ΔN-Mod by GraFix, followed by SDS-PAGE analysis (top) and comparison between reference-free experimental class averages generated for SWR1-ΔC-Mod and the corresponding projections and class averages of full SWR1 (bottom).

We performed single-particle alignment and classification of the data to obtain 2D class averages, or views, of the sub-complexes. A comparison of these views with those from the full complex and 2D re-projections of the SWR1 structure led to two major observations. First, in the absence of either ~300 kDa module, the remaining SWR1 components assemble into a structure very similar to that of the corresponding portion of the full complex (Figure 2.6C-D, bottom). Of particular note is that in SWR1-ΔN-Mod, a ~400 amino-acid truncation in the core Swr1 polypeptide did not significantly impact assembly of the remaining subunits, suggesting that the N- and C-terminal halves of Swr1 fold independently of each other. Second, we observed that two prominent features are retained in both sub-complexes: the Rvb1/2 ring and a prominent density distal to it (Figure 4C and S4B,D). Since SWR1-ΔC-Mod and SWR1-ΔN-Mod only share Rvb1, Rvb2, and the catalytic, ATPase-containing bulk of Swr1, we conclude that the catalytic portion of Swr1 occupies the large density distal to the Rvb1/2 ring (Figure 4D).

Next, we performed difference mapping between class averages of each sub-complex (SWR1-ΔC-Mod or SWR1-ΔN-Mod) and of full SWR1 for three different characteristic views of the complex (Figure 4C). This analysis identified the locations of the C- and N-Modules. They form structurally discrete entities arranged side-by-side and bracketed by the Rvb1/2 ring and Swr1 (Figure 4C and D). These results allowed us to generate a low-resolution annotation of the 3D map (Figure 4D). Further support of this annotated map was provided by general

agreement between the theoretical molecular weights of the modules with those enclosed in the corresponding densities in the EM map (Figure 2.8).

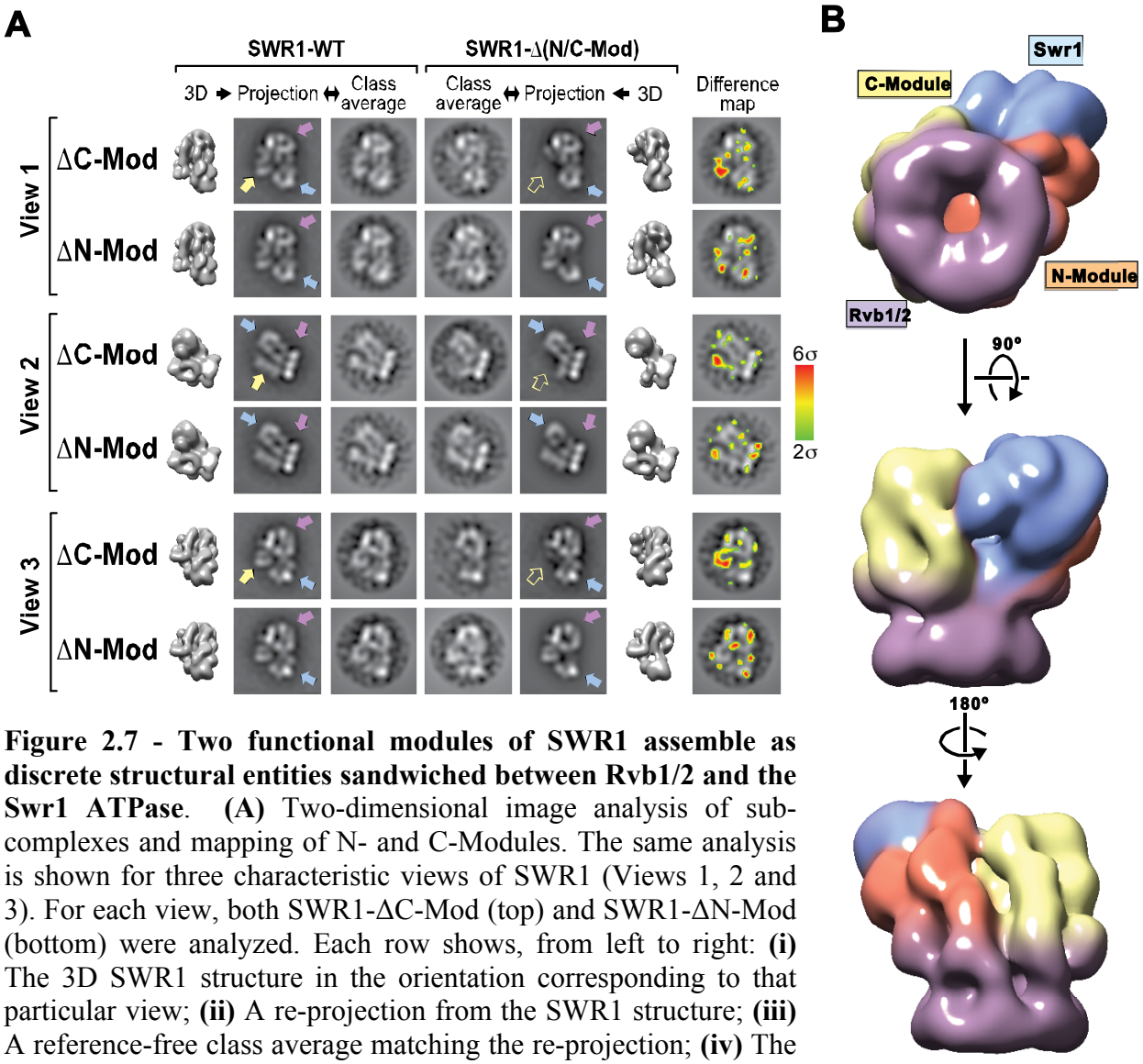

Figure 2.7 - Two functional modules of SWR1 assemble as discrete structural entities sandwiched between Rvb1/2 and the Swr1 ATPase. **(A)** Two-dimensional image analysis of sub-complexes and mapping of N- and C-Modules. The same analysis is shown for three characteristic views of SWR1 (Views 1, 2 and 3). For each view, both SWR1-ΔC-Mod (top) and SWR1-ΔN-Mod (bottom) were analyzed. Each row shows, from left to right: **(i)** The 3D SWR1 structure in the orientation corresponding to that particular view; **(ii)** A re-projection from the SWR1 structure; **(iii)** A reference-free class average matching the re-projection; **(iv)** The corresponding reference-free class average for the sub-complex; **(v)** A re-projection from a 3D model of SWR1 where the N- or C-Module were digitally removed; **(vi)** The 3D model of SWR1 used to generate the re-projection in (v); **(vii)** A difference map calculated by subtracting the reference-free class average of the sub-complex (iv) from the reference-free class average of full SWR1 (iii). The difference map is colored according to the scale shown to the right and is overlaid on top of the reference-free class average of full SWR1. The purple and blue arrows point to those structures that are present in both SWR1 and the two sub-complexes and are color-coded according to the final assignment of molecular identities shown in (D). The yellow arrows point to large features that are present in SWR1 (solid arrow) but absent in SWR1-ΔC-Mod (hollow arrow). **(B)** The same three views of SWR1

shown in Figure 1E are now color-coded according to the identity of the four functional modules: Swr1; Rvb1/2; N-Module and C-Module.

The difference mapping also revealed that removal of the N-Module has a more noticeable effect, relative to deletion of the C-Module, on the overall structure of SWR1; we observed changes in the position of both the Rvb1/2 ring and the Swr1 protuberance between SWR1 and SWR1-ΔN-Mod (Figure 2.7A).

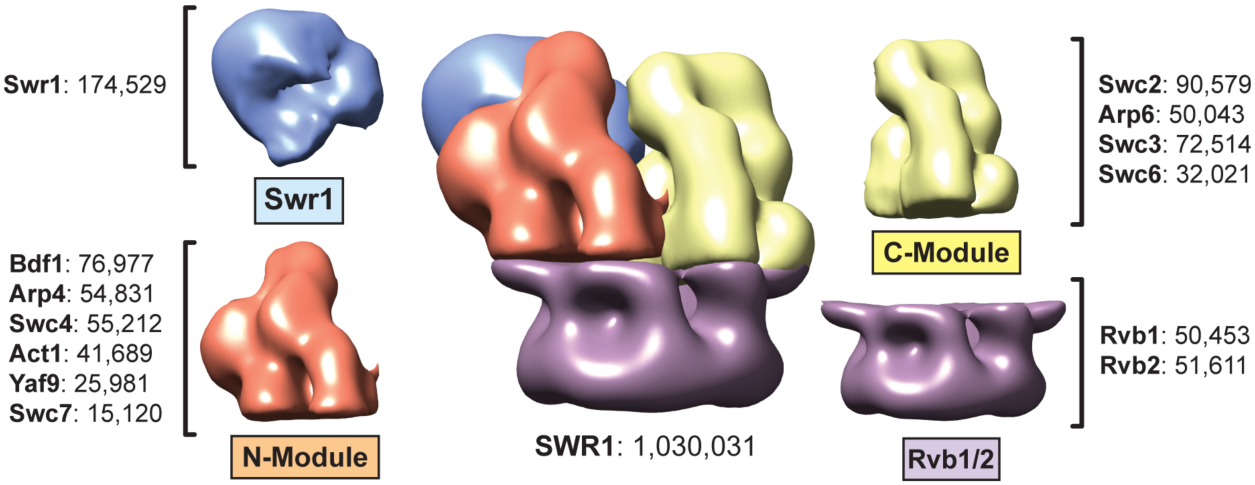

	Theoretical MW	MW of segmented volume
Swr1	174,529 Da	173 kDa
N-Module	269,810 Da	250 kDa
C-Module	245,157 Da	264 kDa
Rvb1/2	306,192 Da	373 kDa

Figure 2.8 – Measurements of segmented 3D densities agree with the molecular weights of the functional modules. The 3D EM map of SWR1 was segmented according to the module boundaries identified in Figure 2.7. The subunits present in each of the four functional modules are indicated along with their calculated weights. The table at the bottom shows the theoretical MW obtained from adding the subunits in each module and the calculated MW obtained from the number of voxels enclosed by each segmented density.

Cross-linking and mass spectrometry map subunit interactions within SWR1

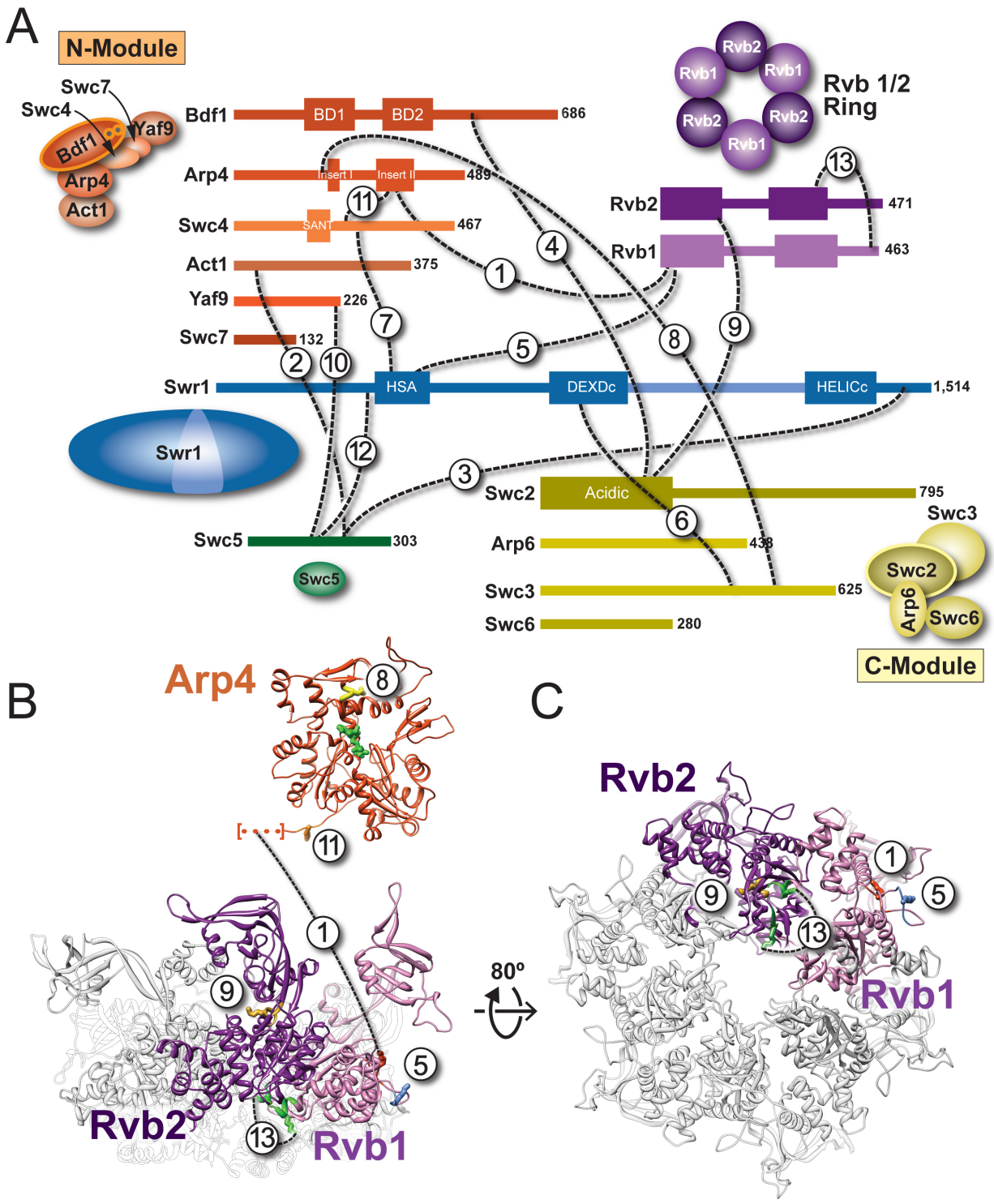

Figure 2.9 - Isotopic cross-linking and mass spectrometry analysis of the SWR1 complex. **(A)** Schematic representation of the cross-links detected by isotopic cross-linking and mass spectrometry of SWR1 complexes. The 14 components of SWR1 are color-coded according to the diagram shown in Figure 2.1A and are drawn proportionally to their mass. The number of

amino acids in each polypeptide is indicated to its right. The SWR1 components are separated into the N-Module, the C-Module, the Rvb1/2 ring, the catalytic subunit Swr1 and the Swc5 subunit. The cross-links identified in this study are shown with dashed black lines and numbered (1-13). **(B)** Mapping of the cross-links involving Rvb1, Rvb2 and Arp4 to their crystal structures. The Arp4 structure is that of the *S.cerevisiae* protein (3QB0) (Fenn et al., 2011) while the Rvb1/2 heterohexamer is a homology model generated for this study using the crystal structure of the human ortholog RuvBL1 (2C9O) (Matias et al., 2006). The amino acids involved in the cross-links are highlighted and color-coded according to the same scheme used in (A) (except for the residues involved in the Rvb1-Rvb2 cross-link, which are colored green). The number placed next to the cross-linked lysines refers to the cross-links shown in (A). The dotted line within square brackets in Arp4 indicates the location of a cross-link we observed that maps to a portion of the sequence not seen in the crystal structure. **(C)** A view of the Rvb1/2 ring perpendicular to its plane, showing the location of the identified cross-links.

In order to gain further insight into the architecture of SWR1, we used a combination of isotopic cross-linking and mass spectrometry (CX-MS) (Leitner et al., 2010) to map spatial proximity between subunits in the complex. In addition to establishing the heteromeric nature of the Rvb1/2 ring (discussed above), our cross-linking data confirmed a number of the previously determined interactions (Figure 2.9 and Table 2.2). Specifically, we observed cross-links connecting the N-Module with the N-terminal half of Swr1 (Swc4-Swr1); the C-Module with the C-terminal half of Swr1 (Swc3-Swr1); and Arp4 and Swc4 within the N-Module (Figure 2.9A and Table 2.2). Additionally, we obtained two cross-links connecting the small subunit Swc5 with both the N- and C-terminus of Swr1, in agreement with data showing that Swc5 requires both termini of Swr1 to be present in the complex (Wu et al., 2009).

We also observed a number of additional cross-links not predicted by the previous biochemical mapping of SWR1 interactions, which suggest a high degree of interconnectedness among SWR1's functional modules. The Rvb1/2 ring, previously shown to require the long insert in the ATPase domain of Swr1 to assemble into the full complex (Wu et al., 2005), cross-linked to the N-terminal half of Swr1 (its HSA domain) *via* Rvb1, the N-Module (Rvb1-Arp4) and the C-Module (Rvb2-Swc2) (Figure 2.9A-B and Table 2.2). The N- and C-Modules also

cross-linked to each other, through Bdf1-Swc2 and Arp4-Swc3 (Figure 2.9A and Table 2.2). Finally, Swc5 cross-linked to the N-Module *via* two interactions with Act1 and Yaf9 (Figure 2.9A and Table 2.2). Understanding the functional significance of these novel spatial relationships will require future work combining biochemistry and finer subunit mapping in SWR1.

Table 2.2 - Inter- and intra-protein cross-links identified *via* isotopic crosslinking and mass spectrometry

INTERPROTEIN CROSS-LINKS							
Cross-linked peptides (Protein1-Protein2)	**Protein1**	**Xlink1 (AA)**	**Protein2**	**Xlink2 (AA)**		**Ca-Ca (Å)**	**Id score**
HQGIMVGMGQKDSYVGDEAQSKR-TKSNESR	|P60010|ACT1	K50	|P38326|SWC5	K205			37.31
LLAQAEDEDDVKAANLAMR-TKSNESR	|Q05471|SWR1	K1456	|P38326|SWC5	K205			33.74
KIIQERIR-SKGRSGSK	|Q03388|VPS72	K218	|P35817|BDF1	K504			33.21
GLGLDESGVAKRVEGGFVGQIEAR-FAVQAVKKR	|Q03940|RVB1	K42	|Q05471|SWR1	K418			32.2
FAPGFKVLTYYGSPQQR-EKGVK	|Q05471|SWR1	K772	|P31376|SWC3	K407			30.55
SAAEIAEEEALVVESKK-SSTKARIAR	|P53201|SWC4	K262	|Q05471|SWR1	K371			30.05
FINHLIKKALEPK-EIEKFKTK	|P80428|ARP4	K195	|P31376|SWC3	K498			29.43
HKEQESQHMLTQEER-KSIGIK	|Q03388|VPS72	K228	|Q12464|RVB2	K123			29.19
LLSSSGKVGSVLDGSKEAR-LENLVKQEAINGS	|P38326|SWC5	K138	|P53930|YAF9	K219			28.5
NDYVPLKR-KKYLQR	|P80428|ARP4	K323	|P53201|SWC4	K238			26.85
LLSSSGKVGSVLDGSKEAR-ETDSLQPITSKEIK	|P38326|SWC5	K138	|Q05471|SWR1	K326			26.64
STKILETSANYL-GVSKTR	|Q03940|RVB1	K454	|Q12464|RVB2	K331		14.5Å	26.33
HQGIMVGMGQKDSYVGDEAQSKR-TKSNESR	|P60010|ACT1	K61	|P38326|SWC5	K205			25.82
TAAHTHIKGLGLDESGVAKR-SDKKVTPTEEK	|Q03940|RVB1	K31	|P80428|ARP4	K335			25.1
INTRAPROTEIN CROSS-LINKS							
Cross-linked peptides (Protein1-Protein2)	**Protein1**	**Xlink1 (AA)**	**Protein2**	**Xlink 2 (AA)**	**|AA1 - AA2|**	**Ca-Ca (Å)**	**Id score**
RAAGVILKMVQNGTIAGR-GVSKTR	|Q12464|RVB2	K59	|Q12464|RVB2	K331	272	33.6Å	44.18
IESESGGLIKTR-NKVDYSR	|P38326|SWC5	K79	|P38326|SWC5	K64	15		38.33
SNSGVVKTWR-NDYVPLKR	|P80428|ARP4	K313	|P80428|ARP4	K323	10	26.0Å	38.27
KSESAYAEQLLK-QRQEMQTALKR	|P53201|SWC4	K372	|P53201|SWC4	K370	2		38.01
STTAAQQEDKILIER-VGSVLDGSKEAR	|P38326|SWC5	K151	|P38326|SWC5	K138	13		37.34
STTAAQQEDKILIER-TKSNESR	|P38326|SWC5	K151	|P38326|SWC5	K205	54		37.08
SNSGVVKTWR-NDYVPLKR	|P80428|ARP4	K313	|P80428|ARP4	K323	10	26.0Å	36.76
SIIITTKSYNEQEIK-GVSKTR	|Q12464|RVB2	K357	|Q12464|RVB2	K331	26	23.9Å	36.65
AGLNDELVLHNKDGFLAR-VGSAEDERYKELR	|P38326|SWC5	K263	|P38326|SWC5	K285	22		36.61

GTNYKSPHGLPLDLLDR-GVSKTR	|Q12464|RVB2	K338	|Q12464|RVB2	K331	7	4.1Å	35.52
FGPSTNKKPFR-SYKGEMR	|Q12509|ARP6	K23	|Q12509|ARP6	K144	121		34.91
RKSESAYAEQLLK-QEMQTALKRK	|P53201|SWC4	K372	|P53201|SWC4	K370	2		34.13
LKTVVTYDMKR-DKKNK	|P35817|BDF1	K525	|P35817|BDF1	K520	5		33.06
IESESGGLIKTRR-NKVDYSR	|P38326|SWC5	K79	|P38326|SWC5	K64	15		32.75
VGSAEDERYKELR-TKSNESR	|P38326|SWC5	K285	|P38326|SWC5	K205	80		32.68
KDEEEQLKR-WNMAEKAYR	|Q05471|SWR1	K433	|Q05471|SWR1	K426	7		32.54
AGLNDELVLHNKDGFLAR-TKSNESR	|P38326|SWC5	K263	|P38326|SWC5	K205	58		32.54
FAVQAVKKR-WNMAEKAYR	|Q05471|SWR1	K418	|Q05471|SWR1	K426	8		32.1
KTVVHTVSLHEIDVINSR-ASGKITK	|Q12464|RVB2	K233	|Q12464|RVB2	K198	35	13.5Å	32.04
SNSGVVKTWR-FINHLIKK	|P80428|ARP4	K313	|P80428|ARP4	K195	118	31.5Å	31.37
SDIKRDETTNEDSDDQVR-IQDPISKEEGR	|Q03388|VPS72	K754	|Q03388|VPS72	K746	8		31.02
KSESAYAEQLLKDFNSDER-QRQEMQTALKR	|P53201|SWC4	K372	|P53201|SWC4	K370	2		30.66
FINHLIKK-KPEFIKK	|P80428|ARP4	K195	|P80428|ARP4	K218	23	19.5Å	30.04
GSKKR-IRKER	|P35817|BDF1	K497	|P35817|BDF1	K488	9		29.96
FAVQAVKKR-WNMAEKAYR	|Q05471|SWR1	K418	|Q05471|SWR1	K426	8		29.59
ILRKDEEEQLK-WNMAEKAYR	|Q05471|SWR1	K433	|Q05471|SWR1	K426	7		29.54
EKVLAGDVISIDKASGK-SITGGHKQGK	|Q12464|RVB2	K183	|Q12464|RVB2	K154	29	19.5Å	29.17
ETHLSLEERGEKFTDDVAK-KGTNGDLTR	|Q05471|SWR1	K74	|Q05471|SWR1	K82	8		28.88
HKKSLAR-KAKEEER	|Q05471|SWR1	K407	|Q05471|SWR1	K400	7		28.84
HKKSLAR-KAKEEER	|Q05471|SWR1	K407	|Q05471|SWR1	K400	7		28.34
WNMAEKAYRILR-KDEEEQLKR	|Q05471|SWR1	K426	|Q05471|SWR1	K433	7		27.87
GTNYKSPHGLPLDLLDR-GVSKTR	|Q12464|RVB2	K338	|Q12464|RVB2	K331	7	4.1Å	27.26
KVTPTEEKEQEAVSK-TKPSGVNKSDK	|P80428|ARP4	K336	|P80428|ARP4	K332	4	N/A	26.23
STKILETSANYL-LLFLDAKR	|Q03940|RVB1	K454	|Q03940|RVB1	K450	4	4.9Å	26.19
ADDENAEKQQSKEAK-SSKTAATEPEPKK	|P31376|SWC3	K380	|P31376|SWC3	K371	9		25.41
YGFAEELFLPKEDDIPANWPR-TLEETKTELSSTAKR	|P80428|ARP4	K296	|P80428|ARP4	K259	37	21.2Å	25.35

DISCUSSION

Using a combination of structural, biochemical and proteomic approaches, we have dissected the three-dimensional architecture of the ATP-dependent chromatin remodeling complex SWR1. By analyzing stable sub-complexes missing defined components, we were able to locate two major functional modules as well as Swr1, the catalytic ATPase, in our cryo-negative stain map. Our structural data indicate that the two modules are bracketed by the catalytic ATPase and the putative AAA+ helicases Rvb1 and Rvb2, which assemble as a single hetero-hexameric ring. Our cross-linking / mass-spectrometry data, which revealed a high degree of spatial inter-connectedness among all components of the complex, is also in agreement with the structure.

Functional modules assemble as structurally discrete entities in SWR1

Our analysis of SWR1 and sub-complexes lacking either the N or C-Module revealed an assembly of structurally discrete domains. In this assembly, the catalytic Swr1 ATPase and the Rvb1/2 ring closely bracket the N- and C-Modules, which are arranged side-by-side (Figure 2.7). The spatial proximity among all of SWR1's components is in agreement with our cross-linking and mass spectrometry results (Figure 2.9); we observed cross-links corresponding to all possible pairwise combinations of the functional domains—Swr1, the Rvb1/2 ring and the N and C Modules. Based on the combination of structural and proteomics data, we can approximate the locations of several SWR1 subunits in our cryo-NS map (Figure 2.10).

We mapped the ATPase-containing bulk of the core subunit Swr1 to a location distal to the Rvb1/2 ring, where its position within the complex appears to be supported mainly by the N Module (Figure 4D). Consistent with this arrangement, the SWR1-ΔN-Mod sub-complex exhibited relatively more widespread structural changes than SWR1-ΔC-Mod, with some

changes in the Rvb1/2 ring detected in the 2D difference maps (Figure 4C). Therefore, we propose that the N-Module serves an important structural role by positioning and orienting the catalytic subunit. Within this module, our cross-linking data indicate that Arp4 mediates the module's interaction with the Rvb1/2 ring (Figure 5). ATP binding by Arp4 has been shown to regulate its association with macromolecular complexes *in vivo* (Sunada et al., 2005). Given its role in SWR1, this property of Arp4 presents a potential regulatory mechanism that targets assembly and thus activity of the complex.

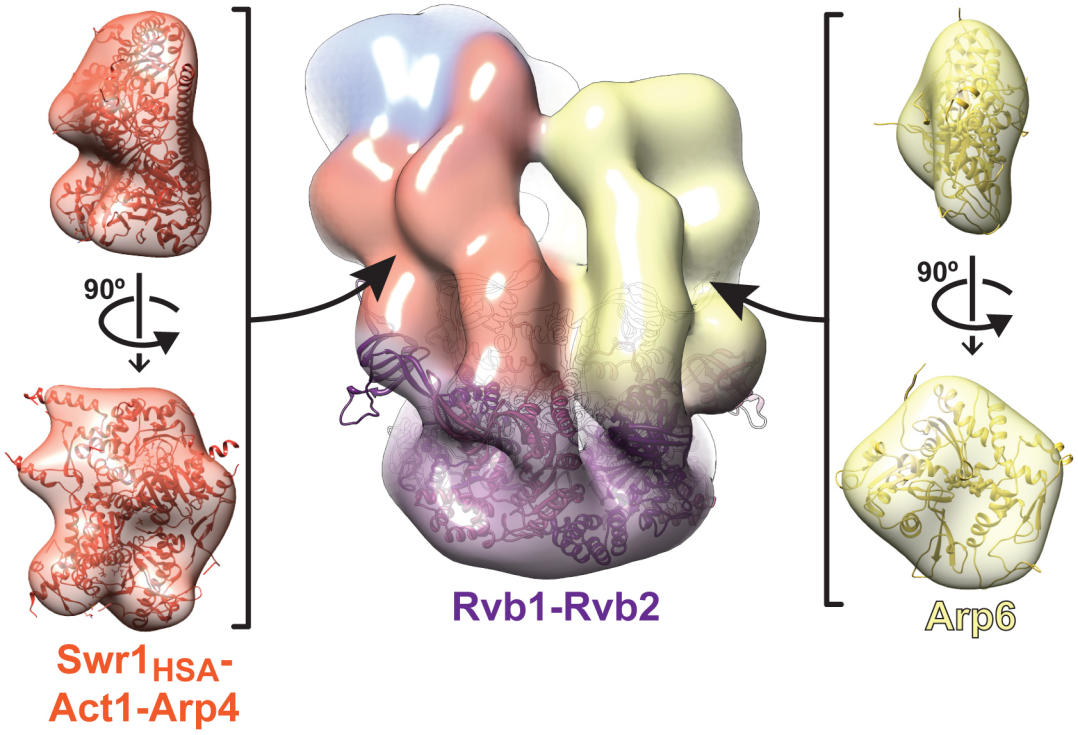

Figure 2.10 - Molecular architecture of SWR1. The SWR1 reconstruction, colored to highlight the different functional modules is shown in the center with the Rvb1/2 homology model docked into the density. Known structures for homologs of components of SWR1 are shown to highlight their compatibility with the structural features of the SWR1 EM map. The left side shows the crystal structure of Snf2HSA-Arp7-Arp9-Rtt102 (PDB: 4I6M) (Schubert et al., 2013) inside a density representing the structure at 28Å resolution as a proxy for Swr1HSA-Act1-Arp4. The right side shows the crystal structure of yeast Arp4 (PDB: 3QB0 and Fenn et al, 2011, EMBO J.) inside a density representing the structure at 28Å resolution as a proxy for Arp6.

While there were localized structural changes in both sub-complexes, we observed that the remaining components largely retained the spatial arrangement they adopt in the full complex (Figure 2.7), suggesting that the N- and C-Modules associate with the complex independently of each other. This is consistent with the fact that these sub-complexes are sufficiently stable for purification and structural studies. Thus, our data support a modular assembly model in which pre-assembled, multi-subunit modules associate with a complex independently of each other. SWR1 components that can assemble in isolation are also found in functionally related complexes. Rvb1/2, which can form a hetero-hexameric ring outside of the complex (Gribun et al., 2008), and the heterodimer Arp4-Act1 (Fenn et al., 2011; Nishimoto et al., 2012) are also found in the SWR1-related INO80 complex. These complexes share functions in H2A.Z localization (Mizuguchi et al., 2004; Papamichos-Chronakis et al., 2011) and DNA repair (Morrison and Shen, 2009). SWR1 also shares Swc4, Yaf9, Arp4 and Act1—a majority of its N-Module—with the histone acetyltransferase NuA4 (Lu et al., 2009), whose acetylation of H2A and H4 enhances SWR1 activity (Altaf et al., 2010). Interesting, all three complexes—SWR1, INO80, and NuA4—converge functionally at H2A.Z and compositionally at Arp4-Act1. Modular assembly has also been observed biochemically for INO80 (Chen et al., 2011; Kapoor et al., 2013) and may also occur in NuA4 (Chittuluru et al., 2011). Although it is unclear whether these complexes can shuffle common functional modules among them, we speculate that sharing of modules might play an important role in cooperative recruitment and collective activity of functionally related complexes.

The Rvb1/2 ring provides an assembly platform that connects all functional modules in the complex

In SWR1, the core subunit Swr1 recruits the N-Module to its N-terminal half and the C-Module and Rvb1/2 to the C-terminal half (Wu et al., 2005; 2009). This assembly map places Swr1 at the center of the complex, where it brings together individual modules *via* separate domains. Our structural data modify this model by showing that Swr1 adopts a peripheral position in the complex, with most of its mass, including the catalytic ATPase domain, spatially separated from the Rvb1/2 ring (Figure 2.7). Their interaction across the complex may be supported by the unique extra-long insert within the Swr1 ATPase (Wu et al., 2005). While we were unable to identify cross-links between this insert domain and the Rvb's, we found that the N-terminal HSA domain in Swr1 and the HSA-associated Arp4 subunit directly cross-linked to Rvb1 (Figure 2.9A,B). This indicates that the N-terminal half of Swr1 extends across the complex and may play a role in the interaction between the N-Module and the Rvb1/2 ring. We propose that while Swr1 functions as a recruitment platform for the N- and C-Modules (Wu et al., 2009), the Rvb1/2 ring serves as an assembly platform that coordinates and stabilizes their side-by-side arrangement, resulting in a complex in which all functional components are interconnected.

While Rvb1 and Rvb2 have been reported to adopt various oligomeric states that confer different levels of activity in isolation (Cheung et al., 2010a), they have not been structurally characterized in the context of a larger complex. We determined structurally and biochemically that Rvb1 and Rvb2 associate with the SWR1 complex as a single hetero-hexameric ring (Figure 2.5). The Rvb insert domains are well resolved in the 3D map, allowing us to unambiguously establish the orientation of the ring relative to the rest of the complex (Figure 2.5D,H). The Rvb

inserts, which are known to be flexible (López-Perrote et al., 2012; Petukhov et al., 2012), face the core of SWR1, with their globular regions protruding from the 3D map. These regions could be accommodated by the adjacent globular densities in the map upon an upward rotation towards the core of the complex (Figure 2.5H). A similar rearrangement has been shown for the dodecameric structure of yeast Rvb1/2, where two hexameric rings interact *via* their rearranged Rvb insert domains (Torreira et al., 2008). Our data indicate that interactions between the ring and the core of SWR1 are also mediated by the Rvb inserts in a rearranged conformation. Furthermore, while it has been proposed that in solution the Rvb's alternate between single and double-ring conformations with distinct functions (Cheung et al., 2010a), their orientation in SWR1 renders the Rvb inserts unavailable for interaction with a second ring, thus preventing formation of the dodecameric structures. Our biochemical quantitation of the Rvb1:Rvb2:Swr1 stoichiometry is in agreement with the 3:3:1 ratios indicated by the structural and proteomic data (Figure 2.5I). Although ~6:6:1 ratios have previously been reported for the highly related INO80 complex (Kapoor et al., 2013; Shen et al., 2000), suggesting the presence of 2 hexameric rings, our quantitation in INO80 also resulted in ~3:3:1 stoichiometry (Figure 2.5J). Therefore, we conclude that remodelers in the INO80 sub-family are characterized by the presence of a single hetero-hexameric Rvb1-Rvb2 ring.

This study presents the 3D structure of SWR1, revealing an interconnected assembly of discrete functional domains. This is also the first structural characterization of the functionally diverse AAA+ proteins Rvb1 and Rvb2 in the context of a larger complex. In SWR1, they form a single hetero-hexameric ring and serve as an assembly platform that connects all functional modules within the complex. In isolation, the highest levels of activity—DNA-stimulated ATPase activity and nucleotide-dependent conformational changes (Gribun et al., 2008)—have

been reported for a single Rvb1/2 hetero-hexamer. Together with our structural data, this observation allows for the possibility that nucleotide- or substrate-dependent conformational changes in the ring serve to mediate global structural dynamics involved in the dimer-exchange reaction.

EXPERIMENTAL PROCEDURES

Protein purification

SWR1 was affinity-purified from *S. cerevisiae* as previously described (Luk et al., 2010). We prepared a glycerol-formaldehyde gradient in a 4 mL ultracentrifuge tube (Beckman Ultra-Clear™) by layering 2 mL of "SWR1 buffer" (25 mM HEPES-KOH, pH 7.6, 1 mM EDTA, 2 mM $MgCl_2$, 0.01% NP-40, 1 mM DTT, 100 mM KCl) containing 10% glycerol and 0.2% formaldehyde over 2 mL of SWR1 buffer containing 60% glycerol and 1.5% formaldehyde. The gradient was formed using a GradientMaster instrument (Model 107ip, BioComp). After applying 4-10 pmoles of SWR1 to the top of the gradient, we centrifuged the sample in a SW 60 Ti rotor (Beckman) at 35,000 rpm and 4°C for 20 hours. We then manually fractionated the gradient from bottom to top into 100 μL fractions and quenched the formaldehyde in each fraction using 80 mM glycine. We stored the fractions at 4°C.

To determine the best fraction to image, we reversed the cross-links for 15 μL of each fraction in 0.3 M Tris, 0.1% SDS, and β-mercaptoethanol for 12 hours at 65°C and 30 minutes at 95°C in a thermocycler (Jackson, 1999). We screened for fractions containing the full complement of 14 subunits by running the treated samples in a 10% SDS-PAGE gel and silver-staining it. All samples used for EM data collection were dialyzed against SWR1 buffer without glycerol before staining.

Electron Microscopy

Sample preparation

We obtained the initial models of SWR1 using negatively stained samples. We applied 5-10 μL of the peak fraction to EM holey grids coated with a thin layer of carbon, let the sample absorb

for 15-30 minutes at 4^0C, rinsed them directly on drops of stain (2% uranyl formate) and then floated a second layer of thin carbon ("sandwich") before drying the grid under a flow of N_2 gas.

The initial models were refined against cryo-negative stain (cryo-NS) data. For cryo-NS samples, we stained as described above but, instead of drying, we froze the stained grids in liquid nitrogen (De Carlo and Stark, 2010).

Imaging

To build the initial 3D models for SWR1, we collected images under low-dose conditions at $+45^o$ and -45^o in a Tecnai G2 Spirit microscope (FEI, Hillsboro, OR), equipped with a US4000 4k x 4k CCD camera (Gatan, Inc, Pleasanton, CA) at a nominal magnification of 60,000 and with a dose of ~ 20 electrons/Å^2. The pixel size at the sample level was 1.65Å.

To obtain data for refinement, we collected untilted cryo-negative data at liquid-nitrogen temperature and under low-dose conditions. We used a field-emission gun (FEG) Tecnai G2 F20 transmission electron microscope (FEI) operating at 120 keV and equipped with a Gatan 4k x 4k CCD. Images were collected at a nominal magnification of 62,000x and an electron dose of ~20 electrons/Å^2. The pixel size at the sample level was 1.73 Å.

Initial model generation

In order to extract the molecular images from the micrographs we windowed out particles in one set of micrographs (-45^o) using the Boxer interface in EMAN1 (Ludtke et al., 1999) and used custom-built SPIDER (Frank et al., 1996) scripts to calculate alignment parameters between the $+45^o$ and -45^o micrographs and extract the tilt mates in the $+45^o$ (Leschziner, 2010). We estimated and corrected for the Contrast Transfer Function (CTF) using the program CTFTILT (Mindell and Grigorieff, 2003) and the SPIDER command TF CT. Single particles were binned

by 2, resulting in a pixel size of 3.3 Å. We combined the +45^{o} and -45^{o} datasets into a stack of ~32,000 particles and performed 2D alignment and classification in IMAGIC (Van Heel et al., 1996). We computed initial models from classes containing 100-200 members using the Orthogonal Tilt Reconstruction approach as described (Leschziner, 2010).

Projection-matching refinement

We initially refined the OTR models against 2D class averages of cryo-negative data. To generate the class averages, we extracted particles from the micrographs as described above and performed CTF estimation and phase flipping using the EMAN2 workflow (Tang et al., 2007). Then, the particles were binned by 2, resulting in a pixel size of 3.45 Å. We subjected ~32,000 particles to reference-free 2D alignment and classification in IMAGIC (Van Heel et al., 1996). In order to minimize heterogeneity, we generated classes with relatively few (15-20) particles.

We filtered the OTR models to 80 Å resolution and performed 15-23 iterations of projection matching refinement using angular steps of 25^{o}, 20^{o}, 15^{o}, 10^{o}, and 8^{o}-5^{o} (every degree) against 2D class averages in SPIDER (Frank et al., 1996) using the AP SH and BP 32F commands. To minimize noise in the reconstructions, we applied a threshold mask calculated for 500% to 150% the theoretical molecular weight of the sample (1.0 MDa). The mask was gradually tightened throughout refinement and its filtration was determined by the resolution of the 3D map, computed according to the 0.5 FSC criterion. Refinement results were stable after 15 iterations, and the resolutions of the 3D maps were 50-60 Å. We then refined the resulting 3D maps (without additional filtration) against single cryo-negative particles. For this step, we carried out 15 iterations of projection-matching refinement at angular steps 25^{o}, 21^{o}, 18^{o}, 15^{o},

13^{o}, 11^{o} and 10^{o}-4^{o} (every degree). Threshold masks computed for 500% to 100% the MW were also utilized.

Alignment of 2D images

To compare 3D maps against experimental class averages, we generated 2D re-projections of the filtered maps at defined theta values using the PJ 3Q command in SPIDER (Frank et al., 1996). The re-projections and experimental class averages were aligned to each other using the AP SH and RT SQ commands in SPIDER (Frank et al., 1996).

Visualization of and docking into 3D maps

We performed 3D structure analysis and image rendering using the UCSF Chimera package (Pettersen et al., 2004). EM-like 3D maps were generated from published crystal coordinates using the CP FROM PDB command in SPIDER (Frank et al., 1996). To dock 3D maps or crystal structures into our EM densities, we roughly placed the former into the latter and used Chimera's "Fit in Map" function for the final fitting.

Segmentation of the SWR1 3D map

We segmented the SWR1 3D map using the eraser tool in Chimera. We used the results from our module mapping (Figure 4) to guide the segmentation. Once we had obtained a segmented module using the eraser, we calculated the molecular weight of the enclosed volume by obtaining the number of voxels in Chimera.

Difference mapping

We performed 2D difference mapping of class averages by first aligning, rotating, and shifting them in IMAGIC (Van Heel et al., 1996) using the MSA-ALIGN command. Then, we normalized and subtracted the aligned images in SPIDER (Frank et al., 1996).

The difference maps were normalized (mean = 0, standard deviation = 1). Threshold masks were calculated for each of them, setting values below 2s to 0 and these masks were then applied to the normalized difference maps. The resulting images were colored in Photoshop by turning them into RGBs and converting the grayscale values to a rainbow gradient. The gradient begins at 2s (as determined by the thresholding) and ends at around 6s, based on the maximum pixel values present in each of the difference maps. These maxima changed slightly between difference maps, ranging from ~6s to ~7s. We used a single color scale for the figure for simplicity, even though it ignores small differences in the heights of the peaks among the images shown.

Homology model generation

The 3D homology model of *S. cerevisiae* Rvb1/2 hetero-hexamer was computed using the SWISS-MODEL interface (Bordoli and Schwede, 2012). We used the crystal structure of the human Rvb1 homolog (2C9O, (Matias et al., 2006)) as the template to align sequences for *Saccharomyces cerevisiae* Rvb1 (YDR190C) and Rvb2 (YPL235W). With the 3D homology models for the Rvb1 and Rvb2 monomers, we generated the hetero-hexameric Rvb1/2 model in PyMOL (The PyMOL Molecular Graphics System, Version 1.5.0.4 Schrödinger, LLC) by computationally aligning each monomer to the corresponding homolog in the crystal structure of the truncated human Rvb1/2 hexameric ring (2XSZ, (Gorynia et al., 2011)). The composite final

structure was saved as a PDB file. Subsequent analyses involving this homology model were carried out in UCSF Chimera (Pettersen et al., 2004).

Stoichiometry quantification

Purified SWR1 and INO80 complexes were resolved on 4-12 % Bis-Tris gel (Novex) with MOPS running buffer. Protein gels were stained with Coomassie or Sypro Orange dye and imaged on Fuji Image Quant LAS 3000. Intensity of relevant protein bands was measured using Image Quant TL software (GE). The ratios of Swr1 or Ino80 to Rvb1 and Rvb2 were calculated after normalizing the band intensities for protein size.

Chemical cross-linking coupled to mass spectrometry

We cross-linked roughly 45 μg of sample with 1 mM disuccinimidyl suberate d0/d12 (DSS, Creativemolecules Inc.) directly in SWR1 buffer at 37°C for 30 minutes and subsequently quenched the reaction by adding ammonium bicarbonate to a final concentration of 50 mM for 10 minutes at 37° C.

We reduced the sample with 2.5 mM Tris (2-Carboxyethyl) phosphine hydrochloride (TCEP, Pierce) in 8 M urea at 37° C for 30 minutes and subsequently alkylated it with 5 mM iodoacetamide (Sigma-Aldrich) for 30 minutes at room temperature in the dark. For digestion, we diluted the sample with ammonium bicarbonate to a 1M final concentration of urea and added 2% w/w trypsin (Promega). Digestion was carried out at 37° C over night and stopped by acidification to 2 % (w/v) trifluoroacetic acid (TFA). We purified peptides with Sep-Pak C18 MicroSpin columns (Waters, Milford, MA), according to the manufacturer's protocol, followed by enrichment of cross-linked peptides using size exclusion chromatography (Leitner et al.,

2012). We carried out LC-MS/MS analysis on an Orbitrap Elite mass spectrometer (Thermo Scientific, San Jose, CA).

We searched the data using XQuest (Rinner et al., 2008) in iontag mode against a database containing the protein sequences of all 14 previously identified SWR1 proteins with a precursor mass tolerance of up to 20 ppm. For matching of fragment ions tolerances of 0.2 Da for common-ions and 0.3 Da for cross-link ions were used. We identified cross-linked peptides with a linear discriminant (ld) score > 25 and further analyzed them by visual inspection in order to ensure good matches of ion series on both cross-linked peptide chains for the most abundant peaks

REFERENCES

Altaf, M., Auger, A., Monnet-Saksouk, J., Brodeur, J., Piquet, S., Cramet, M., Bouchard, N., Lacoste, N., Utley, R.T., Gaudreau, L., et al. (2010). NuA4-dependent acetylation of nucleosomal histones H4 and H2A directly stimulates incorporation of H2A.Z by the SWR1 complex. J Biol Chem *285*, 15966–15977.

Bordoli, L., and Schwede, T. (2012). Automated protein structure modeling with SWISS-MODEL Workspace and the Protein Model Portal. Methods Mol Biol *857*, 107–136.

Boyer, L.A., Latek, R.R., and Peterson, C.L. (2004). The SANT domain: a unique histone-tail-binding module? Nat Rev Mol Cell Biol *5*, 158–163.

Chandramouli, P., Hernandez-Lopez, R., Wang, H.-W., and Leschziner, A.E. (2011). Validation of the orthogonal tilt reconstruction method with a biological test sample. J Struct Biol *175*, 85–96.

Chen, J., Miller, A., Kirchmaier, A.L., and Irudayaraj, J.M.K. (2012). Single Molecule Tools Elucidate H2A.Z Nucleosome Composition. Journal of Cell Science.

Chen, L., Cai, Y., Jin, J., Florens, L., Swanson, S.K., Washburn, M.P., Conaway, J.W., and Conaway, R.C. (2011). Subunit organization of the human INO80 chromatin remodeling complex: an evolutionarily conserved core complex catalyzes ATP-dependent nucleosome remodeling. J Biol Chem *286*, 11283–11289.

Cheung, K.L.Y., Huen, J., Houry, W.A., and Ortega, J. (2010a). Comparison of the multiple oligomeric structures observed for the Rvb1 and Rvb2 proteins. Biochem Cell Biol *88*, 77–88.

Cheung, K.L.Y., Huen, J., Kakihara, Y., Houry, W.A., and Ortega, J. (2010b). Alternative oligomeric states of the yeast Rvb1/Rvb2 complex induced by histidine tags. Journal of Molecular Biology *404*, 478–492.

Chittuluru, J.R., Chaban, Y., Monnet-Saksouk, J., Carrozza, M.J., Sapountzi, V., Selleck, W., Huang, J., Utley, R.T., Cramet, M., Allard, S., et al. (2011). Structure and nucleosome interaction of the yeast NuA4 and Piccolo–NuA4 histone acetyltransferase complexes. Nature Structural & Molecular Biology *18*, 1196–1203.

Clapier, C.R., and Cairns, B.R. (2009). The biology of chromatin remodeling complexes. Annu Rev Biochem *78*, 273–304.

De Carlo, S., and Stark, H. (2010). Cryonegative staining of macromolecular assemblies. Meth Enzymol *481*, 127–145.

Draker, R., Ng, M.K., Sarcinella, E., Ignatchenko, V., Kislinger, T., and Cheung, P. (2012). A Combination of H2A.Z and H4 Acetylation Recruits Brd2 to Chromatin during Transcriptional Activation. PLoS Genet *8*, e1003047.

Durant, M., and Pugh, B.F. (2007). NuA4-directed chromatin transactions throughout the

Saccharomyces cerevisiae genome. Molecular and Cellular Biology *27*, 5327–5335.

Fan, J.Y., Gordon, F., Luger, K., Hansen, J.C., and Tremethick, D.J. (2002). The essential histone variant H2A.Z regulates the equilibrium between different chromatin conformational states. Nat Struct Biol *9*, 172–176.

Fan, J.Y., Rangasamy, D., Luger, K., and Tremethick, D.J. (2004). H2A.Z alters the nucleosome surface to promote HP1alpha-mediated chromatin fiber folding. Molecular Cell *16*, 655–661.

Fenn, S., Breitsprecher, D., Gerhold, C.B., Witte, G., Faix, J., and Hopfner, K.-P. (2011). Structural biochemistry of nuclear actin-related proteins 4 and 8 reveals their interaction with actin. Embo J *30*, 2153–2166.

Frank, J., Radermacher, M., Penczek, P., Zhu, J., Li, Y., Ladjadj, M., and Leith, A. (1996). SPIDER and WEB: processing and visualization of images in 3D electron microscopy and related fields. J Struct Biol *116*, 190–199.

Galarneau, L., Nourani, A., Boudreault, A.A., Zhang, Y., Héliot, L., Allard, S., Savard, J., Lane, W.S., Stillman, D.J., and Côté, J. (2000). Multiple links between the NuA4 histone acetyltransferase complex and epigenetic control of transcription. Molecular Cell *5*, 927–937.

Gorynia, S., Bandeiras, T.M., Pinho, F.G., Mcvey, C.E., Vonrhein, C., Round, A., Svergun, D.I., Donner, P., Matias, P.M., and Carrondo, M.A. (2011). Structural and functional insights into a dodecameric molecular machine - The RuvBL1/RuvBL2 complex. J Struct Biol *176*, –291.

Gribun, A., Cheung, K.L.Y., Huen, J., Ortega, J., and Houry, W.A. (2008). Yeast Rvb1 and Rvb2 are ATP-dependent DNA helicases that form a heterohexameric complex. Journal of Molecular Biology *376*, 1320–1333.

Guillemette, B., and Gaudreau, L. (2006). Reuniting the contrasting functions of H2A.Z. Biochem Cell Biol *84*, 528–535.

Hartley, P.D., and Madhani, H.D. (2009). Mechanisms that specify promoter nucleosome location and identity. Cell *137*, 445–458.

Jackson, V. (1999). Formaldehyde cross-linking for studying nucleosomal dynamics. Methods *17*, 125–139.

Jacobson, R.H., Ladurner, A.G., King, D.S., and Tjian, R. (2000). Structure and function of a human TAFII250 double bromodomain module. Science *288*, 1422–1425.

Jónsson, Z.O., Jha, S., Wohlschlegel, J.A., and Dutta, A. (2004). Rvb1p/Rvb2p recruit Arp5p and assemble a functional Ino80 chromatin remodeling complex. Molecular Cell *16*, 465–477.

Kapoor, P., Chen, M., Winkler, D.D., Luger, K., and Shen, X. (2013). Evidence for monomeric actin function in INO80 chromatin remodeling. Nature Structural & Molecular Biology *20*, 426–432.

Kastner, B., Fischer, N., Golas, M.M., Sander, B., Dube, P., Boehringer, D., Hartmuth, K., Deckert, J., Hauer, F., Wolf, E., et al. (2008). GraFix: sample preparation for single-particle electron cryomicroscopy. Nat Meth *5*, 53–55.

Kobor, M.S., Venkatasubrahmanyam, S., Meneghini, M.D., Gin, J.W., Jennings, J.L., Link, A.J., Madhani, H.D., and Rine, J. (2004). A protein complex containing the conserved Swi2/Snf2-related ATPase Swr1p deposits histone variant H2A.Z into euchromatin. PLoS Biol *2*, E131.

Krogan, N.J., Keogh, M.C., Datta, N., Sawa, C., Ryan, O.W., Ding, H., Haw, R.A., Pootoolal, J., Tong, A., Canadien, V., et al. (2003). A Snf2 family ATPase complex required for recruitment of the histone H2A variant Htz1. Molecular Cell *12*, 1565–1576.

Leitner, A., Reischl, R., Walzthoeni, T., Herzog, F., Bohn, S., Förster, F., and Aebersold, R. (2012). Expanding the chemical cross-linking toolbox by the use of multiple proteases and enrichment by size exclusion chromatography. Mol Cell Proteomics *11*, M111.014126.

Leitner, A., Walzthoeni, T., Kahraman, A., Herzog, F., Rinner, O., Beck, M., and Aebersold, R. (2010). Probing native protein structures by chemical cross-linking, mass spectrometry, and bioinformatics. Mol Cell Proteomics *9*, 1634–1649.

Leschziner, A. (2010). The orthogonal tilt reconstruction method. Meth Enzymol *482*, 237–262.

López-Perrote, A., Muñoz-Hernández, H., Gil, D., and Llorca, O. (2012). Conformational transitions regulate the exposure of a DNA-binding domain in the RuvBL1-RuvBL2 complex. Journal of Biological Chemistry.

Lu, P.Y.T., Lévesque, N., and Kobor, M.S. (2009). NuA4 and SWR1-C: two chromatin-modifying complexes with overlapping functions and components. Biochem Cell Biol *87*, 799–815.

Ludtke, S.J., Baldwin, P.R., and Chiu, W. (1999). EMAN: semiautomated software for high-resolution single-particle reconstructions. J Struct Biol *128*, 82–97.

Luk, E., Ranjan, A., Fitzgerald, P.C., Mizuguchi, G., Huang, Y., Wei, D., and Wu, C. (2010). Stepwise histone replacement by SWR1 requires dual activation with histone H2A.Z and canonical nucleosome. Cell *143*, 725–736.

Matias, P.M., Gorynia, S., Donner, P., and Carrondo, M.A. (2006). Crystal structure of the human AAA+ protein RuvBL1. J Biol Chem *281*, 38918–38929.

Mindell, J.A., and Grigorieff, N. (2003). Accurate determination of local defocus and specimen tilt in electron microscopy. J Struct Biol *142*, 334–347.

Mizuguchi, G., Shen, X., Landry, J., Wu, W.-H., Sen, S., and Wu, C. (2004). ATP-driven exchange of histone H2AZ variant catalyzed by SWR1 chromatin remodeling complex. Science *303*, 343–348.

Morrison, A.J., and Shen, X. (2009). Chromatin remodelling beyond transcription: the INO80

and SWR1 complexes. Nat Rev Mol Cell Biol *10*, 373–384.

Nishimoto, N., Watanabe, M., Watanabe, S., Sugimoto, N., Yugawa, T., Ikura, T., Koiwai, O., Kiyono, T., and Fujita, M. (2012). Heterocomplex Formation by Arp4 and β-Actin Involved in Integrity of the Brg1 Chromatin Remodeling Complex. Journal of Cell Science.

Pamblanco, M., Poveda, A., Sendra, R., Rodríguez-Navarro, S., Pérez-Ortín, J.E., and Tordera, V. (2001). Bromodomain factor 1 (Bdf1) protein interacts with histones. Febs Letters *496*, 31–35.

Papamichos-Chronakis, M., Watanabe, S., Rando, O.J., and Peterson, C.L. (2011). Global regulation of H2A.Z localization by the INO80 chromatin-remodeling enzyme is essential for genome integrity. Cell *144*, 200–213.

Park, Y.-J., Dyer, P.N., Tremethick, D.J., and Luger, K. (2004). A new fluorescence resonance energy transfer approach demonstrates that the histone variant H2AZ stabilizes the histone octamer within the nucleosome. J Biol Chem *279*, 24274–24282.

Pettersen, E.F., Goddard, T.D., Huang, C.C., Couch, G.S., Greenblatt, D.M., Meng, E.C., and Ferrin, T.E. (2004). UCSF Chimera--a visualization system for exploratory research and analysis. J Comput Chem *25*, 1605–1612.

Petukhov, M., Dagkessamanskaja, A., Bommer, M., Barrett, T., Tsaneva, I., Yakimov, A., Quéval, R., Shvetsov, A., Khodorkovskiy, M., Käs, E., et al. (2012). Large-Scale Conformational Flexibility Determines the Properties of AAA+ TIP49 ATPases. Journal of Biological Chemistry *20*, 1321–1331.

Puri, T., Wendler, P., Sigala, B., Saibil, H., and Tsaneva, I.R. (2007). Dodecameric structure and ATPase activity of the human TIP48/TIP49 complex. Journal of Molecular Biology *366*, 179–192.

Ranjan, A., Mizuguchi, G., Fitzgerald, P.C., Wei, D., Wang, F., Huang, Y., Luk, E., Woodcock, C.L., and Wu, C. (2013). Nucleosome-free Region Dominates Histone Acetylation in Targeting SWR1 to Promoters for H2A.Z Replacement. Cell *154*, 1232–1245.

Rinner, O., Seebacher, J., Walzthoeni, T., Mueller, L.N., Beck, M., Schmidt, A., Mueller, M., and Aebersold, R. (2008). Identification of cross-linked peptides from large sequence databases. Nat Meth *5*, 315–318.

Schubert, H.L., Wittmeyer, J., Kasten, M.M., Hinata, K., Rawling, D.C., Heroux, A., Cairns, B.R., and Hill, C.P. (2013). Structure of an actin-related subcomplex of the SWI/SNF chromatin remodeler. Pnas *110*, 3345–3350.

Shen, X., Mizuguchi, G., Hamiche, A., and Wu, C.-H. (2000). A chromatin remodelling complex involved in transcription and DNA processing. Nature *406*, 541–544.

Stark, H. (2010). GraFix: stabilization of fragile macromolecular complexes for single particle cryo-EM. Meth Enzymol *481*, 109–126.

Sunada, R., Görzer, I., Oma, Y., Yoshida, T., Suka, N., Wintersberger, U., and Harata, M. (2005). The nuclear actin-related protein Act3p/Arp4p is involved in the dynamics of chromatin-modulating complexes. Yeast *22*, 753–768.

Suto, R.K., Clarkson, M.J., Tremethick, D.J., and Luger, K. (2000). Crystal structure of a nucleosome core particle containing the variant histone H2A.Z. Nat Struct Biol *7*, 1121–1124.

Szerlong, H., Hinata, K., Viswanathan, R., Erdjument-Bromage, H., Tempst, P., and Cairns, B.R. (2008). The HSA domain binds nuclear actin-related proteins to regulate chromatin-remodeling ATPases. Nature Structural & Molecular Biology *15*, 469–476.

Tang, G., Peng, L., Baldwin, P.R., Mann, D.S., Jiang, W., Rees, I., and Ludtke, S.J. (2007). EMAN2: an extensible image processing suite for electron microscopy. J Struct Biol *157*, 38–46.

Torreira, E., Jha, S., López-Blanco, J.R., Arias-Palomo, E., Chacón, P., Cañas, C., Ayora, S., Dutta, A., and Llorca, O. (2008). Architecture of the pontin/reptin complex, essential in the assembly of several macromolecular complexes. Structure *16*, 1511–1520.

Van Heel, M., Harauz, G., Orlova, E.V., Schmidt, R., and Schatz, M. (1996). A new generation of the IMAGIC image processing system. J Struct Biol *116*, 17–24.

Venters, B.J., and Pugh, B.F. (2009). A canonical promoter organization of the transcription machinery and its regulators in the Saccharomyces genome. Genome Research *19*, 360–371.

Wu, W.-H., Alami, S., Luk, E., Wu, C.-H., Sen, S., Mizuguchi, G., Wei, D., and Wu, C. (2005). Swc2 is a widely conserved H2AZ-binding module essential for ATP-dependent histone exchange. Nature Structural & Molecular Biology *12*, 1064–1071.

Wu, W.-H., Wu, C.-H., Ladurner, A., Mizuguchi, G., Wei, D., Xiao, H., Luk, E., Ranjan, A., and Wu, C. (2009). N terminus of Swr1 binds to histone H2AZ and provides a platform for subunit assembly in the chromatin remodeling complex. J Biol Chem *284*, 6200–6207.

Yen, K., Vinayachandran, V., and Pugh, B.F. (2013). SWR-C and INO80 Chromatin Remodelers Recognize Nucleosome-free Regions Near +1 Nucleosomes. Cell *154*, 1246–1256.

Zhang, H., Roberts, D.N., and Cairns, B.R. (2005). Genome-wide dynamics of Htz1, a histone H2A variant that poises repressed/basal promoters for activation through histone loss. Cell *123*, 219–231.

Chapter Three

Substrate-dependent conformational dynamics of the SWR1 complex

Part of this work was completed in collaboration with Anand Ranjan, Feng Wang, and Debbie Wei in Carl Wu's group (NIH/NCI/HHMI). A.R and D.W performed purification of endogenous SWR1 from *Saccharomyces cerevisiae* and *in vitro* assembly of recombinant mononucleosomes. F.W designed and purified H2A.Z/H2B dimers.

INTRODUCTION

Histone-dimer exchange by SWR1 involves the remodeler recruiting its two obligate substrates—the nucleosome and the H2A.Z/H2B dimer (Z/B). Interestingly, *in vitro*, these binding events appear to occur independently and synergistically activate SWR's ATPase activity (Luk et al., 2010). Biochemical analysis of SWR1-nucleosome interaction unveiled a marked preference of the enzyme for substrates harboring extranucleosomal, or linker, DNA (Ranjan et al., 2013). This study found that there is a significant difference in affinity of the enzyme for the substrate containing between 40 and 50 basepairs of linker DNA. ChIP data on the *in vivo* footprint of SWR1 corroborated the biochemical results, indicating that the complex contacts 60 basepairs of linker DNA on the promoter side of the +1 nucleosome (Yen et al., 2013). These two studies also assigned the recognition of linker DNA to the Swc2 subunit. A patch of basic residues residing on the conserved N-terminal region of the Swc2 polypeptide has been identified as the DNA-interaction domain (Ranjan et al., 2013) (Figure 3.1B). Thus, the nucleosome-depleted region directly contacts Swc2 and likely serves as a major recruitment feature for the SWR1 complex.

Remarkably, the *in vivo* footprint of the catalytic subunit Swr1, obtained using ChIP, showed that it contacts the nucleosome at a site very close to the linker DNA (Figure 3.1A) (Yen et al., 2013). This is in marked contrast to all other characterized remodelers, whose catalytic ATPase domains interact with the nucleosome around SHL-2 (Figure 1.9) (Dechassa et al., 2012; 2008; Gangaraju et al., 2009; Saha et al., 2005; Schwanbeck et al., 2004). Swr1's contact site is between SHL-7 and SHL-5, where histone-DNA interactions are energetically weak (Figure 1.4) (Hall et al., 2009). Interestingly, binding here brings the translocase close to a region of relatively strong interactions, between SHL-5 and 4, where the H2A/H2B dimer is found (Figure

1.4). This site is likely to be SWR1's main energetic barrier towards ejection of the canonical dimer, which is an obligate step in dimer exchange. Therefore, SWR1, like octamer-sliding remodelers, may have evolved to interact with the substrate nucleosome at a site most energetically favorable for its specialized function.

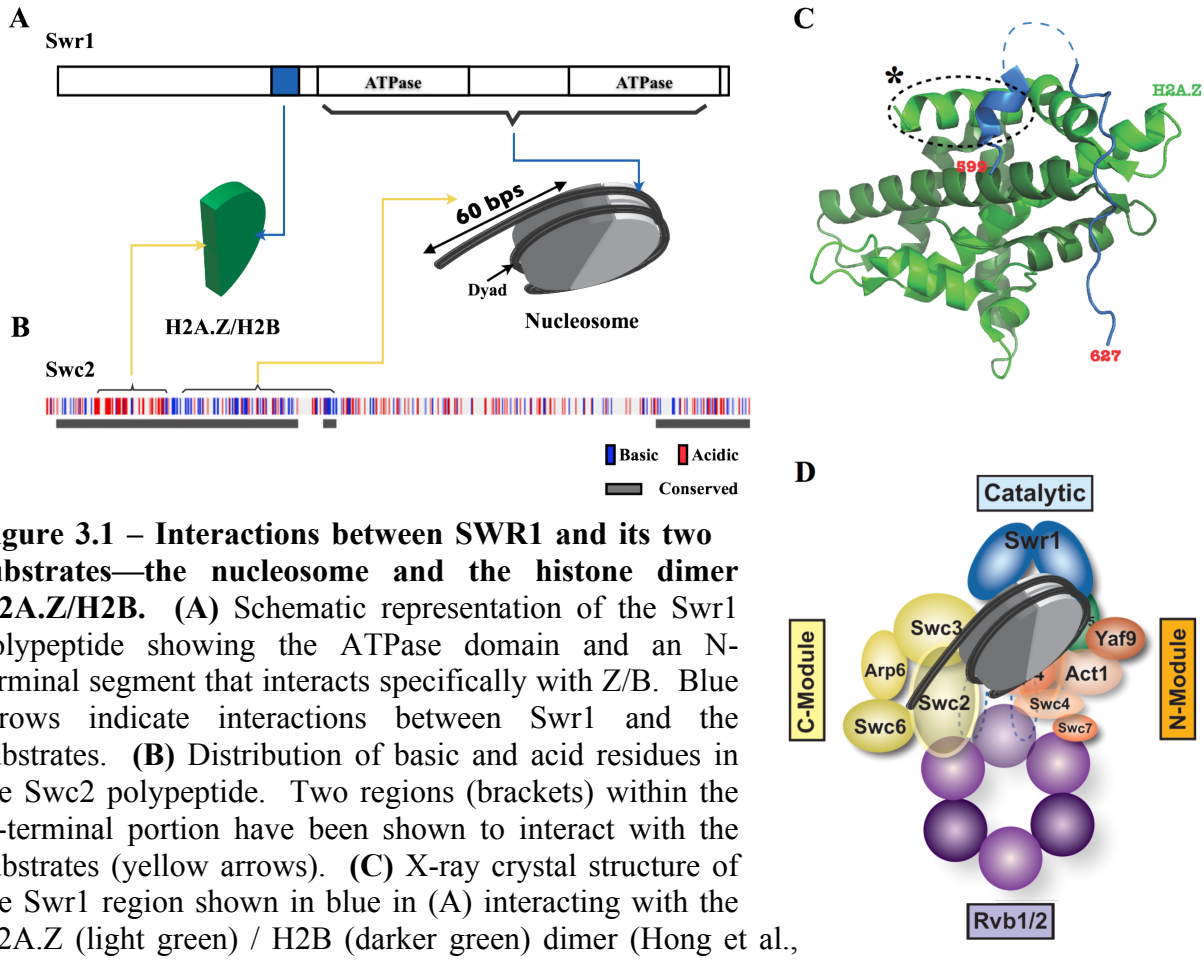

Figure 3.1 – Interactions between SWR1 and its two substrates—the nucleosome and the histone dimer H2A.Z/H2B. **(A)** Schematic representation of the Swr1 polypeptide showing the ATPase domain and an N-terminal segment that interacts specifically with Z/B. Blue arrows indicate interactions between Swr1 and the substrates. **(B)** Distribution of basic and acid residues in the Swc2 polypeptide. Two regions (brackets) within the N-terminal portion have been shown to interact with the substrates (yellow arrows). **(C)** X-ray crystal structure of the Swr1 region shown in blue in (A) interacting with the H2A.Z (light green) / H2B (darker green) dimer (Hong et al., 2014). Dashed oval and asterisk indicate an interaction with an H2A.Z-specific region. **(D)** Schematic representation of the SWR1-nucleosome interaction based on available information.

Swr1 and Swc2 not only recognize the substrate nucleosome but also contain domains that interact specifically with the Z/B dimer (Figure 3.1A-B). An acidic patch within the conserved N-terminal segment of the Swc2 polypeptide, immediately adjacent to the DNA-binding region (Figure 3.1B), interacts specifically with Z/B (Wu et al., 2005). Recently, a short

28 amino-acid segment of Swr1, N-terminal and adjacent to the ATPase domain, has been demonstrated to bind specifically to Z/B (Figure 3.1A) (Hong et al., 2014). The crystal structure of this interaction revealed electrostatic contacts of this region with the αC helix that characterizes H2A.Z (Figure 3.1C). Therefore, Swr1 also harbors a Z/B-binding domain. Since H2A.Z's αC helix provides the interaction surface for both Swr1 and Swc2 (Hong et al., 2014; Wu et al., 2005), it is unlikely that a single Z/B binds both subunits simultaneously. The mechanistic implication of two potentially independent Z/B binding sites in SWR1 is unclear, especially considering that dimer exchange is a stepwise process—only one of two H2A/H2B dimers is exchanged per reaction (Luk et al., 2010).

Despite the recent insights into substrate binding by SWR1, it is not known how the complex spatially coordinates its substrates to facilitate dimer exchange. Having two potential Z/B binding sites in SWR1 makes the enzyme-substrate stoichiometry an important question to address. Using the annotated apo-SWR1 structure as a model, we have characterized a SWR1-nucleosome complex and shown that the enzyme undergoes a significant conformational change upon contacted a surprisingly limited region in the nucleosome core particle. Knowledge of substrate preference has allowed us to assemble and purify a more biochemically stable SWR1-nucleosome complex, which we aim to characterize structurally. Lastly, we have also purified a homogenous sample containing the SWR1-nucleosome-Z/B ternary complex. Pursuing its structure will allow us to address important questions regarding substrate stoichiometry and spatial coordination.

RESULTS

SWR1 adopts an extended conformation in the presence of a nucleosome

Our 3D reconstruction of SWR1 does not show a deep central cavity that could accommodate a nucleosome, as has been observed for the RSC complex (Chaban et al., 2008; Leschziner et al., 2007). This suggested the possibility that SWR1 interacts with its substrate nucleosome in a different manner. To explore this possibility, we obtained the structure of SWR1 bound to a nucleosome. We carried out an *in vitro* nucleosome-binding reaction in the absence of nucleotide (Figure 3.2A) and purified the sample using the GraFix method, as we had done with SWR1 alone (Figure 3.2B). Western blotting confirmed the co-sedimentation of histones with SWR1 in the glycerol gradient (Figure 3.2C). Furthermore, the sample exhibited retarded electrophoretic mobility on a native gel relative to SWR1 alone that had been similarly purified (Figure 3.4A). This suggested that a majority of the SWR1 + nucleosome sample contained nucleosome-bound complexes. We imaged this sample under cryo-negative stain conditions.

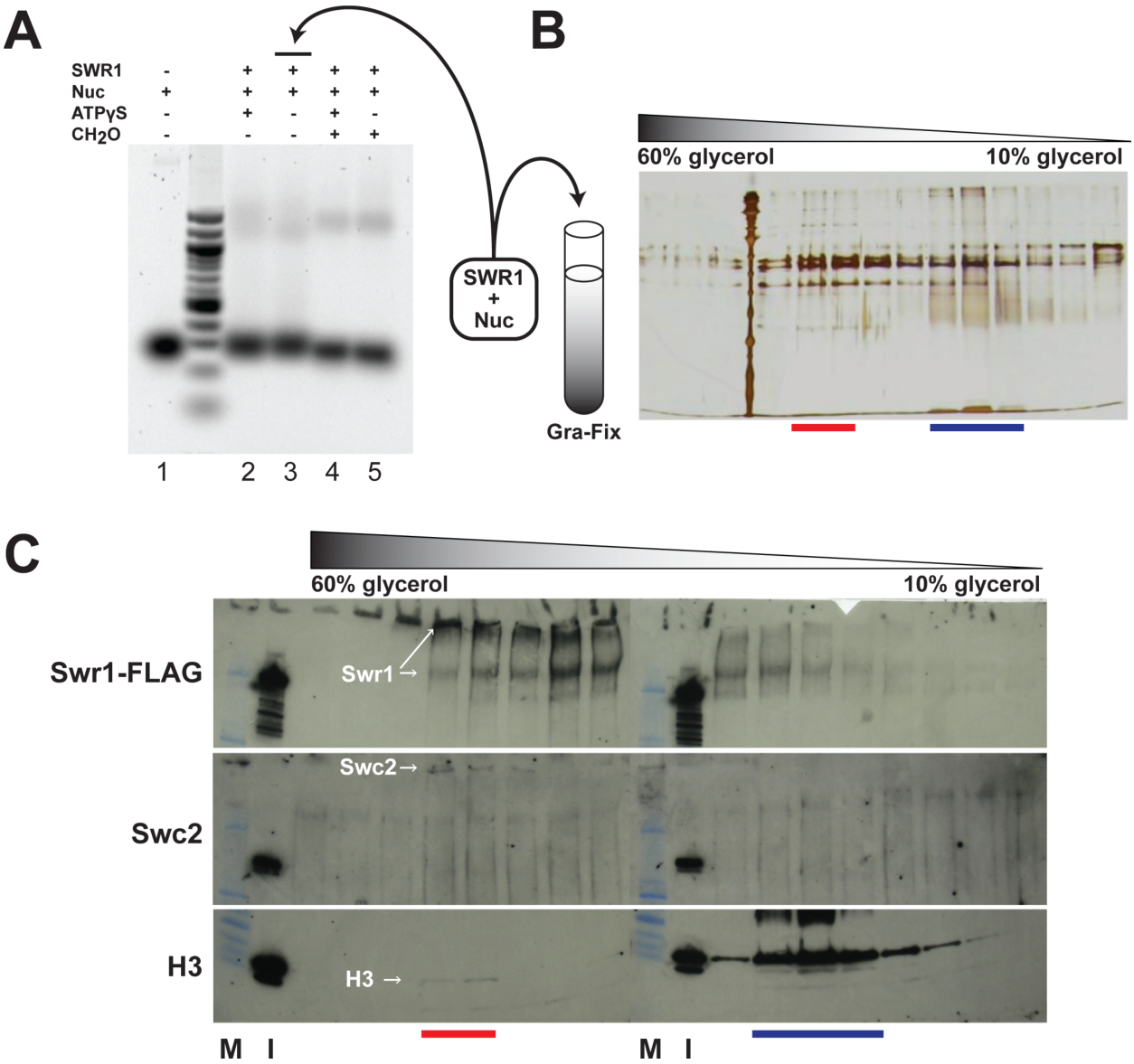

Figure 3.2 - Assessment of nucleosome binding by SWR1 after GraFix purification. (A) Agarose gel electrophoresis of nucleosome-binding reactions. SWR1 was incubated with recombinant nucleosomes in the presence (lanes 2 and 4) or absence (lanes 3 and 5) of ATPgS and formaldehyde (lanes 4 and 5). After incubation, the reactions were resolved on a 1.3% agarose gel at 4°C in 0.2X TB buffer, stained with Sybr Green I, and imaged using the Typhoon equipment. A free-nucleosome marker was run on lane 1. **(B)** The SWR1 + nucleosome sample (equivalent to that in lane 3) was stabilized and purified through a GraFix gradient. **(C)** Samples from selected GraFix fractions were electrophoresed in a 10% SDS-PAGE, transferred to a nitrocellulose membrane. Western blot was performed to identify H3, Swc2, and Swr1-FLAG. Due to incomplete reversal of formaldehyde crosslinking, the large subunits Swr1 and Swc2 were immobilized at the bottoms of the wells. Red and blue horizontal lines mark peaks for nucleosome-bound SWR1 and free nucleosomes, respectively. M: molecular weight marker. I: GraFix Input

To obtain the 3D reconstruction of the SWR1-nucleosome complex, we first refined our apo-SWR1 model against 2D class averages generated from the SWR1-nucleosome data (Figure 3.3A). Using the resulting 3D map as a starting model, we performed maximum-likelihood-based 3D classification of the entire single-particle SWR1-nucleosome dataset (Scheres, 2012a). We obtained 5 classes that displayed overall structural similarity (Figure 3.3B); however, several

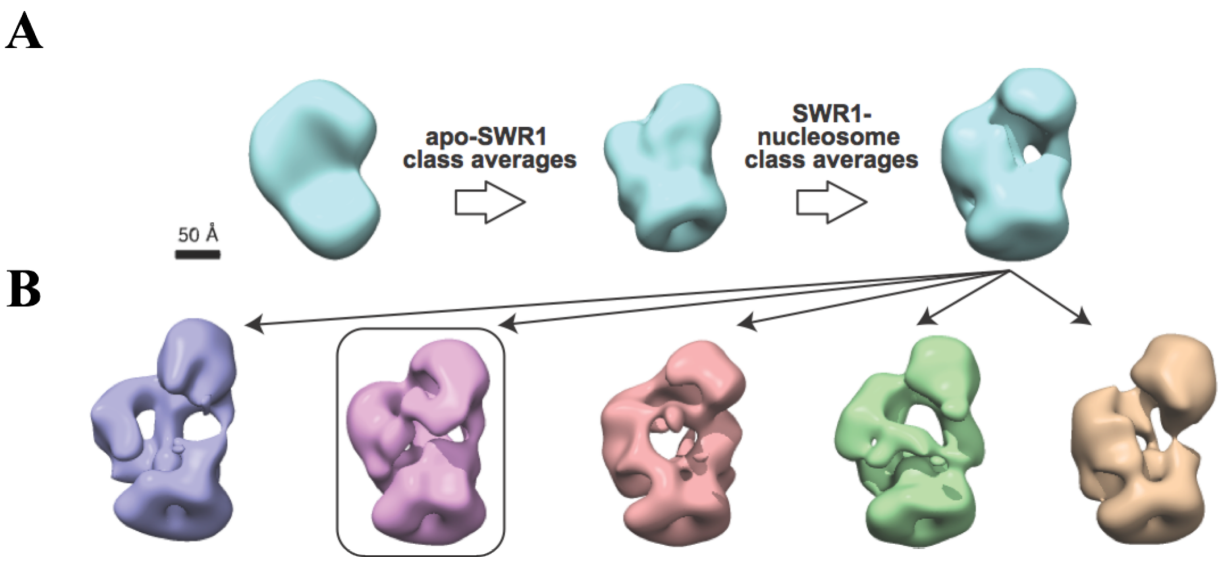

Figure 3.3 – Model generation and 3D classification of SWR1-Nucleosome data. (A) The initial 3D reconstruction of SWR1-nucleosome was generated using a strategy analogous to that used for the apo-SWR1 structure. The OTR initial model (left) was first refined by projection matching against reference-free class averages generated from untilted, cryo-negative stain (cryo-NS) images of apo-SWR1. The resulting structure (middle) was filtered to 60Å and refined by projection matching against reference-free class averages generated from untilted, cryo-NS images of SWR1-nucleosome. The final refined structure is shown to the right. **(B)** The 3D map obtained after the initial refinement (A) was used as the starting model to classify the SWR1-nucleosome data into five different reconstructions using the RELION software package (Scheres, 2012b). This panel shows the final five reconstructions generated by 3D classification. The boxed model was selected for single-model refinement against single particles assigned to the class.

of them were missing densities corresponding to either N- or C-Module (Figure 3.3B). Therefore, we selected the class in which we could account for all modules identified in the apo-SWR1 structure for projection-matching refinement. To minimize heterogeneity in the dataset,

we refined this model only against those images assigned to the specific class by the 3D classification procedure; this data set accounted for ~20% of the images. The resulting 3D structure had a resolution of 34 Å (Figure 3.4C,D).

The SWR1-nucleosome structure is elongated relative to apo-SWR1 along an axis perpendicular to the Rvb1/2 ring (Figure 3.4B-E). This elongation appears to be the result of an extension, away from the Rvb1/2 ring, of Swr1 and the C-Module (Figure 3.4B,C). Difference maps calculated between the apo-SWR1 and SWR1-nucleosome structures support this conformational change (Figure 3.4F-G), as does a comparison between re-projections of the apo-SWR1 3D map with reference-free class averages of the SWR1-nucleosome data (Figure 3.4I). At the reported resolution, we did not observe significant changes in the Rvb1/2 ring; Swr1 and the C-Module are the major densities that differ in position between the two structures (Figure 3.4F,G). We note that the sample used in this analysis was purified and imaged under identical conditions to nucleosome-free SWR1. Therefore, experimental and computational variations are unlikely to have contributed to the observed conformational difference.

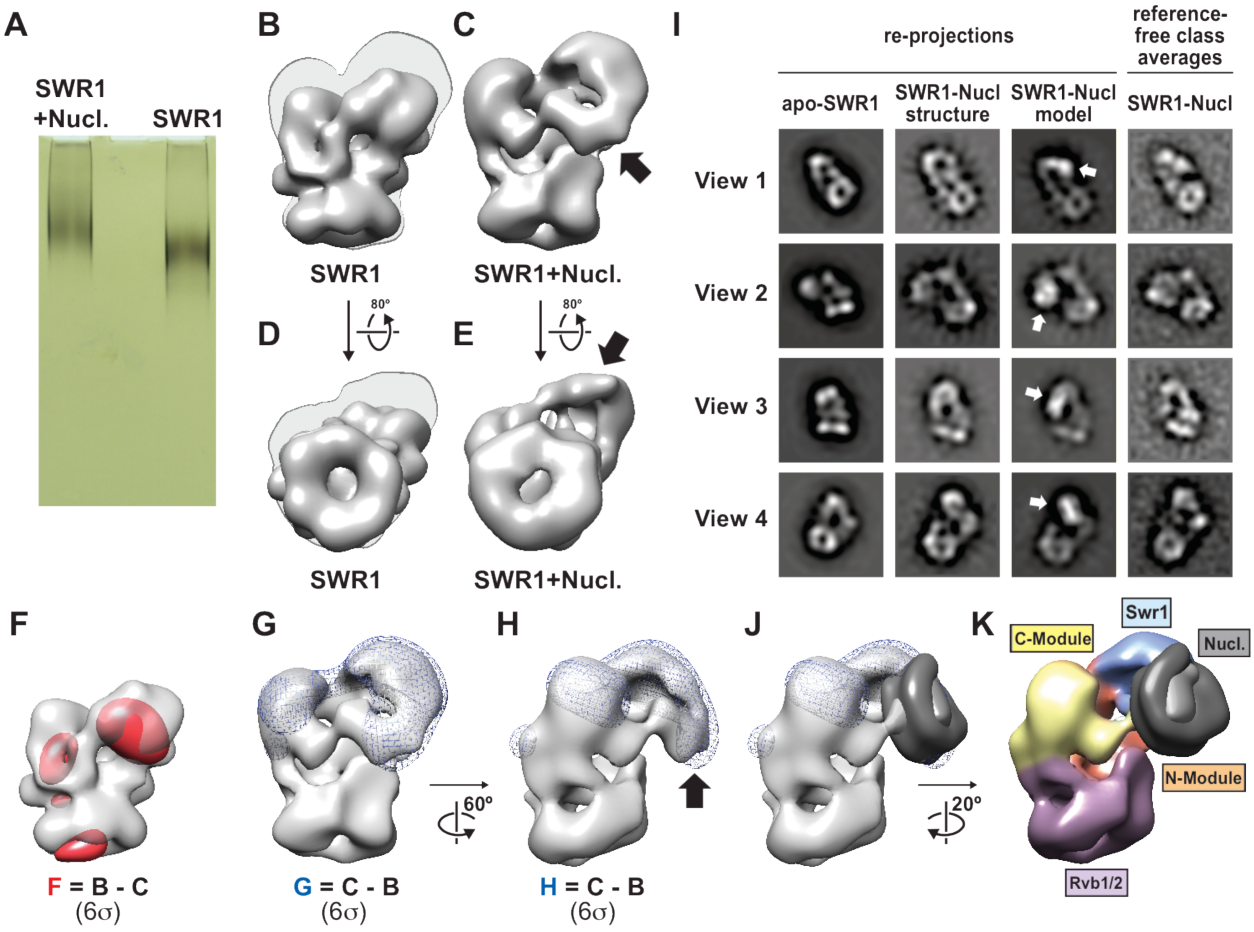

Figure 3.4 - SWR1 undergoes a conformational change in the presence of a nucleosome. (A) Native PAGE of GraFix-stabilized SWR1 + nucleosome (left) and SWR1 alone (right). **(B)** The structure of SWR1 (apo-SWR1) filtered to 34Å resolution. **(C)** Three-dimensional reconstruction of a SWR1-nucleosome complex at a resolution of 34Å. The shadow shown in (B) is the silhouette of the structure in (C) to highlight the overall elongation of the structure. **(D and E)** The structures in (B) and (C) are seen from the Rvb1/2 ring. The silhouette of the structure in (E) is shown behind the structure in (D). The arrows in (C) and (E) point to new densities visible in the SWR1-nucleosome reconstruction. **(F, G)** Difference maps obtained by subtracting: (F) SWR1-nucleosome (C) from apo-SWR1 (B) (red densities, superimposed on apo-SWR1) or (G) apo-SWR1 (B) from SWR1-nucleosome (C) (blue mesh, superimposed on SWR1-nucleosome). The structures were filtered to 60Å before calculating the difference maps. The difference maps were contoured to 6s and represent either those parts of the structure present in apo-SWR1 but absent in SWR1-nucleosome (F) or present in SWR1-nucleosome but absent in apo-SWR1 (G). **(H)** A partial side view of the structure in (G) (rotated by 60°), showing the superposition between the new density and a peak in the difference map (black arrow). **(I)** Two-dimensional image analysis of SWR1-nucleosome data for four different views of the complex. The panel shows, from left to right: (i) re-projections of apo-SWR1 that best match the view of SWR1-nucleosome analyzed; (ii) the corresponding re-projections of the SWR1-nucleosome reconstruction shown in (C,E); (iii) the corresponding re-projections of the SWR1-nucleosome 3D model shown in (I) (the white arrow points to the nucleosome); (iv) the corresponding

reference-free class averages from the SWR1-nucleosome data. **(J)** 3D model for the SWR1-nucleosome complex. A nucleosome, filtered to 34Å, was placed in the peak in the difference map based on the 2D image analysis shown in (I). The nucleosome is shown in grey with the H2A/H2B histone dimer in a lighter shade. **(K)** The SWR1-nucleosome model shown in (J), rotated by 20^{o} around the vertical axis, is color-coded according to the identity of the four functional modules. The nucleosome is colored as in (J).

SWR1 engages the nucleosome core particle via the catalytic subunit Swr1

The SWR1-nucleosome reconstruction showed a new density that is contiguous with that of the core subunit Swr1 and extends towards the Rvb1/2 ring (Figure 3.4C). This prominent protrusion from Swr1 is also observed in 2D class averages (Figures 3.4I) and coincides with a peak in the difference map calculated by subtracting apo-SWR1 from SWR1-nucleosome (Figure 3.4G,H). We docked a 3D map of the yeast nucleosome crystal structure (White et al., 2001), filtered to the resolution of the SWR1-nucleosome map (34Å), into the EM density. We observed that the bulk of the nucleosome could be accommodated by the extra density in our 3D map (Figure 3.4J). However, this density was not fully resolved, likely due to heterogeneity, both conformational and biochemical, in the data. The 3D map also indicated that the most significant contact between SWR1 and the nucleosome core particle is mediated by the ATPase-containing portion of Swr1 (Figure 3.4K). Taken together, our data suggest that SWR1 engages the nucleosome core particle in a significantly extended conformation, mainly *via* the Swr1 subunit. However, this observation does not exclude the possibility that flexible regions of the nucleosome, such as linker DNA (43 bp were present in our nucleosome construct) and/or histone tails, could interact with components of the complex. These potentially labile contacts are unlikely to be resolved in our 3D structure.

To confirm the orientation of the bound nucleosome suggested by our data (Figure 3.4K), we generated a 3D map containing the docked nucleosome (Figure 3.4J) and compared its re-

projections against experimental 2D class averages. This analysis indicated that the location and orientation of the modeled nucleosome were in general agreement with the experimental data (Figure 3.4I). In this orientation, the nucleosome appears to be stabilized over a central depression formed between the Swr1 ATPase and the Rvb1/2 ring. One side of the octamer faces the complex, while the other side is completely exposed. Since we know the location of the C-Module, which binds to the H2A.Z/H2B dimer that will replace H2A/H2B, we chose a nucleosome orientation in our model that has its H2A/H2B dimers pointing towards the C-Module (Figure 3.4K).

Biochemical purification of a stable SWR1-Nucleosome complex using a preferred substrate

Incomplete resolution of the bound substrate in the complex suggested that the nucleosome did not bind sufficiently stably to SWR1. In order to improve this property, which may allow us to better determine the orientation of the bound nucleosome, we purified a more stable SWR1-nucleosome (SN) sample by using a substrate containing 60 basepairs of linker DNA, as opposed to the 43 basepair linker present in the previously utilized substrate. The longer linker has been shown to significantly enhance the affinity of the nucleosome for SWR1 *in vitro* (Ranjan et al., 2013). It is also the length contacted by SWR1 *in vivo* (Yen et al., 2013). We incubated affinity-purified SWR1 with a 3 fold excess of nucleosomes and biochemically assessed binding using agarose gel electrophoresis (Figure 3.5A). In the presence of SWR1, the nucleosomes were clearly electrophoretically retarded, indicative of complex formation. Interestingly, this shifted species migrated on the gel as a more distinct band than that previously

observed for the shorter-linker substrate (compare with Figure 3.2A, lanes 2 and 3). This may represent our biochemical support for the preference of the enzyme toward this substrate.

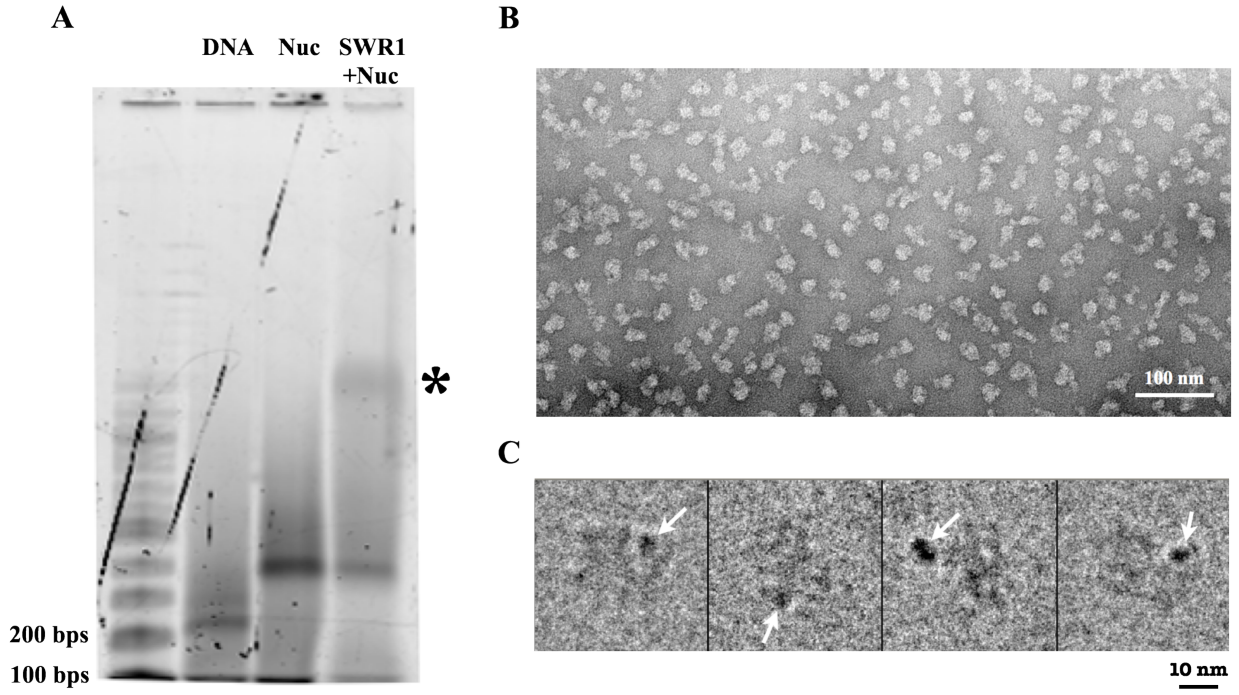

Figure 3.5 – Biochemical purification and initial imaging of SWR1 complexed with a preferred nucleosome substrate. (A) SWR1 was incubated with a 3 fold excess of 60 basepair-linker nucleosomes at 4°C for 4 hours. The reaction was analyzed on a native agarose gel (1.3% agarose, 0.2X TB) and stained for nucleic acids using Sybr Green I. Naked DNA identical in sequence to nucleosomal DNA and free nucleosomes (Nuc) were used as controls. Left lane: 100 bp markers. Asterisk marks nucleosomes shifted in the presence of SWR1. **(B)** GraFix-treated and glycerol-removed samples were negatively stained and imaged using the electron microscope. A representative micrograph is shown. **(C)** A similarly prepared sample containing nucleosomes with Nanogold®-labeled DNA was imaged under cryo conditions. Representative micrographs of single particles are shown. White arrows mark high-contrast features that may correspond to the labels.

The sample was purified using the GraFix method as described. To determine if the resulting sample was suitable for an EM study, we imaged select GraFix fractions in negative stain after glycerol removal. This allowed us to select 2-3 fractions in which the sample appeared homogeneous (Figure 3.5B). To confirm that the sample was enriched in nucleosome-bound complexes, we covalently labeled the DNA ends with commercially available Nanogold®

and assembled the nucleosome substrate *in vitro* using this DNA. SWR1 complexed to this substrate was purified using an identical protocol and imaged under cryo conditions, which are ideal for visualization of the electron-dense gold labels. We were able to identify single particles exhibiting high-contrast features that may correspond to the gold labels (Figure 3.5C). Since the reconstituted nucleosomes were purified through a sucrose gradient, free gold-labeled DNA should not be present in the binding reaction. Therefore, the particles we observed should be SN. However, we have not determined enrichment of this species in the selected fractions. Furthermore, unambiguous assignment of the gold-label signals requires future alignment and classification of the single particles.

Biochemical purification of the SWR1-Nucleosome-Z/B ternary complex

Generating the SWR1-Nucleosome-Z/B ternary complex (SNZ) *in vitro* is complicated by the high affinity of the dimers, which must be present in excess, for the long linker DNA. As this feature directly interacts with SWR1 *via* Swc2 (Ranjan et al., 2013), the dimers would be a major competitor for SWR1 in nucleosome binding. We have determined a biochemical protocol to successfully form the ternary complex *in vitro* (Figure 3.6A). We first incubated SWR1 with a 3 fold excess of nucleosomes for 4 hours at 4^{o}C so that the binding reaction could reach equilibrium. This sample should be enriched for the SWR1-nucleosome complex (SN). Then, we added Z/B at 5 fold excess of SWR1 and incubated the three-component binding reaction for an additional 2 hours at 4^{o}C. Native agarose electrophoresis of the sample showed that addition of Z/B generated a nucleosome-containing species with distinctly lower electrophoretic mobility from the presumably SN species (Figure 3.6B), suggesting that the final sample was enriched for SNZ. This analysis also indicated that SNZ was the main nucleosome-

bound species of SWR1, as the resulting band appeared sharp and distinct from the SN band. It was also evident from the up-shift of the free nucleosomes that the excess dimers was titrated towards the linker DNA (Figure 3.6B, SNZ lane).

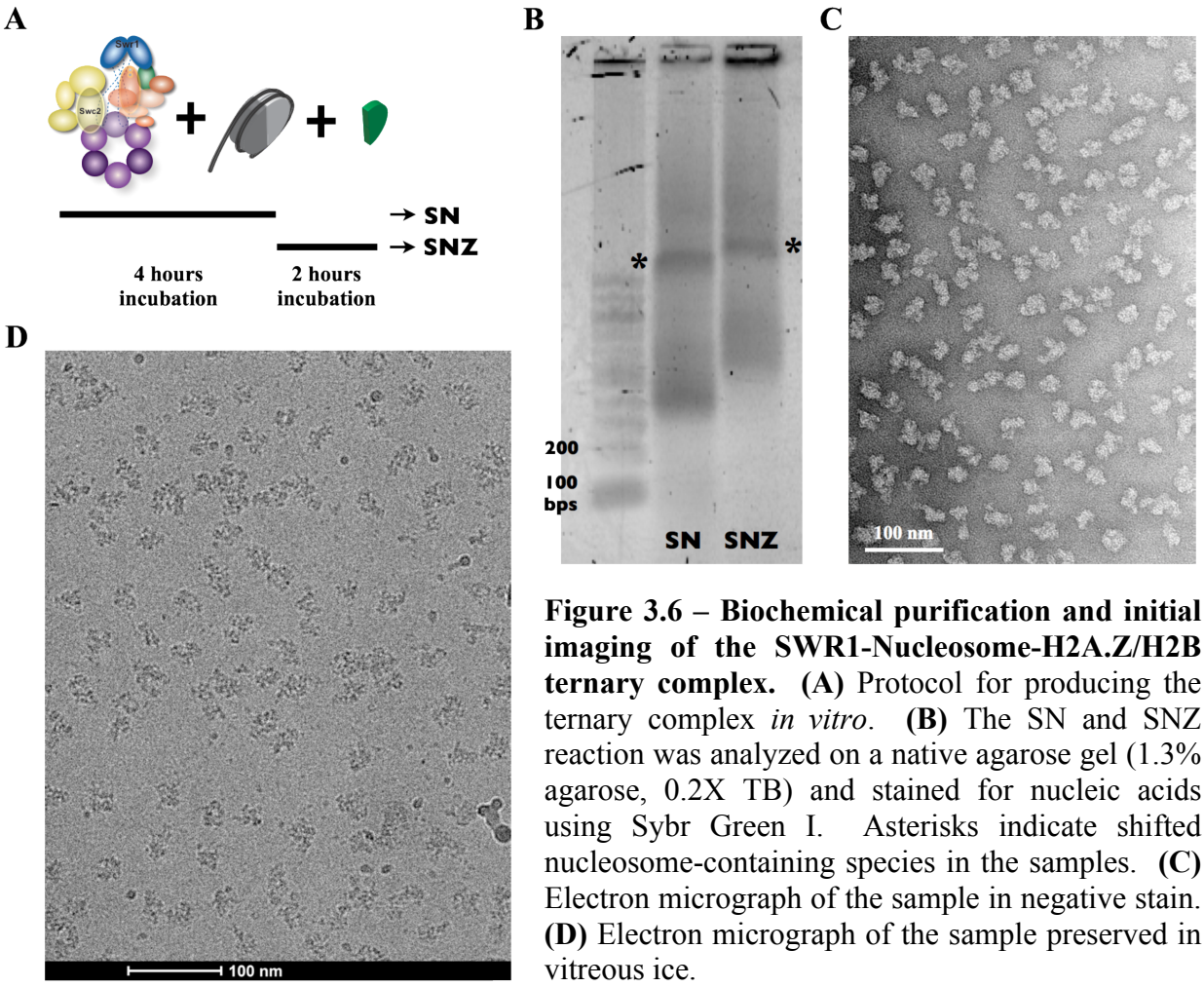

Figure 3.6 – Biochemical purification and initial imaging of the SWR1-Nucleosome-H2A.Z/H2B ternary complex. **(A)** Protocol for producing the ternary complex *in vitro*. **(B)** The SN and SNZ reaction was analyzed on a native agarose gel (1.3% agarose, 0.2X TB) and stained for nucleic acids using Sybr Green I. Asterisks indicate shifted nucleosome-containing species in the samples. **(C)** Electron micrograph of the sample in negative stain. **(D)** Electron micrograph of the sample preserved in vitreous ice.

We selected for GraFix fractions containing the most homogeneous sample using NS-EM (Figure 3.6C). The sample was most homogeneous in the bottom 300 µL of the gradient, where the glycerol concentration was ~60%. Thus, the migratory property of this sample in the glycerol gradient was significantly different from that of apo-SWR1, which was found at ~50% glycerol (Figure 2.2A), suggesting that it contained more massive complexes. This sample was

also well-behaved in vitreous ice, allowing high-quality cryo-EM data to be collected (Figure 3.6D).

DISCUSSION

Nucleosome binding by SWR1

Conformational changes have been reported for nucleosome-bound remodelers (Gangaraju et al., 2009); however, they have yet to be visualized. In this study, the 3D structure of SWR1-nucleosome, together with the annotated 3D map of SWR1 alone, allowed us to characterize the structural changes that the complex undergoes upon substrate binding (Figure 3.7). We observed a significant extension of Swr1 and the C-Module away from the Rvb1/2 ring, which appears to be required to accommodate the substrate between Swr1 and the ring. This extension occurred in the absence of nucleotides, suggesting that recognition of nucleosomal features, such as linker DNA, nucleosomal DNA, and/or histone tails, by various components of the complex is sufficient to drive this ATP-independent conformational change. This rearrangement can also be mediated, at least in part, by the Rvb1/2 ring. A recent structural study has shown that the ring adopts primarily two nucleotide-independent conformations in solution: “compact” and “stretched”. Their structures significantly differ in the extension of the insert domains relative to the nucleotide-binding AAA+ domains (López-Perrote et al., 2012). Since our data indicate that flexibility of the Rvb inserts is involved in their association with SWR1 (Figure 2.5H), these two conformations of the Rvb1/2 ring may also exist in the complex. It is possible that the interconnectedness exhibited by apo-SWR1 stabilizes the “compact” conformation of the ring. This function may be overcome by substrate recognition, thus allowing the complex to extend and engage the nucleosome. While this model remains to be

tested in SWR1, similar regulatory mechanisms involving release of auto-inhibition have been demonstrated for other remodelers (Clapier and Cairns, 2012; Hauk et al., 2010).

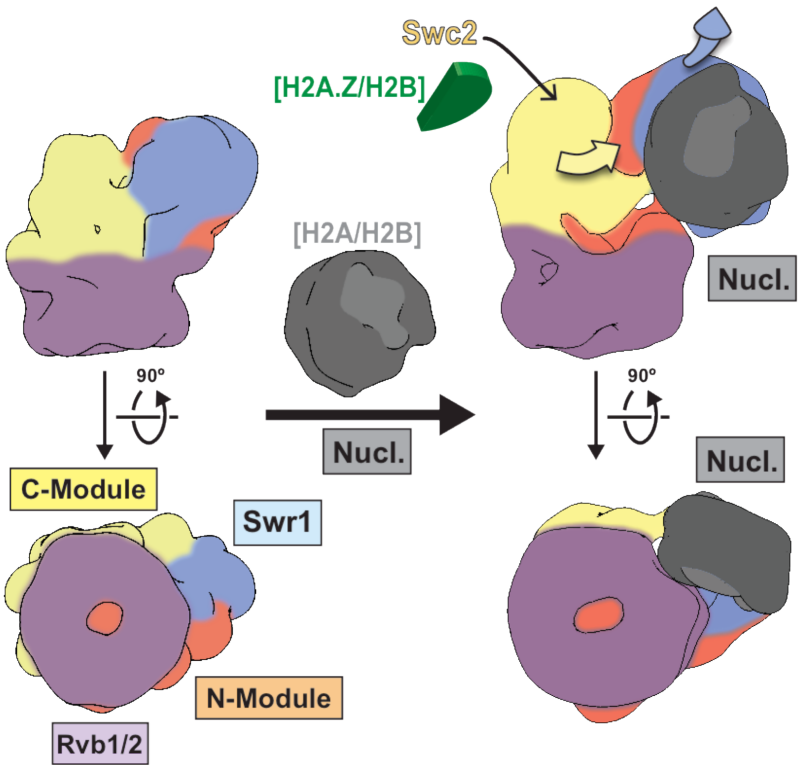

Figure 3.7 – Nucleosome-induced conformational change in SWR1. Schematic representation of the conformational changes observed in this work between apo-SWR1 and SWR1-nucleosome. Apo-SWR1 (left) and SWR1-nucleosome (right) are shown from two different orientations. The four functional domains are labeled at the bottom left and follow the same color conventions used throughout the chapter. The arrows (top right) indicate the major conformational changes observed upon addition of nucleosome to SWR1. The nucleosome is shown in grey with the H2A/H2B dimers in a lighter shade. The location of subunits involved in binding to the H2A.Z/H2B dimer (green) that will be inserted (Swc2 in the C-Module).

We showed that SWR1 makes only limited contact with the nucleosome, mediated primarily by the catalytic core of Swr1. This is in contrast to other characterized remodelers, which exhibit significantly more extensive interactions with their substrate. For example, the RSC complex binds both faces of the nucleosome (Chaban et al., 2008; Saha et al., 2005); the related SWI/SNF complex contacts ~50 bps, or nearly one gyre, of nucleosomal DNA (Dechassa et al., 2008); and the smaller ISW2 complex forms discrete contacts across one face of the nucleosome (Dang and Bartholomew, 2007). The limited contact formed between SWR1 and the nucleosome core particle has not been observed in any other remodeler. We speculate that while

different remodelers exhibit different patterns of substrate handling, extensive interactions may be a feature of remodelers that slide the histone octamer. As nucleosomal DNA is unraveled from the octamer, these interactions may serve to prevent substrate disintegration. SWR1, however, is the only known remodeler that does not slide the octamer (A.R, C.W, unpublished data). Furthermore, ATP-dependent mobilization of nucleosomal DNA by SWR1 has been shown to be extremely limited (Jónsson et al., 2004; Papamichos-Chronakis et al., 2011). Therefore, chromatin remodeling by SWR1 may not require large-scale disruptions of histone-DNA contacts, as seen for sliding reactions. We suggest that the limited contact observed between SWR1 and the nucleosome may reflect this mechanistic distinction.

Our 3D results currently do not address contacts that the complex makes with linker DNA (Ranjan et al., 2013; Yen et al., 2013), as observed for SWI/SNF (Dechassa et al., 2008), ISWIs (Dang and Bartholomew, 2007; Yamada et al., 2011), and suggested for the SWR1-related INO80 complex (Udugama et al., 2010). Histone tails may also interact with components of the N-Module, such as Swc4 and Arp4 (Boyer et al., 2004; Galarneau et al., 2000; Sunada et al., 2005). All of these potential interactions, which would occur outside of the nucleosome core particle, could stabilize the substrate-bound conformation revealed by the 3D map. Having purified SWR1 bound to a preferred substrate, which appears homogeneous, we will pursue determination of a higher-resolution 3D structure of a stable SN complex within which the nucleosome core particle is well resolved. The Nanogold®-labeled SN sample will provide complementary data to allow determination of the nucleosome's orientation when bound to SWR1.

It has been shown that while ATPase activity of SWR1 is enhanced upon binding to an H2A-containing nucleosome, it achieves the highest level of stimulation when its second

substrate—the H2A.Z/H2B dimer—is bound (Luk et al., 2010). Our successful biochemical purification of the SNZ complex will allow the structural characterization of this highly activated ternary complex. Interestingly, the revelation that there are two specific dimer binding sites in SWR1 (Hong et al., 2014; Wu et al., 2005; 2009) makes it an important goal to map the location(s) of the bound dimer(s) in our SNZ reconstruction. Furthermore, it remains to be seen how ATP binding and/or hydrolysis by Swr1 and perhaps Rvb1/2 may further affect the overall structure of the substrate-bound complexes. Analysis of SWR1's conformational dynamics in the presence of nucleotides should provide important new insights into the mechanism of dimer exchange.

CONCLUSIONS

This thesis work has accomplished a detailed dissection of SWR1's molecular architecture and provided a structural foundation upon which conformational dynamics may be characterized. However, it has also been a reminder that remodelers are challenging research subjects and that our understanding, both structural and mechanistic, is still extremely limited. Analysis of the core translocase domains must also take into account how the remaining components of the complexes may dictate their remodeling activities. In terms of SWR1, we are still far from understanding how this sophisticated assembly exchanges histone dimers. Structural studies, which must now consider pushing the resolution thanks to recent advances in EM technologies, should be combined with biochemical and single-molecule studies that address the enzyme's dynamics in solution.

At the same time as the release of this study, the 3D EM structure of the INO80 complex was reported (Tosi et al., 2013). Considered to be sister complexes, SWR1's and INO80's

common subunits include Rvb1/Rvb2 and amount to >50% of their molecular weights. Their catalytic subunits are also highly similar in sequence (Morrison and Shen, 2009). The two reported structures for SWR1 (this work) and INO80 (Tosi et al., 2013), both from *S. cerevisiae* but were obtained using different biochemical and computational approaches, are largely dissimilar. Tosi, Haas, Herzog and colleagues suggested that INO80 contains a dodecameric assembly of Rvb1/2, although the double rings are not well accommodated within the assigned density. Furthermore, our biochemical data disagree with the structural results. The oligomeric state of the AAA+ proteins has major mechanistic implications (Gribun et al., 2008) and thus should be accurately determined. Future validations are required for a meaningful comparative analysis of the INO80 complexes.

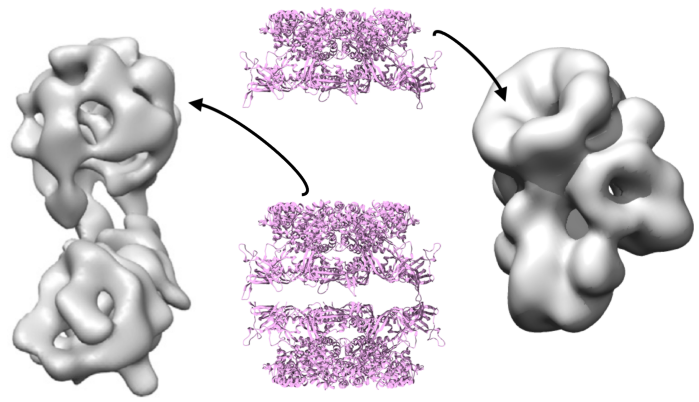

Figure 3.8 – Comparison between 3D EM structures of INO80 and SWR1. The NS-EM structure of INO80 (left) (Tosi et al., 2013) and the cryo-NS-EM structure of SWR1 (right) (Nguyen et al., 2013) are visually aligned and displayed side by side. The crystal structure of the RUVBL1 hexamer (Matias et al., 2006) is shown to scale. INO80 was determined to contain a dodecamer (arrow points to the assigned density) and SWR1 a single hexamer.

Despite their compositional similarity, the two sole members of the INO80 subfamily are functionally different. Unlike SWR1, INO80 is a robust octamer slider *in vitro* (Udugama et al., 2010). It may also possess dimer-exchange activity which reverses that of SWR1 (Papamichos-Chronakis et al., 2011). *In vivo*, these two complexes have been shown to regulate the distribution of H2A.Z and also to collaborate in DNA repair and other processes (Morrison and

Shen, 2009; Papamichos-Chronakis et al., 2011). However, it is still being debated whether INO80 is a dedicated, robust dimer exchanger, as demonstration of this activity has not been successfully reproduced by other research groups. Thus, dimer exchange may be a shared function of the INO80 subfamily, or it may be unique to SWR1. In either case, this pair of highly related remodelers offers the chromatin remodeling field an excellent opportunity to address how remodelers functionally diverge and how structure could influence function within this class of molecular machines.

EXPERIMENTAL PROCEDURES

Purification of substrate-bound SWR1 complexes

SWR1-nucleosome (43-bp linker)

SWR1 was affinity-purified from *S. cerevisiae* as previously described (Luk et al., 2010). Nucleosomes were prepared by Anand Ranjan (Wu Lab – NCI/NIH) and contained recombinant fly H3-H4, yeast H2A-H2B and 193 bp DNA bearing the 601 nucleosome-positioning sequence (NPS) and a 43 bp asymmetric linker. To obtain nucleosome-bound SWR1, we carried out an *in vitro* binding reaction with 40 pmoles reconstituted nucleosomes and 10 pmoles SWR1 in a 120 µL reaction for 30 minutes at room temperature. We then proceeded to purify SWR1-Nucl using GraFix as described in Chapter 2.

SWR1-nucleosome (60-bp linker)

We carried out *in vitro* reconstitution of nucleosomes using recombinantly expressed canonical histones from *D. melanogaster* and a DNA construct containing the 601 NPS, 60 bps of linker DNA on one side and 10 bps on the other side. We used salt-gradient dialysis as describe (Dyer et al., 2004). The sample was further purified using a sucrose gradient, pooled, and dialyzed into storage buffer (20 mM Tris, pH 7.5, 1 mM EDTA, 1 mM TCEP)

We added ~60 pmoles of nucleosomes to ~20 pmoles of purified SWR1 in exchange buffer (25 mM HEPES-KOH, pH 7.6, 0.37 mM EDTA, 0.35 mM EGTA, 10% glycerol, 0.017% NP-40, 1 mM TCEP, 70 mM KCl, 3.6 mM $MgCl_2$). The total reaction (40-50 µL) was incubated at 4^{o}C for 4 hours. A 5 µL aliquot was taken and electrophoresed in 1.3% agarose (0.2X TB buffer), using TE+sucrose as loading buffer. The gel was stained with Sybr Green I and imaged using the Typhoon.

The sample was purified using a GraFix gradient as described, but with formaldehyde gradient changed to 0.5% to 2%.

SWR1-Nucleosome-H2A.Z/H2B

We pre-charged SWR1 with the nucleosomes by incubating them as described. After 4 hours, a 5 μL aliquot was put aside for native gel analysis (SN sample). We added ~100 pmoles of H2A.Z/H2B (recombinantly expressed and purified by Feng Wang – Wu Lab), or 5 fold excess. The three-component reaction was incubated for another 2 hours at 4^{o}C. Another 5 μL aliquot was retrieved (SNZ sample) for native gel. We electrophoresed, as described, both SN and SNZ aliquots simultaneously.

GraFix was then carried out on this sample.

Native gel electrophoresis and Western Blot

Native gel electrophoresis

To qualitatively assess nucleosome occupancy in the GraFix-treated sample, we compared the electrophoretic mobility of this sample against that of apo-SWR1, which was similarly purified. After dialysis, cross-linked samples from single fractions were electrophoresed in a NuPAGE® Novex 3-8% Tris-Acetate, 1.0 mm gel (Invitrogen) at 4^{0}C. Sample loading buffer contained 10% glycerol, 0.01% w.v. bromophenol blue, 43 mM imidazole, 35 mM HEPES, pH 7.4. Electrophoresis buffer contained 43 mM imidazole and 35 mM HEPES, pH 7.4. The gel was silver-stained.

Western Blot

To confirm co-migration of nucleosomes and SWR1 in the glycerol gradient, we quenched and reversed the formaldehyde crosslinking as described above. Then, an aliquot of each fraction was electrophoresed in pre-cast PROTEAN 4-20% polyacrylamide gel (Bio-Rad). Proteins were transferred onto a nitrocellulose membrane and blotted for,

- H3 using rabbit α-H3 (AB1791) and GαRb 2^0 at 1:3,000 dilution at 1:5,000 dilution
- Swr1-3xFLAG using mouse α-FLAG (Bio-Rad) at 1:3,000 dilution and RAM 2^0 at the same dilution
- Swc2 using chicken α-Swc2 (Wu et al., 2009) at 1:10,000 dilution and α-chicken HRP at 1:5,000 dilution

Membranes were exposed to Kodak chemiluminescence films.

Electron Microscopy

Sample preparation

To prepare cryo-negative samples, we applied 5-10 μL of the peak fraction to Quantifoil® grids coated with a thin layer of carbon, let the sample absorb for 15-30 minutes at 4^0C in a sealed apparatus to prevent evaporation. Then, we rinsed them directly on drops of stain (2% uranyl formate), floated a second layer of thin carbon ("sandwich") and froze the stained grids in liquid nitrogen (De Carlo and Stark, 2010).

To prepare cryo samples, we absorbed the sample onto carbon as described. We used the Vitrobot (FEI) system to carry out vitrification of the sample in liquid ethane. The chamber was maintained at 4^oC and 100% humidity. Typical blotting parameters are 20-25 force and 4s-5s time, with no drain time before plunging.

Imaging

We collected untilted cryo-negative data at liquid-nitrogen temperature and under low-dose conditions. We used a field-emission gun (FEG) Tecnai G2 F20 transmission electron microscope (FEI) operating at 120 keV and equipped with a Gatan 4k x 4k CCD. Images were collected at a nominal magnification of 62,000x and an electron dose of ~20 electrons/Å^2. The pixel size at the sample level was 1.73 Å.

Alignment of 2D images

To compare 3D maps against experimental class averages, we generated 2D re-projections of the filtered maps at defined theta values using the PJ 3Q command in SPIDER (Frank et al., 1996). The re-projections and experimental class averages were aligned to each other using the AP SH and RT SQ commands in SPIDER (Frank et al., 1996).

Visualization of and docking into 3D maps

We performed 3D structure analysis and image rendering using the UCSF Chimera package (Pettersen et al., 2004). EM-like 3D maps were generated from published crystal coordinates using the CP FROM PDB command in SPIDER (Frank et al., 1996). To dock 3D maps or crystal structures into our EM densities, we roughly placed the former into the latter and used Chimera's "Fit in Map" function for the final fitting.

To generate the composite nucleosome-bound SWR1 map, we generated a 3D map of the yeast nucleosome from the published crystal coordinates (PDB: 1IDB, (White et al., 2001)) as described above. Then, we placed this map into our experimental map and converted the former's 3D coordinate system to the latter *via* resampling (*vop resample* command in Chimera). The two maps were then normalized, added, and filtered in SPIDER (Frank et al., 1996)

3D classification of SWR1-nucleosome reconstructions

To obtain the 3D structure of nucleosome-bound SWR1, we used the 3D map we obtained after refinement of the OTR model against SWR1 class averages. This model was low-pass filtered to 60 Å and refined against 2D class averages generated from cryo-negative data of the nucleosome-bound sample. The SWR1-nucleosome class averages were obtained as described above for nucleosome-free SWR1. Using the resulting 3D map as a starting model, we performed maximum-likelihood-based 3D classification (Scheres, 2012a) using the RELION program (Scheres, 2012b). We generated 5 classes using ~45,000 single particles, obtained under identical conditions to those for the apo-SWR1 sample. Single particles were phase-flipped in EMAN2 (Tang et al., 2007), binned by 3 for a resulting pixel size of 5.17 Å, and normalized in XMIPP (Sorzano et al., 2004). After 3D classification, we performed single-model refinement by using the "autorefine" option in RELION. Because a majority of the resulting 3D maps exhibited missing densities, we selected a model in which densities for all modules identified in the apo-SWR1 structure were account for. We refined it against single-particles assigned to the corresponding class by 3D classification.

REFERENCES

Boyer, L.A., Latek, R.R., and Peterson, C.L. (2004). The SANT domain: a unique histone-tail-binding module? Nat Rev Mol Cell Biol *5*, 158–163.

Chaban, Y., Ezeokonkwo, C., Chung, W.-H., Zhang, F., Kornberg, R.D., Maier-Davis, B., Lorch, Y., and Asturias, F.J. (2008). Structure of a RSC-nucleosome complex and insights into chromatin remodeling. Nature Structural & Molecular Biology *15*, 1272–1277.

Clapier, C.R., and Cairns, B.R. (2012). Regulation of ISWI involves inhibitory modules antagonized by nucleosomal epitopes. Nature.

Dang, W., and Bartholomew, B. (2007). Domain architecture of the catalytic subunit in the ISW2-nucleosome complex. Molecular and Cellular Biology *27*, 8306–8317.

De Carlo, S., and Stark, H. (2010). Cryonegative staining of macromolecular assemblies. Meth Enzymol *481*, 127–145.

Dechassa, M.L., Hota, S.K., Sen, P., Chatterjee, N., Prasad, P., and Bartholomew, B. (2012). Disparity in the DNA translocase domains of SWI/SNF and ISW2. Nucleic Acids Research.

Dechassa, M.L., Zhang, B., Horowitz-Scherer, R., Persinger, J., Woodcock, C.L., Peterson, C.L., and Bartholomew, B. (2008). Architecture of the SWI/SNF-nucleosome complex. Molecular and Cellular Biology *28*, 6010–6021.

Dyer, P.N., Edayathumangalam, R.S., White, C.L., Bao, Y., Chakravarthy, S., Muthurajan, U.M., and Luger, K. (2004). Reconstitution of nucleosome core particles from recombinant histones and DNA. Meth Enzymol *375*, 23–44.

Frank, J., Radermacher, M., Penczek, P., Zhu, J., Li, Y., Ladjadj, M., and Leith, A. (1996). SPIDER and WEB: processing and visualization of images in 3D electron microscopy and related fields. J Struct Biol *116*, 190–199.

Galarneau, L., Nourani, A., Boudreault, A.A., Zhang, Y., Héliot, L., Allard, S., Savard, J., Lane, W.S., Stillman, D.J., and Côté, J. (2000). Multiple links between the NuA4 histone acetyltransferase complex and epigenetic control of transcription. Molecular Cell *5*, 927–937.

Gangaraju, V.K., Prasad, P., Srour, A., Kagalwala, M.N., and Bartholomew, B. (2009). Conformational changes associated with template commitment in ATP-dependent chromatin remodeling by ISW2. Molecular Cell *35*, 58–69.

Gribun, A., Cheung, K.L.Y., Huen, J., Ortega, J., and Houry, W.A. (2008). Yeast Rvb1 and Rvb2 are ATP-dependent DNA helicases that form a heterohexameric complex. Journal of Molecular Biology *376*, 1320–1333.

Hall, M.A., Shundrovsky, A., Bai, L., Fulbright, R.M., Lis, J.T., and Wang, M.D. (2009). High-resolution dynamic mapping of histone-DNA interactions in a nucleosome. Nature Structural & Molecular Biology *16*, 124–129.

Hauk, G., Mcknight, J.N., Nodelman, I.M., and Bowman, G.D. (2010). The chromodomains of the Chd1 chromatin remodeler regulate DNA access to the ATPase motor. Molecular Cell *39*, 711–723.

Hong, J., Feng, H., Wang, F., Ranjan, A., Chen, J., Jiang, J., Ghirlando, R., Xiao, T.S., Wu, C., and Bai, Y. (2014). The Catalytic Subunit of the SWR1 Remodeler Is a Histone Chaperone for the H2A.Z-H2B Dimer. Molecular Cell *53*, 498–505.

Jónsson, Z.O., Jha, S., Wohlschlegel, J.A., and Dutta, A. (2004). Rvb1p/Rvb2p recruit Arp5p and assemble a functional Ino80 chromatin remodeling complex. Molecular Cell *16*, 465–477.

Leschziner, A.E., Saha, A., Wittmeyer, J., Zhang, Y., Bustamante, C., Cairns, B.R., and Nogales, E. (2007). Conformational flexibility in the chromatin remodeler RSC observed by electron microscopy and the orthogonal tilt reconstruction method. Proc Natl Acad Sci USA *104*, 4913–4918.

López-Perrote, A., Muñoz-Hernández, H., Gil, D., and Llorca, O. (2012). Conformational transitions regulate the exposure of a DNA-binding domain in the RuvBL1-RuvBL2 complex. Journal of Biological Chemistry.

Luk, E., Ranjan, A., Fitzgerald, P.C., Mizuguchi, G., Huang, Y., Wei, D., and Wu, C. (2010). Stepwise histone replacement by SWR1 requires dual activation with histone H2A.Z and canonical nucleosome. Cell *143*, 725–736.

Matias, P.M., Gorynia, S., Donner, P., and Carrondo, M.A. (2006). Crystal structure of the human AAA+ protein RuvBL1. J Biol Chem *281*, 38918–38929.

Morrison, A.J., and Shen, X. (2009). Chromatin remodelling beyond transcription: the INO80 and SWR1 complexes. Nat Rev Mol Cell Biol *10*, 373–384.

Nguyen, V.Q., Ranjan, A., Stengel, F., Wei, D., Aebersold, R., Wu, C., and Leschziner, A.E. (2013). Molecular Architecture of the ATP-Dependent Chromatin-Remodeling Complex SWR1. Cell *154*, 1220–1231.

Papamichos-Chronakis, M., Watanabe, S., Rando, O.J., and Peterson, C.L. (2011). Global regulation of H2A.Z localization by the INO80 chromatin-remodeling enzyme is essential for genome integrity. Cell *144*, 200–213.

Pettersen, E.F., Goddard, T.D., Huang, C.C., Couch, G.S., Greenblatt, D.M., Meng, E.C., and Ferrin, T.E. (2004). UCSF Chimera--a visualization system for exploratory research and analysis. J Comput Chem *25*, 1605–1612.

Ranjan, A., Mizuguchi, G., Fitzgerald, P.C., Wei, D., Wang, F., Huang, Y., Luk, E., Woodcock, C.L., and Wu, C. (2013). Nucleosome-free Region Dominates Histone Acetylation in Targeting SWR1 to Promoters for H2A.Z Replacement. Cell *154*, 1232–1245.

Saha, A., Wittmeyer, J., and Cairns, B.R. (2005). Chromatin remodeling through directional DNA translocation from an internal nucleosomal site. Nature Structural & Molecular Biology *12*,

747–755.

Scheres, S.H.W. (2012a). A Bayesian view on cryo-EM structure determination. Journal of Molecular Biology *415*, 406–418.

Scheres, S.H.W. (2012b). RELION: implementation of a Bayesian approach to cryo-EM structure determination. J Struct Biol *180*, 519–530.

Schwanbeck, R., Xiao, H., and Wu, C. (2004). Spatial contacts and nucleosome step movements induced by the NURF chromatin remodeling complex. J Biol Chem *279*, 39933–39941.

Sorzano, C.O.S., Marabini, R., Velázquez-Muriel, J., Bilbao-Castro, J.R., Scheres, S.H.W., Carazo, J.M., and Pascual-Montano, A. (2004). XMIPP: a new generation of an open-source image processing package for electron microscopy. J Struct Biol *148*, 194–204.

Sunada, R., Görzer, I., Oma, Y., Yoshida, T., Suka, N., Wintersberger, U., and Harata, M. (2005). The nuclear actin-related protein Act3p/Arp4p is involved in the dynamics of chromatin-modulating complexes. Yeast *22*, 753–768.

Tang, G., Peng, L., Baldwin, P.R., Mann, D.S., Jiang, W., Rees, I., and Ludtke, S.J. (2007). EMAN2: an extensible image processing suite for electron microscopy. J Struct Biol *157*, 38–46.

Tosi, A., Haas, C., Herzog, F., Gilmozzi, A., Berninghausen, O., Ungewickell, C., Gerhold, C.B., Lakomek, K., Aebersold, R., Beckmann, R., et al. (2013). Structure and Subunit Topology of the INO80 Chromatin Remodeler and Its Nucleosome Complex. Cell *154*, 1207–1219.

Udugama, M., Sabri, A., and Bartholomew, B. (2010). The INO80 ATP-dependent chromatin remodeling complex is a nucleosome spacing factor. Molecular and Cellular Biology.

White, C.L., Suto, R.K., and Luger, K. (2001). Structure of the yeast nucleosome core particle reveals fundamental changes in internucleosome interactions. Embo J *20*, 5207–5218.

Wu, W.-H., Alami, S., Luk, E., Wu, C.-H., Sen, S., Mizuguchi, G., Wei, D., and Wu, C. (2005). Swc2 is a widely conserved H2AZ-binding module essential for ATP-dependent histone exchange. Nature Structural & Molecular Biology *12*, 1064–1071.

Wu, W.-H., Wu, C.-H., Ladurner, A., Mizuguchi, G., Wei, D., Xiao, H., Luk, E., Ranjan, A., and Wu, C. (2009). N terminus of Swr1 binds to histone H2AZ and provides a platform for subunit assembly in the chromatin remodeling complex. J Biol Chem *284*, 6200–6207.

Yamada, K., Frouws, T.D., Angst, B., Fitzgerald, D.J., DeLuca, C., Schimmele, K., Sargent, D.F., and Richmond, T.J. (2011). Structure and mechanism of the chromatin remodelling factor ISW1a. Nature *472*, 448–453.

Yen, K., Vinayachandran, V., and Pugh, B.F. (2013). SWR-C and INO80 Chromatin Remodelers Recognize Nucleosome-free Regions Near +1 Nucleosomes. Cell *154*, 1246–1256.